2011

Testing and improving the luminosity relations for Gamma-Ray Bursts

Andrew Collazzi
Louisiana State University and Agricultural and Mechanical College

TESTING AND IMPROVING THE LUMINOSITY RELATIONS FOR GAMMA-RAY BURSTS

A Dissertation

Submitted to the Graduate Faculty of the
Louisiana State University and
Agricultural and Mechanical College
in partial fulfillment of the
requirements for the degree of
Doctor of Philosophy

in

The Department of Physics and Astronomy

by
Andrew Collazzi
B.S., Vanderbilt University, 2006
M.S., Louisiana State University, 2010
August, 2011

Acknowledgments

Above all else, I would like to thank my adviser, Bradley Schaefer, for everything he has done to help me through these years. Without his constant support, direction, patience, and fantastic attitude, I would not have made it through these years.

I would also like to specially thank Robert Hynes for helping me expand my horizons as an astronomer. In particular, I would like to thank him for allowing me to participate in his X-Ray Binary group here at LSU. Finally, I wish to thank him for his generosity, without which these last few months would have been far more difficult.

In addition, I would like to thank the faculty and staff of the LSU Department of Physics and Astronomy for their support. In particular, Dana Browne, Amy Campbell, Michael Cherry, Geoffrey Clayton, Jonathan Dowling, Juhan Frank, James Giammanco, Mark Jarrell, Arlo Landolt, James Matthews, and Joel Tohline.

Thank you to many of the Vanderbilt physics and astronomy faculty who opened up the Universe for me. In particular, I would like to thank Robert Knop for giving me my first real experience in astrophysical research and the wonderful opportunity to go to CTIO. Without those experiences, I would never have made it to LSU. I would also like to thank David Weintraub and Kevian Stassun of Vanderbilt University for all they did in helping me become a better student and scientist.

I would like to thank all my friends and colleagues for their support and companionship. In particular: Jonathan Ahlbin, Andrew Banecker, Robert Beaird, Charles Bradley, Christopher Britt, Zachary Byerly, Matthew Cael, James Clem, Robert Collyer, David Donovan, Tiffany Driscoll, Wesley Even, Anne Gibbons, Bobby Gibbons II, Vayujeet Gokhale, Andrew Greenwood, Charles Jasper, Mark Kirkland, Drew Lanclos, Kristen Landis, Tyler Landis,

Lisa Lee, James Legeai III, Hayes Lewis, Laura Linhardt, Jarrod Marsh, David Mashburn, Whitney Mashburn, Valerie Mikles, Ashley Pagnotta, Matthew Patterson, Samuel Reid, Erich Schoeller, Lawrence Staten, Sulakshana Thanvanthri, Joshua Thibodaux, Sai Vinjanampathy, Frank Womack, and Limin Xiao.

Thank you to my entire family for all their support and remarkable patience throughout graduate school. In particular, I would like to thank my parents, Edith and Charles Collazzi, for all their support and encouragement. My brother, Timothy Collazzi, also deserves a special thank you, especially for all those mid-afternoon calls that helped me get through the day.

This work has been supported, in part, by grant AST-0708079 of the United States National Science Foundation and grants NNG05GH22H and NNX10AI40H of The Louisiana Space Consortium. Thank you for your support.

Table of Contents

Acknowledgments ii

List of Tables vii

List of Figures viii

Abstract x

1. Introduction 1
   - 1.1 A Brief History of Gamma-Ray Bursts 1
   - 1.2 Gamma-Ray Bursts as a Cosmological Tool 7
   - 1.3 Gamma-Ray Bursts as Standard Candles 12
   - 1.4 The Gamma-Ray Burst Luminosity Relations 15
   - 1.5 Problems With the Luminosity Relations 17
   - 1.6 This Work 21

2. Evaluating and Improving the Luminosity Relations 22
   - 2.1 Applying Generalized Tests for the Gamma-Ray Burst Luminosity Relations 22
   - 2.2 Testing Existing Luminosity Relations 25
   - 2.3 How Accurately Are the Luminosity Indicators Being Measured? 27
   - 2.4 Extending the Nakar and Piran Tests 29
   - 2.5 Using Individual Pulse Properties 31
   - 2.6 Conclusions and the Future 37

3. Generalized Tests for the Luminosity Relations 38
   - 3.1 Introduction 38
   - 3.2 The Generalized Test 39
   - 3.3 Test for Ambiguity in Deriving Results 43
   - 3.4 Test for Violators 47

4. Does the Addition of a Duration Improve the $E_{peak} - L_{iso}$ Relation for Gamma-Ray Bursts? - An Examination of the 'Firmani Relation' 50
   - 4.1 Introduction 50
   - 4.2 Testing the Firmani Relation 52
   - 4.3 Seeking the Optimal Duration 61
   - 4.4 Discussion 65

5. How Accurately Is E_{peak} Being Measured? 69
   - 5.1 Introduction 69
   - 5.2 Types of Uncertainty in E_{peak} 72
   - 5.3 Specific Examples 75
   - 5.4 Typical $\sigma_{Poisson}$ 77

5.5 Quantifying $\sigma_{\rm Choice}$ . . . 78
5.6 Measuring $\sigma_{\rm Det}$ . . . 81
5.7 Measuring $\sigma_{\rm Def}$ . . . 87
5.8 Are GRBs Thermostated? . . . 91
5.9 Implications . . . 95

6. A Significant Problem with Using the Amati Relation for Cosmological Purposes . . . 98
6.1 Background . . . 98
6.2 The $S_{\rm bolo}$ - $E_{\rm peak}$ Diagram and the Amati Relation . . . 100
6.3 Generalizing the Test to Many Detectors . . . 107
6.3.1 Amati et al. (2006) Data . . . 109
6.3.2 Schaefer (2007) Data . . . 109
6.3.3 BATSE Data . . . 111
6.3.4 *HETE*-2 Data . . . 114
6.3.5 *Swift* Data . . . 114
6.3.6 *Suzaku* Data . . . 118
6.3.7 *Swift* - *Suzaku* Data . . . 118
6.3.8 *Konus* Data . . . 120
6.3.9 *Beppo-Sax* Data . . . 123
6.3.10 Overview of Results . . . 123
6.4 The Amati Relation from a Combination of Selection Effects . . . 126
6.4.1 Trigger Thresholds . . . 126
6.4.2 Threshold For Measuring $E_{\rm peak,obs}$ . . . 128
6.4.3 The $E_{\rm peak,obs}$ Distribution . . . 129
6.4.4 The $S_{\rm bolo}$ Distribution . . . 129
6.4.5 The Effects in Combination . . . 130
6.5 Beaming Factor and the $S_{\rm bolo}$ - $E_{\rm peak}$ Diagram . . . 135
6.6 Short Bursts . . . 139
6.7 Conclusions . . . 140

7. The Burst Pulse Paradigm . . . 144
7.1 Introduction . . . 144
7.2 Data . . . 146
7.3 The Hakkila Pulse Model . . . 148
7.4 The Two Sided Gaussian Pulse Model . . . 150
7.5 Calculating $E_{\rm peak}$ . . . 157
7.6 Conclusions . . . 163

8. Conclusions . . . 165
8.1 The Work . . . 165
8.2 New Luminosity Relations? . . . 167
8.3 The Path Forward . . . 168

Bibliography . . . 170

Appendix. Letters of Permission 177
A.1 Permission to Reproduce Previously Published Work 177
A.2 Permission to Reproduce Figure 1.2 177

Vita 178

List of Tables

1.1 The Seven GRB Luminosity Relations 16

3.1 Generalized Tests of the Luminosity Relations 42

4.1 Burst Properties Used Throughout This Chapter 57

4.2 Expanding the Firmani Relation 59

4.3 RMS and Systematic Errors Values For Durations 64

5.1 $\sigma_{\rm Choice}$ in the BATSE Era 80

5.2 $\sigma_{\rm Sat}$ in the *Swift* Era 86

6.1 Demographics of the Data Samples 108

6.2 Beaming Factors for Each Data Sample 138

7.1 Two-Sided Gaussian Fits to *Swift* Data - Individual Channel Data 154

7.2 Two-Sided Gaussian Fits to *Swift* Data - Summed 4 Channel Data 155

7.3 Double Sided Gaussian Fits to *Swift* Data 156

7.4 XSPEC $\rm E_{peak}$ Fits to *Swift* Data 159

7.5 Sakamoto Check 161

7.6 Sakamoto Check 2 161

7.7 Robustness Test 162

List of Figures

1.1 Three examples of Gamma-Ray Bursts 2

1.2 The BATSE discovery of isotropy in the GRB distribution 4

1.3 The Hubble Diagram using both supernovae and GRBs 11

1.4 Model differences in cosmologies 13

1.5 The calibration plots for two GRB luminosity relations 19

2.1 The Amati relation and the Nakar and Piran test 24

3.1 $\mathcal{F}(z)/\mathcal{F}_{\max}$ for the eight luminosity relations 45

3.2 $\mathcal{F}(z)/\mathcal{F}_{\max}$ for two relations 48

4.1 The Firmani relation with Firmani's data 54

4.2 The Firmani relation with independent data for the same 19 GRBs 59

4.3 The Firmani relation when extended to 60 GRBs 62

5.1 A visualization of the scatter of E_{peak} due to σ_{choice} Alone 82

5.2 Another visualization of the scatter of E_{peak} due to σ_{choice} Alone 83

6.1 The basics of the Nakar and Piran test in graphical form 102

6.2 1,000 simulated bursts based on the Amati relation with no measurement errors 103

6.3 1,000 simulated bursts based on the Amati relation with realistic measurement errors 105

6.4 10,000 simulated bursts without the Amati relation 106

6.5 The Nakar and Piran test for 50 bursts from Amati et al. (2006) 110

6.6 The Nakar and Piran test for 27 bursts from Schaefer (2007) 112

6.7 1654 BATSE bursts from the future 5B BATSE catalog (Goldstein et al. 2011) 113

6.8 *HETE*-2 data from Sakamoto et al. (2005) 115
6.9 *Swift* data from Butler et al. (2007) 117
6.10 *Suzaku* data 119
6.11 Combined data from *Swift* and *Suzaku* 121
6.12 *Konus* bursts 122
6.13 *Beppo-Sax* bursts 124
6.14 The selection effects 132
6.15 Beaming and the Ghirlanda limit 137

Abstract

Gamma Ray Bursts (GRBs) have several luminosity relations where a measurable property of a burst light curve or spectrum is correlated with the burst luminosity. These luminosity relations are calibrated for the fraction of bursts with spectroscopic redshifts and hence the known luminosities. GRBs have thus become known as a type of 'standard candle'; where standard candle is meant in the usual sense that their luminosities can be derived from measurable properties of the bursts. GRBs can therefore be used for the same cosmology applications as Type Ia supernovae, including the construction of the Hubble Diagram and measuring massive star formation rate. The greatest disadvantage of using GRBs as standard candles is that their accuracy is lower than desired. With the recent advent of GRBs as a new standard candle, every effort must be made to test and improve the distance measures.

Here, several methods are employed to do just that. First, generalized forms of two tests are performed on all of the luminosity relations. All the luminosity relations pass the second of these tests, and all but two pass the first. Even with this failure, the redundancy in using *multiple* luminosity relations allows all the luminosity relations to retain value. Next, the 'Firmani relation' is shown to have poorer accuracy than first advertised. In addition, it is shown to be exactly derivable from two other luminosity relations. For these reasons, the Firmani relation is useless for cosmology. The Amati relation is then revisited and shown to be an artifact of a combination of selection effects. Therefore, the Amati relation is also not good for cosmology. Fourthly, the systematic errors involved in measuring a popular luminosity indicator (E_{peak}) are measured. The result is that an irreducible systematic error of 28% exists. After that, a preliminary investigation into the usefulness of breaking GRBs

into individual pulses is conducted. The results of an 'ideal' set of data do not provide for confident results due to large error bars. Finally, the work concludes with a discussion about the impact of the work and the future of GRB luminosity relations.

1. Introduction

1.1 A Brief History of Gamma-Ray Bursts

Gamma-Ray Bursts (GRBs) are commonly called the 'biggest explosions since the big bang'. They appear as flashes in the sky lasting anywhere between fractions of a second to several minutes. These flashes, comprised mostly of gamma-rays, have peaks in their flux spectrum ranging from a few keV to a few MeV. During outburst, they are brighter than all other gamma-ray sources combined (Fishman & Meegan 1995), and generally have an average total energy of $\sim 10^{52}$ ergs. This equates to an average intensity of $\sim 10^{-7} - 10^{-5}$ ergs cm^{-2} s^{-1}. GRBs were first discovered in 1973 (Klebesadel et al. 1973), observed only in the gamma-ray range of the spectrum. Until the discovery of their X-ray, optical and radio counterparts (Costa et al. 1997; van Paradijs et al. 1997; Frail et al. 1998), they were 'objects without precedent' (Fishman & Meegan 1995) as they had previously had no detected counterparts in any other energy range. This made them exotic objects, which sparked the interest of many astronomers. From the early measurements through modern observation techniques, GRBs are renowned for having a wide range of durations, light curves (see Figure 1.1) and spectral variations, which has made modeling *all* bursts very difficult.

There are two main classifications of GRBs. This is done largely by the duration of the burst, with any burst less than two seconds being referred to as 'short' and any burst longer than that to be 'long'. Long GRBs have vastly more known about them, and are much better understood than short GRBs. This is largely due to there being much more in the way of afterglow data on long GRBs. In addition to their shorter durations, short GRBs have a harder spectral profile than that of a long GRB, thus earning them the moniker "short hard

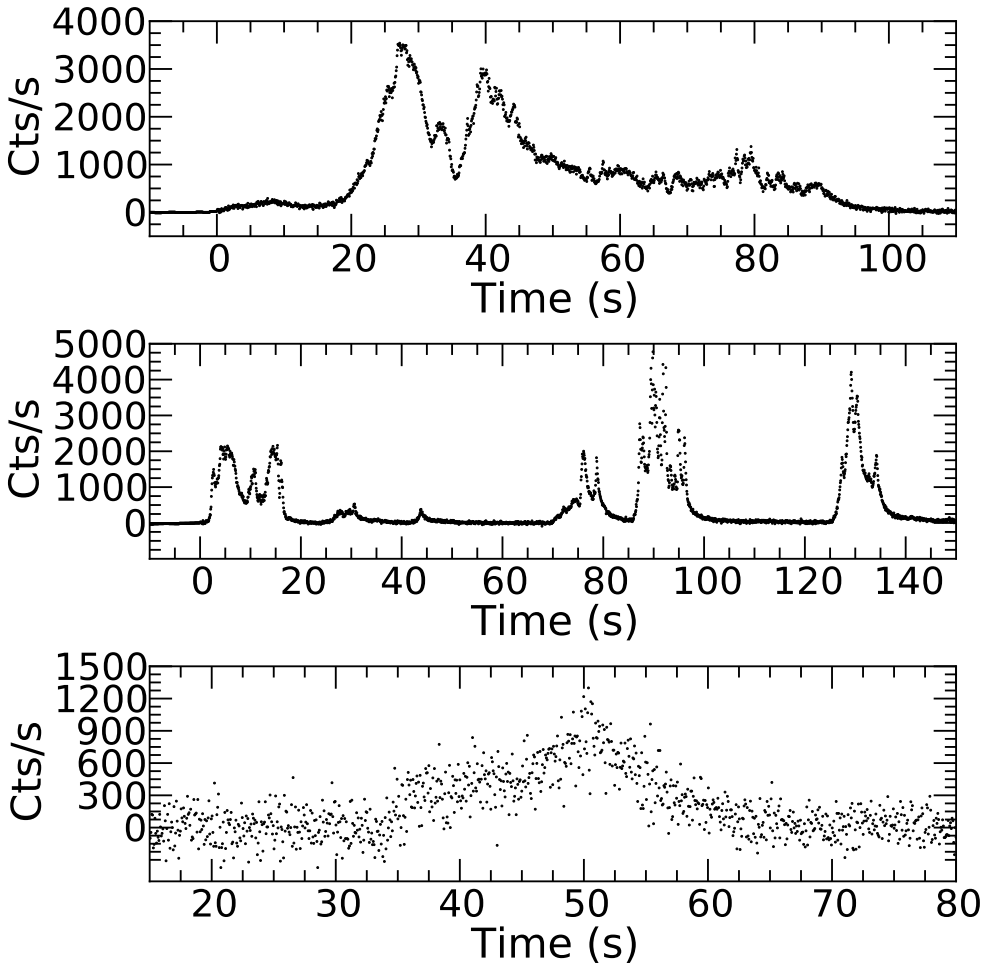

Figure 1.1 Three examples of Gamma-Ray Bursts. The y-axis is in counts of gamma-ray photons (the energy range depending on the spacecraft). The first two light curves, GRB 990123 and GRB 990506, are data from BATSE and the last light curve, GRB 050126, is data from *Swift* . GRBs have no consistent pattern, except in their chaotic nature. GRB 050126 shows an example of Poisson variations on a faint burst, although GRBs can certainly be much more ambiguous. GRB 990123 shows one style of a GRB, with one sustained burst (although with multiple peaks). GRB 990506 is an example of a burst with multiple separated pulses, making it difficult to describe the duration of the burst.

bursts". The emission mechanism for short GRBs is therefore assumed to be different than that of long GRBs. For the purposes of this thesis, whenever the term GRB is used, it refers to long bursts (unless specifically referred to otherwise).

One of the biggest questions that dominated many of the early GRB conferences was the geometrical question of where GRBs were coming from. In the broadest sense, there were two camps on the issue: galactic and extra-galactic. Indeed, before 1991 and even into the middle 1990's, a majority of workers on GRBs believed the source to be galactic neutron stars. The strongest evidence for galactic GRBs came from Murakami et al. (1988), who found absorption lines at 20-70 keV. This is consistent with cyclotron radiation in highly magnetic fields typical of a neutron star. Another strong argument made by the galactic source supporters was that the Eddington luminosity for neutron stars is 10^{38} erg s^{-1}, which places bursts at distances within the galaxy. An extragalactic model would require such a tremendous amount of energy that no one conceived of how such huge energies could be produced in such a short period (the rest mass energy of a star is on the order of 10^{52} erg). Arguments for the galactic models were strengthened by early distribution maps (e.g. Golenetskii, 1988; Figure 5 of Higdon & Ligenfelter 1990). Golenetskii used this distribution to argue for a concentration towards the galactic plane. In addition, the distribution did not coincide with galaxies or galaxy clusters. One of the more famous tests on this distribution was the 'V/V_{max}' test (Schmidt 1968, Schmidt et al. 1988, Higdon & Schmidt 1990), which confirmed a spatial uniformity of bursts, which is a conflicting conclusion - that GRBs were coming from extra-galactic sources.

It was not until GRB detectors like BATSE (Burst Alert and Transient Source Experiment) on CGRO (Compton Gamma Ray Observatory; Meegan et al. 1992), that a sufficient number of bursts were observed to answer the question as to the origin of GRBs. While

Figure 1.2 The BATSE discovery of isotropy in the GRB distribution. This graph shows the positions of the first ∼1,000 BATSE bursts in galactic co-ordinates. The findings solidified GRBs as coming not only from outside the galaxy but from *distant* galaxies. Many workers in GRB astronomy still consider this result to be one of the greatest achievements of GRB astronomy. This figure is Figure 6 of Briggs et al. (1996), and is reproduced by permission of the AAS (see Appendix A).

not much better than *Konus* in giving the astrometry of bursts, BATSE far surpassed its predecessors, seeing greatly more GRBs than any of the previous GRB detectors on other missions. BATSE settled the argument in the minds of most GRB workers. The most compelling piece of evidence provided by BATSE was that the observed distribution of GRBs was isotropic (Fishman 1991; Briggs et al. 1996; Figure 1.2). The lack of any structure to the GRB distribution is a huge indicator of very-distant extra-galactic sources.

However, the angular isotropy of GRBs is not enough proof of the cosmological distances of GRBs. An isotropic distribution could still be obtained by a source that is only observed out to a distance equal to the scale height of the galaxy or out to a distance still within the galaxy's halo. It is for this reason that another piece of evidence was looked to: the log P - log N distribution. If one were to plot the frequency of observations versus the brightness of the bursts in a log-log plot, there will be a -3/2 power law in the distribution

if GRBs are homogenous in their locations. This is a simple consequence of convolution of how many bursts there would be in a given volume by the inverse square law. BATSE saw a significant deviation from this -3/2 power law, which has a deficit of fainter bursts (Figure 13 of Fishman & Meegan 1995). So the debate continued as to where GRBs were coming from for some time. However, as you get finer and finer resolution on how isotropic GRBs are, you need them to be further and further out to still be 'local'. Eventually, the BATSE angular distribution got a fine enough isotropy (again, see Figure 1.2) to convince most everyone that GRBs had to be cosmological in origin.

A big advance for GRB science came with follow-up observations. These are generally done in X-ray, radio, ultraviolet, and optical bands, with the first observations made in 1997 (e.g. Costa et al. 1997; van Paradijs et al. 1997; Frail et al. 1998). The discovery of GRB afterglows allowed for the first arc-second positions of GRB sources. This then led the way for the first host galaxies to be discovered (Kulkarni et al. 1998) and redshifts measured (Metzger et al. 1997). Redshift in this instance refers to the Doppler shifting of light as a result of the expansion of the Universe as it travels to Earth (also called cosmological redshift). GRB afterglows were consequently the final piece of evidence to convince even the most skeptical of GRB workers that GRBs were coming from distant galaxies.

With better locations, GRBs were soon linked to star-forming regions. This ties GRBs to the deaths of massive stars: supernovae (SNe). Direct evidence linked GRBs and Type Ic SNe (Galama et al. 1998; Hjorth et al. 2003; Price et al. 2003; Stanek et al. 2003; Malesani et al. 2004; Campana et al. 2006;). However, Podsiadlowski et al. (2004) pointed out that the GRB rate is one per $\sim 3 \times 10^5$ years per galaxy. This rate is lower than the supernovae rate by more than a factor of 10^3. Therefore, special conditions are required for a SNe to produce a GRB.

One such special condition was deduced from GRB afterglows. In the X-ray, the lightcurve is shown to be a thrice broken power law. These breaks are seen from anywhere from 10^2 to 10^4 seconds after the burst. Likewise, the optical afterglow follows a power law with a single break. This is significant because it confirms that GRBs are not formed in an isotropic explosion. GRBs must therefore come from a collimated jet with high bulk Lorentz factor of 100-1000 (Woosley 1993; MacFadyen et al. 2001; Woosley & Bloom 2006).

With all this, the 'collapsar model' of GRBs became the accepted paradigm for GRB progenitors. As GRBs are connected with not only SNe, but areas of high star-formation, the evidence is that they must come from very massive, low-metallicity stars. As a supermassive star nears the end of its life, it can no longer generate enough energy via fusion to sustain its own mass. The star begins to collapse inwards, forming a black hole at the center. If the progenitor has a high rotation rate, high angular momentum will drive falling material into an accretion disk about the black hole. From there, it is not clear how the material is collimated into jets. The prevailing theory is that magnetic fields in the accretion disk get twisted and cause suitable conditions to create two jets, one from each face of the accretion disk. These jets, fueled by the material of the dying star, punch their way to the surface of the star, gradually accelerating as the stellar density decreases. By the time the leading shock has broken through the star, it will be traveling with a Lorentz factor of $100 - 1000$.

The emission seen from a GRB is believed to come from material collisions within the jet. As different fronts of matter are ejected at slightly different speeds, these fronts will collide with each other. The matter is immediately heated, causing immense motion of particles due to the high kinetic energy. This is known as an 'internal shock', which produces the gamma and X-rays seen in the 'prompt' emission of a GRB (Mészáros & Rees 1997). The emission mechanism that produces the gamma-ray photons is under debate. The debate generally

centers around two possibilities: synchrotron radiation and inverse Compton scattering. In synchrotron radiation, high energy photons are created as a result of a particle being accelerated as it travels in a highly magnetic field. In inverse Compton scattering, relativistic electrons scatter lower energy photons into higher energies (Rees & Mészáros, 1992; 1994).

Later, the slowing jet collides into the interstellar medium (ISM) and this action is what causes the decaying afterglows seen in the other wavelengths, ranging from radio to X-ray (Sari et al. 1998). The mechanism that causes afterglows is not understood. The idea is that synchrotron radiation is occurring as a result of particles being accelerated in a magnetic field. This magnetic field would likely be associated with the relativistic materials moving outward in the jet.

GRBs are, in a sense, an extreme supernova eruption: one that is so immense that the formation of a black hole creates the powerful jet that penetrates through the star and sends out the gamma radiation beam outwards.

1.2 Gamma-Ray Bursts as a Cosmological Tool

It is clear that GRBs are exotic, extreme, and evocative objects that in themselves spark much interest. Indeed, much remains to be uncovered in the field, especially in terms of the mechanics of the eruption itself. However, it is their usefulness as a tool for cosmology that is of significant interest to not only GRB astronomy, but the broader community. GRBs have a unique advantage over all other cosmological tools (e.g. Supernovae Ia, Cepheid Variables, RR Lyrae stars) in that they can be seen out to a redshift of z =8.2 (Tanvir et al. 2009; Salvaterra et al. 2009). While this is the maximum distance that a burst has been observed, there is sufficent evidence that it is very likely that they will be observed at even greater distances (Lamb & Reichart 2000; Bromm & Loeb 2002; 2006). There is a great

deal of cosmological information that can be obtained through GRBs. For example, Lamb & Reichart (2000) suggested that the optical afterglow light from a GRB sufficiently far out could pass through galaxies giving chemical abundances out to extreme redshift galaxies. Another example is given in Tanvir et al. (2009) and Lamb & Reichart (2000) which both suggest that as GRBs are observed at such extreme distances, they allow for measure of the Gunn-Peterson effect (a trough in the spectra of early quasars at energies less than that of Lyman-α which is evidence of the re-ionization of the early Universe). In addition, with the various Gamma-ray observatories in orbit, many optical transients have been discovered in the last decade, providing for sub-arc second positioning of (some) bursts. This provides *exact* positioning of the bursts (which as discussed earlier, was and is a huge problem with bursts without said transients). This provides a means for several telescope teams to find and study extremely high-z galaxies with relative ease. For all these tasks to be realized, redshifts must be obtained through GRBs. Only a fraction of bursts (31% for *Swift* , 5% for *Fermi*) have had red-shifts determined spectroscopically.

As it is now widely accepted that GRBs come from high mass stars undergoing core-collapse supernova, it follows that GRBs can be used as a cosmological tool for star formation rates (SFR). That is, the rate of GRBs will have to be proportional to the SFR of *massive* stars. This is largely due to the stars that are massive enough for core-collapse supernovae that could produce a GRB would have extremely short main-sequence lifetimes. Therefore, a GRB must be occurring at a site of recent star formation. While it might seem that GRBs are at a disadvantage for being an SFR for only massive stars, this is true of all other methods of measuring SFR, as the massive stars are the ones that give the best evidence of their lives and deaths in the high-z Universe. If one can accomplish the goal of obtaining distances to GRBs, then one can map out the GRB rates as a function of redshift, revealing

the Universe's SFR. The importance of SFR is vital for a wide variety of galaxy formation studies as well as determining the best population models. One large hurdle that workers determining the SFR have is with the lack of good data past $z \sim 4.6$ (e.g. Bouwens et al. 2006; Hopkins & Beacom 2006). As GRBs have already have had several detections beyond this range, they promise to break this limit. In addition, they are impervious to extinction (the absorption and scattering of light as it travels through space). Lloyd-Ronning et al. (2002) pointed out a complexity that arises when deriving the GRB SFR is that the burst luminosity function must be cleanly separated from the rate variations with distance. To realize the important result of SFRs for cosmology, one must have reliable and accurate methods of determining a distance to *most*, if not all, GRBs.

Perhaps the greatest contribution GRBs can provide to cosmology is in their invaluable extension of the Hubble Diagram out to high-z. The HD is the graphical representation of Hubble's Law (equation 1.1) (Sandage et al. 1958; Hubble 1929), which states that the distance of a galaxy is directly related to how fast it is moving.

$$v = \mathrm{H}_0 \, \mathrm{D} \quad , \quad \text{where} \quad \mathrm{H}_0 = 71.0 \pm 2.5 \frac{\mathrm{km/s}}{\mathrm{Mpc}} \tag{1.1}$$

The value used here for Hubble's Constant, H_0, is from the latest WMAP result (Jarosik et al. 2011). Hubble's Law is a direct result of the expansion rate of the Universe. The Hubble's constant actually *changes* with time, leading to an apparent change on the larger scale of the Universe. As such, tracing the evolution of Hubble's law to the early Universe (also called the high-z Universe) reveals the evolution of important cosmological factors. Therefore, the more precisely the HD is known, the better one knows the cosmological parameters which dictate how much of the Universe is matter, dark matter and dark energy. By refining these values, one can determine the age and fate of the Universe. This was most famously done by the Supernovae Cosmology Project (SCP) and the High-z Supernovae Search, which are

credited with finding that the Universe's expansion rate was increasing. This was done by fitting supernovae out to $z \sim 0.98$ to the HD.

Type-Ia supernovae have therefore rightfully been trumpeted as a fantastic tool for cosmology. However, it becomes clear how big of a contribution GRBs can be for helping refine the HD as they have been observed well over $z = 6.6$ (Schaefer 2007, Figure 1.3). GRBs become a fantastic extension as supernovae have only been useful out to $z \sim 1.4$ (Riess et al. 2004), and even the best estimates have shown that proposed state-of-the-art instruments like the proposed SNAP satellite would only extend supernovae out to $z \sim 1.7$. Supernovae have been shown to have superb accuracy, with a 1-σ uncertainty in the derived distance modulus of $\sim$ 0.30 mag (Perlmutter et al. 1999; Riess et al. 2004; Astier et al. 2006). This is in contrast to GRBs, which have been shown to have a 1-σ uncertainty of 0.65 mag (Schaefer 2007), although this is only 2.1X worse. Here, distance modulus refers to the difference between the apparent magnitude and the absolute magnitude of an object as given by equation 1.2; where m is the apparent magnitude, M is the absolute magnitude, d_L is the luminosity distance, and μ is the distance modulus.

$$\mu = m - M = 5 \log_{10} d_L - 5 \tag{1.2}$$

GRBs are not used with an optical magnitude, yet nevertheless, μ is a convenient way to represent the distance to the burster. In the next section, an analogous equation will be presented for the GRB peak flux and its luminosity.

There are a variety of cosmological models (that is, models that map the history and fate of the Universe's expansion) that predict differences especially in the early Universe. The differences can largely be attributed to the choice of cosmological parameters: the amount of dark matter, dark energy and 'real matter' that can be (reasonably) attributed, along with other choices for the evolution of certain gravitational models etc. and how these parameters

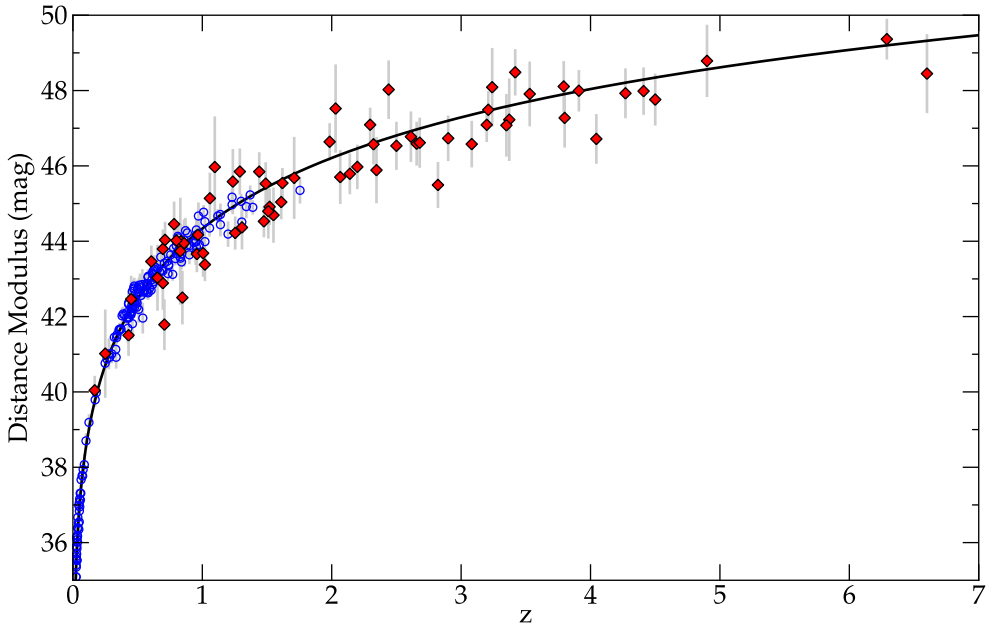

Figure 1.3 The Hubble Diagram using both supernovae and GRBs. The red diamonds are the 69 GRBs from Schaefer (2007). The blue empty circles with $z < 1.4$ are from the 'Union sample' of Type Ia supernovae (Kowalski et al. 2008). In this plot, the strength of both supernovae and GRBs becomes apparent. Supernovae have 2.1X times the accuracy, but are limited to $z < 1.4$ (possibly out to 1.7 with the proposed SNAP mission), whereas GRBs are able to reach out beyond $z = 6$. The shape of the GRB Hubble Diagram is well-defined out to $z \sim 6.5$. The redshift range $z > 1.7$ can only be measured with GRBs, and this range covers unique physics where the equation of state may be changing (thus varying the cosmological parameters). The promise of GRB cosmology is to cover this range that only they can reach. This project is designed to improve the accuracy of GRBs so that there can be greater accuracy in the HD out to high redshifts. To take close historical analogies, no astrophysicist would stop testing or improving the Cepheid period-luminosity relation after Leavitts original work, and the community vigorously pushed, tested and improved the luminosity-decline relation for supernova (type Ia) after the original papers of Phillips (1993) and Hamuy et al. (1996). Similarly, the GRB luminosity relations need a lot of testing and improvement, and that is the work here.

change over the course of the Universe. These cosmological models generally have relatively small differences in their predictions for the HD out to $z < 1.4$, having moderate variations on the order of 0.25 mag in the predicted distance moduli. However, in the very high-z Universe, these differences become very large (Figure 1.4). As an example, at a redshift of $z \sim 5$ the differences in predicted distance moduli are as large as 2 magnitudes. Therefore, a GRB found at these high redshifts are worth ten supernovae found at their extreme redshift, $z = 1.4$.

One can then see that while supernovae are the best choice in determining the best parameters for the *current* state of the Universe (that is, the current equation of state - the ratio of pressure to energy density), they do not cover the range of redshifts to determine these parameters in the early, high-z Universe. GRBs are the only tool for these redshifts, with a range that spans out to $z \sim 8$, they can help cosmological model workers determine more accurately how the Universe's equation of state has changed over time. To do this, one first must have a more accurate means of determining reliable distances to GRBs. GRBs have great potential, especially with data already coming in for free via the multitude of gamma-ray satellites, but first the means of obtaining distances of GRBs must be improved before they can be used to their potential.

1.3 Gamma-Ray Bursts as Standard Candles

In astrophysics, the term 'standard candle' is used quite often, and with good reason. Standard candles are one of the most important tools in modern astrophysics. The concept is that if an object in the sky is identified as a *known* standard candle, one then knows its luminosity. Depending on the type of standard candle this is obtained in a variety of ways, but always is dependent on using observed quantities to derive the luminosity. For example,

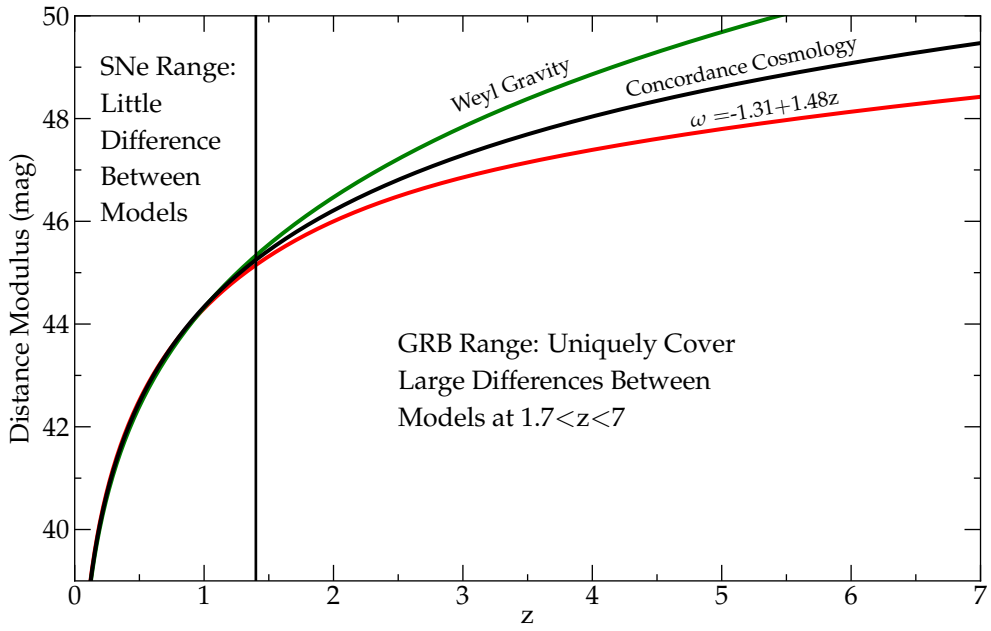

Figure 1.4 Model differences in cosmologies. The middle curve is for the 'concordance cosmology'; The lower curve is for the best fit to the supernova Hubble Diagram with a variable equation of state for the Dark Energy (Riess et al. 2004); and the upper curve is for Weyl gravity (Mannheim 2006; Kazanas & Mannheim 1991), while the Fractal Bubble model (Leith et al. 2008; Wiltshire 2007) is essentially on top of the concordance curve. The first two of these models are considered 'standard cosmologies' while the later two are considered 'non-standard cosmologies'. Nonetheless, one can see that even for a standard cosmology, there are large differences at high redshift. Therefore, while supernovae are indeed 2.1X more accurate than GRBs for the HD, GRBs are the only tool available to determine which models are correct by looking at the high-z Universe.

Cepheid variables are a type of standard candle in which their luminosity can be derived via the period of the oscillation of their observed brightness. Once the luminosity of standard candle is derived, this needs only be compared to the apparent brightness of the object via the inverse square law (equation 1.3).

$$\Phi = \frac{\mathrm{L}}{4\pi\, \mathrm{d}_\mathrm{L}^2} \tag{1.3}$$

In this manner, the distance to distant galaxies are easily obtainable. Much of astrophysics depends on knowing the distance to an object, as it determines the energy output, redshifts and even the structure of space itself. All these things are required components in determining the physics of a system, and so distances become a valuable commodity.

Technically speaking, the term 'standard candle' has two definitions. The first is any set of objects that would all have the same luminosity. An example of this is a street lightbulb. All street light bulbs have the same energy output (luminosity), so it would be intuitive and common to tell how far away a street lamp is by just seeing how bright the bulb appears and using the inverse square law to derive its distance. This ideal situation is of course impossible in astrophysics, so an alternative definition is the one that is typically used in the astrophysical sense. That is, a *class* of objects from whom observables can be used to determine its luminosity. A more appropriate term might have been 'standardizable candles'.

At first glance, it seems that GRB light curves are too chaotic. That is, on first glance, it would seem extremely unlikely that GRBs would be able to be turned into a standard candle. However, a number of relations have been found since 1999 which use some measurable quantity from a GRB as a 'luminosity indicator'. These indicators are typically well correlated with the burst peak luminosity or fluence in an equation known as a 'luminosity relation'.

1.4 The Gamma-Ray Burst Luminosity Relations

The promise of GRBs as standard candles began in late 1999, when two groups made the extraordinary discovery that GRB light curves can be used to derive the intrinsic peak luminosity of their burst (Norris et al. 2000; Fenimore & Ramirez-Ruiz 2000). In simplest terms, the groups found specific quantities can be measured from the GRB that are strongly correlated with the peak luminosity in a 'luminosity relation'. These groups' discovery was a tremendous breakthrough, as GRBs became then a legitimate possibility as a new standard candle. The results showed that given a tight enough correlation, the distance to a GRB could be obtained via the gamma-ray energy alone. This would make it possible to get the distances to almost any GRB without the need of obtaining redshifts from a host galaxy; something that only had a 31% success rate even with the arc-second resolution of *Swift* .

Since the first discovery in 1999, a total of seven luminosity relations have been discovered and seriously analyzed. The most famous relation, termed 'the Amati relation' (Amati et al. 2002; Amati et al. 2006), connects the total burst gamma-ray energy for assumed isotropic emission ($E_{\gamma,iso}$) as a power law to the observed spectral peak energy (E_{peak} , corrected for redshifting to the frame of the burst). Where E_{peak} describes the peak of the E×F(E) curve (proportional to νF_ν), which is the photon energy of the peak spectral flux.

The most accurate of these is the so-called 'Ghirlanda relation' (Ghirlanda et al. 2004). The Ghirlanda relation connects the total burst energy, corrected for the anisotropic emission of the relativistic jet (E_γ), as a power law to E_{peak} . Luminosity has been used in many luminosity relations, for example, it has been connected to the spectral lag (τ_{lag}) in Norris et al. (2000), where τ_{lag} describes the time between the peak of the light curve in the 25-50 keV and the 100-320 keV channels. Luminosity has also been linked to the variability (V) in Fenimore & Ramirez-Ruiz (2000) and Li & Paczynski (2006); where the variability is some

Table 1.1. The Seven GRB Luminosity Relations

Relation	Equation	Source
$\tau_{\rm lag}-{\rm L}$	$\log({\rm L_{iso}}) = 51.25 - 1.01\log\left(\frac{\tau_{\rm lag}}{1+z}\right)$	Norris et al. (2000)
V−L	$\log({\rm L_{iso}}) = 55.50 + 1.77\log(V(1+z))$	Fenimore & Ramirez-Ruiz (2000)
$\rm E_{peak}-L_{iso}$	$\log({\rm L_{iso}}) = 48.05 + 1.68\log({\rm E_{peak}}(1+z))$	Schaefer (2003b)
$\rm E_{peak}-E_{\gamma,iso}$	$\log({\rm E_{\gamma,iso}}) = 47.93 + 2.04\log({\rm E_{peak}}(1+z))$	Amati et al. (2002;2006)
$\rm E_{peak}-E_{\gamma}$	$\log({\rm E_{\gamma}}) = 47.13 + 1.43\log({\rm E_{peak}}(1+z))$	Ghirlanda et al. (2004)
$\tau_{\rm rise}-{\rm L}$	$\log({\rm L_{iso}}) = 51.33 + 1.21\log\left(\frac{\tau_{\rm rise}}{1+z}\right)$	Schaefer (2002)
$\rm N_{peak}-L$	$\log({\rm L_{iso}}) > 50.32 + 2\log({\rm N_{peak}})$	Schaefer (2002)

measure of how 'spiky' the light curve is. The spectral peak energy ($\rm E_{peak}$) has also been connected to the luminosity in Schaefer (2003b) and Yonetoku et al. (2004). The minimum rise time, $\tau_{\rm rise}$, has also been connected to luminosity in Schaefer (2002), where this is the shortest time over which the light curve rises by half the peak flux of the pulse. Finally, luminosity has also been connected to the number of peaks in the light curve, $\rm N_{peak}$, in Schaefer (2002). The specific equations can be found in Table 1.1.

These seven relations have been confirmed by several workers who demonstrate the same relation in independent samples (e.g. Schaefer et al. 2001; Reichart et al. 2001; Amati 2003; Bloom et al. 2003; Amati 2006; Li & Paczynski 2006; Nava et al. 2006; Butler et al. 2010; and most extensively in Schaefer 2007 for 69 GRBs and all seven relations). A number of other relations have been proposed, but they have yet to be extensively tested and thus have not been included above. Lloyd-Ronning & Ramirez-Ruiz (2002) confirmed the existences of both the V−L and the $\rm E_{peak}-L_{iso}$ relations by showing that the predicted $V-\rm E_{peak}$ relation existed using 159 BATSE bursts with unknown redshifts and 8 BATSE bursts with known redshifts. Importantly, the seven relations all have reasonable models

to explain the physics behind them (Kobayashi et al. 2002; Mészáros et al. 2002; Schaefer 2002; Schaefer 2003a; Schaefer 2003b; Eichler & Levinson 2004; Liang et al. 2004; Schaefer 2004; Levinson & Eichler 2005; Rees & Mészáros 2005; Giannos & Spruit 2007; Thompson et al. 2007). In fact, one of the greater victories in the GRB luminosity relations is that *four* of them were originally predicted by theory! (Lloyd-Ronning & Ramirez-Ruiz 2002; Schaefer 2002; Schaefer 2003b) With many different confirmations coupled with understanding of the underlying theory, there is strong confidence in the existence and reliability of these GRB luminosity relations.

The quality of GRB luminosity relations varies considerably, with the $E_{peak}-E_{\gamma}$ relation being the best of the confirmed luminosity relations, and the V−L relation being the worst (as illustrated in Figure 1.5). The work that is proposed is to not only improve the existing luminosity relations, but test other proposed ones. In fact, new, quality, luminosity relations will be of tremendous help and in of themselves even if they are not of superior quality. This is suggested by the work of Schaefer (2007), which showed that by combining the existing luminosity relations as a weighted average, the quality of any single luminosity relation gives for distance is improved by a factor of two.

1.5 Problems With the Luminosity Relations

The luminosity relations are not without criticism, and indeed have a variety of their own problems. This is similar to both Cepheid and Type Ia supernova luminosity relations had heavy criticisms and problems in their early days. The Amati relation, which is the most heavily criticized relation, has had issues because it returns ambiguous redshifts (with a high-z and low-z possibility) when the redshift is unknown (Li 2007; Schaefer & Collazzi 2007). This trouble is irrelevant when the redshift is known (i.e. obtained spectroscopically

from the redshift of the host galaxy), which does not affect current HD work which only uses bursts with known redshifts. There is a complication that has arisen where some fraction of bursts appear to violate the Amati relation (more in Chapters 2, 3 and 6), and that fraction itself is debated (Nakar & Piran 2005; Band & Preece 2005; Schaefer & Collazzi 2007; Goldstein et al. 2010). An issue that has been raised with the Ghirlanda relation is only applicable to a fraction of GRBs. To use the Ghirlanda relation, there needs to be a long photometric time series on the optical afterglow (if present) for a jet break to be observed. An additional confusion arises when X-ray breaks are confused with a jet break (for which the Ghirlanda relation does not work). In addition, there is considerable scatter in the 'variability' and 'rise time' relations, so much that little information is provided for the luminosity of the burst (Schaefer 2007). The relation involving N_{peak} returns only a lower limit on luminosity, and therefore not truly useful for most purposes (Schaefer 2007). Finally, a previously accepted luminosity relation (Firmani et al. 2006, not listed in table 1.1) has been shown to be no significant improvement on either of the two other relations using E_{peak} , from which it was derived (Collazzi & Schaefer 2008).

One problem that has been more one of publicity is a so-called 'circularity problem' in the HD. This problem is that if the luminosities for bursts are derived assuming a certain cosmology, the derived HD cannot be used to test any *other* cosmology than the one the burst luminosities were derived with. This problem has been relatively small for supernovae standard candles, because the calibration of the supernovae luminosity relations operate in a range where the differences in cosmological models are minimal. For GRBs, the circularity problem has already been shown to be ignorably small in size (Schaefer 2007). So some workers (e.g. Wright 2007) have explicitly ignored the issue. Nonetheless, there are two devices that are usually used to avoid this 'problem', both of which are explained in detail in

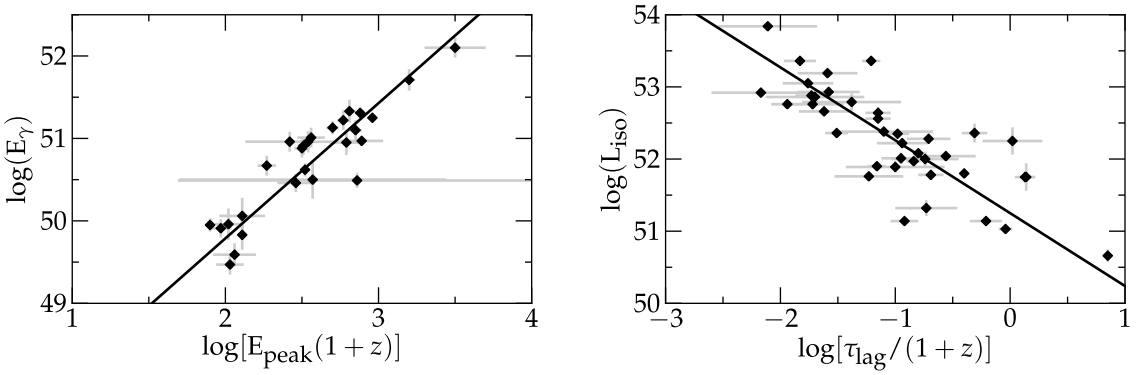

Figure 1.5 The calibration plots for two GRB luminosity relations . Here the Ghirlanda relation (left) and the lag-time relation (right) are displayed. The Ghirlanda relation has the least scatter of any of the GRB luminosity relations , but still is worse than is desirable. The lag time relation has substantially more scatter. These calibration plots were formed using the concordance cosmology, so cannot be used in any other assumed cosmological models.

Schaefer (2007). The first is to calculate the HD for each and every cosmology, and take the chi-squares as correct with extra degrees of freedom for the varying cosmology. The second is to calibrate the luminosity relations for the $z < 1.4$ GRBs based on the cosmology derived from supernovae, with the uncertainties over this redshift range being greatly smaller than the error bars. Therefore, this issue is a publicity one, as there are existing ways of avoiding it, but the issue does still get brought up in the literature (usually by analyst blunder).

Another widely advertised issue claims that the Amati relation is merely the result of detector threshold effects (Butler et al. 2007). This claim has scared off some luminosity relation workers from continuing (e.g. Bromm & Loeb 2007). The claim has been since widely rejected for a wide variety of strong causes, (e.g. Cabrera et al. 2007; Amati et al. 2009; Krimm et al. 2009; Nava et al. 2009; Xiao & Schaefer 2009; Ghirlanda et al. 2010) and has been recanted by the authors themselves in Butler et al. (2009). Nevertheless, this issue will be re-analyzed in Chapter 6.

The most pressing problem with luminosity relations is therefore in their accuracy (see Figure 1.5). The best relation ($E_{peak}-E_{\gamma}$) has an RMS (root-mean square) scatter about its calibration curve of 0.15 in the log of the luminosity, while the worst (V−L and $\tau_{rise}-$ L) relations have RMS scatters of 0.45 in the log of the luminosity. There are a number of reasons why one can not just use the 'best' of these relations and ignore the rest. The biggest of which being that the most accurate relation, the Ghirlanda relation, requires that a jet break is observed, which is only seen in a very few number of bursts. The other reason why one should combine the Ghirlanda relation with other luminosity relations is to alleviate any concerns about the ambiguity in the Ghirlanda relation as pointed out by Li (2007). Combining multiple, independent relations will also help reduce the errors on derived distances. So one is best served by using as many luminosity relations as possible, and getting a weighted average for the distance modulus.

Schaefer (2007) showed that when the luminosities given by all the relations are combined as a weighted average, the *average* error bar is 0.26 in the log of the luminosity. This translates into an uncertainty in the distance modulus (for the HD) of $\sigma_{\mu} = 0.65$ mag. This is a significantly larger than desired uncertainty, especially when compared to existing uncertainties derived using supernovae. The one-sigma errors in the supernovae HD are $\sigma_{\mu} = 0.36$ mag over 42 supernovae (Perlmutter et al. 1999), which improves to $\sigma_{\mu} = 0.29$ with the 'gold sample' of Riess et al. (2004), and improves even further in the Supernovae Legacy Survey (Astier et al. 2006). Thus GRBs are 2.1X worse than even the best supernovae has to offer. This is very encouraging, as it is already substantially lower than what the community expected. This factor can be lowered significantly by fine tuning the GRB luminosity relations.

1.6 This Work

The goal of this work is to improve the accuracy of the luminosity relations, as it is extremely likely that they can be improved. To draw a parallel from history, once supernovae (type Ia) were found at high redshifts, k-corrections were applied (and have been ever since, e.g. Kim et al. 1996). Another example from history would be that the period-luminosity relation was further improved by finding that color was a third dimension that when accounted for would lead to a more accurate period-luminosity-color relation. In a similar fashion, the goal is to improve GRB luminosity relations; the methods of which are explained in Chapter 2, along with some background of current work being by other GRB workers. Chapters 3-7 will detail work that the author has done to improve, test, and add to the luminosity relations. Chapter 8 shall review the impact of the work that the author has done, and comment on what further work needs to be done.

2. Evaluating and Improving the Luminosity Relations

With GRBs being so important for understanding the high-z Universe, methods to test and improve the luminosity relations must be formulated. In this chapter, the underlying concepts of these methods are reviewed. In later chapters, these methods will be fully explored with their implications.

2.1 Applying Generalized Tests for the Gamma-Ray Burst Luminosity Relations

The Amati relation only requires two easily obtainable GRB properties, S_{bolo} and E_{peak}. Recall that S_{bolo} is the total fluence of the burst over the 1-10,000 keV range, and that E_{peak} is the observed energy of the peak in the νF_ν spectrum. E_{peak} can be obtained simply by using the LINUX-based analysis tool XSPEC[1] and finding the peak in the best fit of the spectrum. S_{bolo} can then be obtained by integrating the $E \times \frac{dN}{dE}$ curve over the 1-10,000 keV range. As these values are simple to get, the Amati relation is the simplest of the luminosity relations to critique.

The most widely known of these criticisms is that of Nakar and Piran (2005). This test was based off a simple idea: use the luminosity relation and inverse square law to set up an equality between the redshift-dependent terms and the observable quantities. As an example, start with the Amati relation,

$$E_{\gamma,iso} = A\, E_{peak}^{2.04}\, (1+z)^{2.04}\,. \tag{2.1}$$

[1]Version 12.6.0q, http://heasarc.nasa.gov/xanadu/xspec/

Where, $E_{\gamma,iso}$ is the total gamma ray energy assuming for isotropic emission, and z is the cosmological redshift. A is used here as some constant. The Amati relation describes the total gamma-ray energy as directly proportional to E_{peak} in the burst's rest frame. In contrast, $E_{\gamma,iso}$ is also described by the inverse square law,

$$E_{\gamma,iso} = 4\pi\, d_L^2\, S_{bolo}\, (1+z)^{-1}\,. \tag{2.2}$$

Where d_L is the luminosity distance. The Nakar and Piran test involves putting these two equations together, then isolating the observables from the redshift-dependent terms. In the case of the Amati relation, you would end up with

$$\frac{E_{peak}^{2.04}}{S_{bolo}} = \frac{4\pi\, d_L^2\, (1+z)^{-3.04}}{A}. \tag{2.3}$$

The result is an equation where the left hand side is composed of observable quantities and the terms on the right hand side are functions of distance. As the distance rises, d_L^2 gets larger and $(1+z)^{-3.04}$ gets smaller, which yields a maximum redshift for the function. When the concordance cosmology is used, the function peaks at $z \sim 3.8$ (see Figure 2.1). Specifically, the left hand side of the equation cannot exceed $\sim 10^9$ kev$^{2.04}$erg^{-1}. This becomes a means to test the Amati relation, as the observed quantities are readily available, and can be performed on all bursts, regardless of redshift. The result of the Nakar and Piran (2005) study was that $\sim 48\%$ of their sample (751 BATSE bursts) were in violation of this limit, and therefore they concluded that the Amati relation failed the test.

This test was built upon by Li (2007), who noted that an ambiguity arises as a direct result of the turnover found in the Amati relation by the Nakar and Piran test. Specifically, a degeneracy arises as the value of the left hand side approaches the maximum value for the relation (see Figure 2.1). For example, a burst at a distance of $z \sim 2.8$ would have identical properties to that of a burst at a redshift of $z \sim 5.0$. As both these distances are

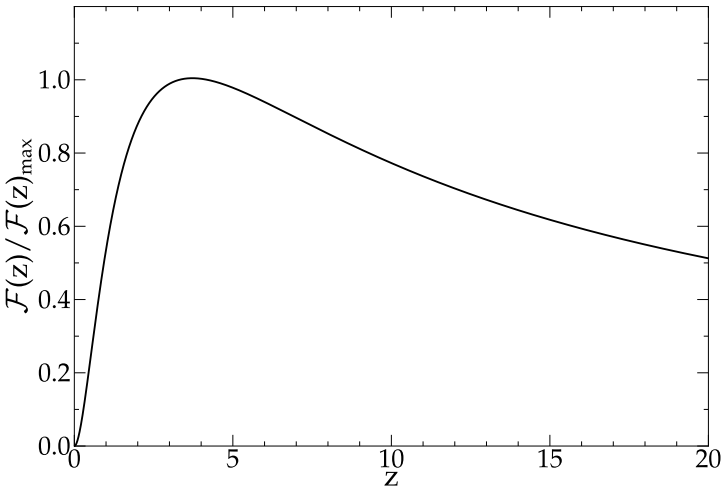

Figure 2.1 The Amati relation and the Nakar and Piran test. The ratio of the observables (normalized to the maximum value) is plotted as a function of redshift. The function has a maximum value that occurs at $z \sim 3.4$. This dictates a maximum value for $E_{peak}^{2.04}/S_{bolo}$ for bursts. Li (2007) built upon this test by noting that a degeneracy exists as a result of this turnover. For example, a burst at a redshift of $z \sim 2.8$ could be mistaken for a burst of $z \sim 5.0$ as the Amati relation would produce the same value for both of these bursts. As both these redshifts are plausible, the degeneracy must be broken through means independent of the Amati relation.

plausible for a GRB, Li (2007) argued that the Amati relation was good only for nearby GRBs, for which the degeneracy could be broken simply because the higher of the values was unreasonable.

In chapter 3, these tests are revisited on a more general scale, and are applied to eight luminosity relations. The result is that all eight of the tested luminosity relations pass the Nakar and Piran test when uncertainties of the data and dispersions of the correlations are taken into proper account. In addition, all the luminosity relations were found to be good when used for purposes when z is already known (e.g. calibrating the luminosity relations and the GRB HD). The result of Li (2007) is confirmed: the Amati relation produces very

large error bars when a redshift is sought $z \gtrsim 1.4$; moreover, it is found that the Ghirlanda relation has a similar peak, with large error bars when seeking a redshift $z \gtrsim 3.4$. None of the other six luminosity relations have this ambiguity issue; therefore, the degeneracies can be broken by simply using more than one of the luminosity relations for a given burst.

2.2 Testing Existing Luminosity Relations

Several luminosity relations have been proposed beyond the ones included in Table 1.1. Most of these relations are not widely tested outside of the groups that have proposed them, and usually do not have any physical explanation for their existence. There is good reason to explore the validity of proposed luminosity relations as any new luminosity relation might provide a tighter relation than any existing one. Another motive for exploring newly proposed luminosity relations is that the scatter in the GRB HD can be brought down by *up to* a factor of $\sqrt{N}$, where N is the number of luminosity relations used.

One such proposed relation was given in Firmani et al. (2006). The relation suggests that the addition of a duration, $T_{0.45}$, greatly reduces the scatter in the $E_{peak} - L_{iso}$ relation. Here, $T_{0.45}$ is the Reichart et al. (2001) definition of a GRB's duration. The duration takes the time interval of the brightest bins in the light curve that contain 45% of the burst's total fluence. Firmani et al. (2006) found a tight correlation with a reduced chi-square of 0.7 over 16 degrees of freedom introducing this duration into the $E_{peak} - L_{iso}$ relation. This result offers hope of improved accuracy of luminosity relations as distance measurement tools. Still, there is no physical reason to expect that the duration would provide for a tighter relation. Therefore, the relation might be tightened further through the use of a different definition of duration. No explanation was provided as to why the Reichart definition was

used, so it is reasonable to expect that a different definition of duration might provide for a better result.

Chapter 4 explores the utility and promise of the Firmani relation as a new luminosity relation. The investigation starts by reproducing the procedures of Firmani et al. (2006) exactly. This is done in order to ensure that the fitting procedure that is performed is identical to that of the original study. The Firmani relation is then tested using the same 19 bursts, except with independently measured values for L_{iso} , E_{peak} , and $T_{0.45}$. The relation gains significant scatter for the independent data set, and erodes to scatter comparable to the $E_{peak} - L_{iso}$ relation when the sample is expanded to 60 GRBs. Therefore, for a significant sample of bursts, the $L_{iso} - E_{peak}\, T_{0.45}$ relation is just as accurate as the $E_{peak} - L_{iso}$ relation. Nonetheless, this does not rule out the possibility that a different definition of duration could provide for a tighter fit to that of the $E_{peak} - L_{iso}$ relation. Thirty-two definitions of duration are tested using the expanded data set. The quality of each fit is compared via the root mean square (RMS) of the scatter of the predicted and observed values of L_{iso} in log space. The quality of the fits are also compared via the predicted systematic errors in the fits (defined as the error needed to bring the reduced chi square to 1). While some duration measurements are found to provide a better fit than others, none of them provide for a significant improvement to the $E_{peak} - L_{iso}$ relation. In addition, a simple derivation shows that the Firmani relation is a combination of the $E_{peak} - L_{iso}$ and $E_{peak} - E_{\gamma,iso}$ relations. Given that the Firmani relation is neither independent or a significant improvement of already existing luminosity relations, it should not be used for GRB cosmology.

2.3 How Accurately Are the Luminosity Indicators Being Measured?

Even with these two investigations, there is still the considerable issue that the GRB luminosity relations have a scatter which is far greater than is desired. One likely cause of this is could lie in simple failures to measure the luminosity indicators with sufficient accuracy. That is, it is possible that the luminosity relations' scatter is dominated by simple measurement noise. One needs only go through the literature to see how a burst measured by two different satellites can have very different results. So a vital question becomes whether the scatter seen in the luminosity relations is merely a result of not knowing the burst well enough. This would confirm that the underlying physics of the luminosity relations is well understood, and the problem of scatter in the luminosity relations lies in the data gathering.

When a burst occurs, there are a variety of points in which uncertainty would be added. For a specific example, one can look to E_{peak}, arguably the most important GRB parameter. The most familiar source of uncertainty would be the calculated contribution from ordinary Poisson errors, $\sigma_{\rm Poisson}$. This is the error as reported in all the literature when values of E_{peak} is given. A second source of uncertainty comes from not knowing the detector response perfectly (an impossible task), which will be referred to as $\sigma_{\rm Det}$. Yet another issue that arises in determining E_{peak} is the various choices that are made in deriving the value. These choices include the exact time and form of the background, the exact time interval over which to accumulate the spectrum, whether to use Bayesian or frequentist statistics, and even their convergence criteria for the fit. Reasonable analysts will make different choices, and there is no 'best' set of choices known. The same set of data therefore can be looked at by two entirely different set of analysts, and would result in two entirely different values. Therefore, this difference between the two is a sort of uncertainty, $\sigma_{\rm Choice}$. The final source

of uncertainty is related to the model used to measure E_{peak} , σ_{Model}. An example of the problem here is illustrated where the same data (i.e. from the same satellite) is measured by the same group, and yet the Band model will yield a different result in a different value than when a cut-off power law is used to fit the data. Another example of this uncertainty is that the value of E_{peak} will be different when integrating over the whole burst, as opposed to just the time of peak flux.

The luminosity relations are all expressed as power laws, with this being appropriate for the physical interpretations of the relations. Also, the various errors described above are multiplicative. Therefore, it is best to consider the logarithm of the luminosity indicators, for example, $\mathrm{Log}(E_{peak})$ or $\mathrm{Log}(\tau_{lag})$. The *total* measurement uncertainty will be labeled as σ_{Total}. As such, as the individual errors are multiplicative, the total errors will be given as

$$\sigma^2_{Total} = \sigma^2_{Poisson} + \sigma^2_{Det} + \sigma^2_{Choice} + \sigma^2_{Model}. \tag{2.4}$$

The task is then to derive σ_{Total} by determining the remaining three sources of individual errors (as $\sigma_{Poisson}$ is already reported in the literature).

In chapter 5, the size of these individual error bars for E_{peak} is explored exhaustively. This investigation goes beyond the basic Poisson statistics to quantify the individual and total uncertainties are in measuring E_{peak} . The one-sigma uncertainty associated with the choices made by analysts is 28%, which equates to $\log_{10}(E_{peak}) = 0.12$. Variations associated with the detector response matrix are found to be negligibly small. The uncertainties caused by commonly-used alternative definitions of E_{peak} is typically 23%-46% (although this varies with application). The final implications of the study are: (1) Even the very best measured E_{peak} values will have systematic uncertainties of 28%. (2) Thus, GRBs have a limitation in accuracy for a single event, with this being reducible by averaging many bursts. (3) The typical one-sigma total uncertainty for collections of bursts is 55%. (4) It is also found that

the width of the distribution for E_{peak} in the burst frame must be near zero, implying that some mechanism must exist to thermostat GRBs. (5) The community can only improve on this situation by using collections of bursts which all have identical definitions for the E_{peak} calculation.

2.4 Extending the Nakar and Piran Tests

Earlier work in applying generalized tests to the GRB luminosity relations have already been performed (see Chapter 3). However, more recent studies, particularly in regards to the Amati relation, have urged a revisit to this of the issue.

In their own work, Nakar & Piran analyzed 751 BATSE bursts, finding 48% of the bursts to violate this limit, concluding that the Amati relation fails the test. Schaefer & Collazzi (2007) later showed that this fraction was what is expected for this relation due to simple scattering effects (see Chapter 3). In the ideal case with no measurement uncertainties, there are no violators, but as soon as noise is introduced, some of the points (especially those near the redshift limit) would be over the limit. Of course, there would be an equal number of bursts that would go up (and thus above the limit) to those who go down (and below the limit). So the real finding is that the differences between the limit and the equation are very small given the known scatter (Schaefer & Collazzi 2007). Thus, the original test by Nakar and Piran actually *confirms* the Amati relation.

Schaefer & Collazzi (2007) extended this test to 69 bursts with known redshifts from many satellites. The result was that the Amati relation passed the Nakar and Piran test (within error bars). The paper goes on to show that this test could be generalized for use to test *all* luminosity relations. In most cases, this resulted in no maximum, or at the very least no maximum within a reasonable redshift range ($z < 20$). A second luminosity relation

was found to have a limit - the Ghirlanda relation, with a limit of $z = 7.4$. In addition, all luminosity relations were shown to have either no bursts failing the test (like the lag-luminosity relation), or a number of failures that is acceptable given measurement errors). The end conclusion is that all known luminosity relations passed the Nakar and Piran test.

A complication arises in Band & Preece (2005), which examined (largely) the same BATSE bursts without known redshifts, finding an 80% failure rate for the Amati relation. This result was later confirmed by Goldstein et al. (2010). So it seems that there is a direct conflict between these four independent tests. Making matters worse, it appears that the 7 bursts from BATSE with spectroscopic redshifts agree with the Amati relation, indicating a possible population problem.

With this critical possibility, it is of great importance to determine what is going on. The luminosity indicators must be extracted from different satellites and tested individually. In doing this, results will be independent of any systematic errors from a single detector. This analysis should also be generalized to test how bursts with redshifts and without redshifts behave. It is critical to these tests to see if GRBs with a known redshift are coming from a separate population.

Another criticism of the Amati relation is that the Amati relation is both dependent on the satellite and that it arises from selection effects (Butler et al. 2007). Butler et al. (2007) pointed out an apparent shift in the Amati relation between *Swift* and pre-*Swift* data sets. Their claim that selection effects will produce the Amati relation were never substantiated by any analysis, examples, or derivations, and the cause of the selection effects was never identified. These claims have scared off some workers from using any luminosity relations (e.g. Bromm & Loeb 2007); however, it has been widely rejected for a variety of strong causes (e.g. Cabrera et al. 2007; Amati et al. 2009; Krimm et al. 2009; Nava et al. 2009;

Xiao & Schaefer 2009; Ghirlanda et al. 2010) and most recently the authors themselves recanted their previous findings (Butler et al. 2010). Nevertheless, the cause and effects for the basic claims of satellite-to-satellite differences are being reconsidered.

In chapter 6, the Nakar and Piran test is revisited explicitly in regards to the Amati relation. In order to satisfactorily address these many issues, data sets from various different GRB detectors are performed independently. That is, the Nakar and Piran test is performed on data sets from each of the BATSE, *Swift* , *Konus* , *Suzaku* , *HETE*-2 and *Beppo-Sax* GRB detectors individually. The first major finding is that all data sets, with the exception of the *HETE*-2 data, have an intolerably high violator rate, and therefore have failed the Nakar and Piran test. The larger result, however, is the discovery that every detector has a different distribution of bursts when placed on a plot of S_{bolo} vs E_{peak} (a graphical representation of the Nakar and Piran test). This requires that selection effects are dominating these distributions. A combination of detector and burst population effects are found to be the cause of this phenomena. For a sufficient set of these selection effects, only bursts which obey the Amati relation are visible. The conclusion is therefore, that the Amati relation is merely the result of selection effects within the burst population and the detector. In a sense, Butler et al (2007) was correct - there is a systematic selection effect in the Amati relation, but for not for the reasons originally thought. As such, the Amati relation, like the Firmani relation, should not be used for cosmological purposes. The failure of the Amati relation is in no way prejudicial against the other luminosity relations.

2.5 Using Individual Pulse Properties

Strong cases haves been made that some of the luminosity relations are really based on the individual pulse properties (Hakkila et al. 2008; Ghirlanda et al. 2010). This would not

apply to either the Amati or Ghirlanda relation as they involve the fluence and are based on the overall burst energetics. The groups have applied the burst properties of several BATSE bursts (Hakkila 2008; Hakkila & Nemiroff 2009; Hakkila & Preece 2011), some *HETE*-2 bursts (e.g. Arimoto et al. 2010), and *Fermi* bursts (e.g. Ghirlanda et al. 2010). Within individual bursts, the groups have demonstrated that the shorter the lags and durations, the lower the peak flux of an individual pulse. In addition, the pulses from the BATSE bursts have shown a fairly tight relation using the lag times and durations of the pulses. This makes good physical sense because the explanations for the relations using luminosity (lag time, minimum rise time, and E_{peak}) all relate to the conditions at the peak of individual pulses (as shown in Schaefer 2003b; Schaefer 2004). That is, a different pulse will show different peak luminosities and thus have different indicators. Therefore, it seems that the relevant unit is actually the pulses of a burst, and not the whole burst itself.

The formalism in finding and fitting the individual pulses in a burst has been laid out in Hakkila et al. (2008). This procedure involves a formula with two shape parameters, τ_1 and τ_2, which are similar to the rise and decay time of the pulse. Norris et al. (1996) and Hakkila & Nemiroff (2009) have applied this fitting routine and have found that it has been very successful in matching observed pulse shapes. Hakkila et al. (2008) provides a routine that fits light curves, starting with a Bayesian Blocks method (Scargle 1998) and uses chi-square tests to ensure the pulses extracted are of sufficient significance. Even with this routine, resolving individual pulses is not an easy task, often times pulses are confused together (Hakkila 2011).

The developed formalism provides several advantages for pulling out the critical values. The primary advantage is that the peak flux obtained directly from a binned light curve becomes more accurate with a fitted functional form. Secondly, the lag times that would be

extracted via individual pulses are more 'pure' than a lag time derived from the whole burst (which is convoluting a number of pulses). Consequently, the definition of rise time should be reconsidered, possibly to be replaced with the τ_1 parameter, which is much less affected by Poisson noise (as the whole burst would be). Finally, a redundancy can be developed in getting multiple measures of key parameters from a burst. In using these multiple values from a single burst, the average distance from these parameters can be used to improve the accuracy of the relation.

The groups testing this fitting procedure have yet to apply it to *Swift* bursts. In addition, the groups have *not* done any work in regards to luminosity relations, they have been mostly concerned with enhancing and advertising their pulse measurement models. As *Swift* has the largest number of GRBs with measured redshifts, this opens the door to model luminosity relations (particularly the $\tau_{\rm rise}-$ L and $\tau_{\rm lag}-$ L relations) based on pulses instead of the whole burst. In addition, improved peak fluxes can also be obtained (which can also improve measurements of luminosities).

While the luminosity indicators are always measured in the Earth's rest frame, the physics of the luminosity relations work in the burst rest frame. Therefore, one needs to properly account for any relativistic effects that have changed the data; that is, the observed data needs to be shifted back into the burst rest frame. Energy values (like $\rm E_{peak}$) will be redshifted as they travel across space by a factor of $(1+z)^{-1}$, and the two timescale related indicators ($\tau_{\rm lag}$ and $\tau_{\rm RT}$) will be time dilated by a factor of $(1+z)$. The one luminosity indicator that is not entirely straightforward is that of the variability. However, the variability seems to act similarly to an inverse timescale, so one can assume that it undergoes a shift of factor $(1+z)^{-1}$. These factors need to be simply reversed in order to shift the observed quantities to what they would be in the burst frame.

A more insidious complication arises in how the luminosity indicators change with their rest frame energy band. The problem is essentially that detectors for GRBs are in a specific band; e.g., BATSE measures the 50-300 keV range. This energy range that the satellite is sensitive to is closely constant for a given detector and in the Earth's frame of reference. This energy band corresponds to a very different energy band for the burst's frame, depending on the distance from us. In addition, the luminosity indicators vary widely depending on the rest energy frame. Specifically, $\tau_{\rm lag}$ and $\tau_{\rm rise}$ increase while $\rm N_{peak}$ and V decrease if the energy band is lowered. A similar issue is that data obtained here on Earth is binned by a constant time interval (on the order of fractions of a second), and of course this binning is different due to time dilation for any given pair of bursts. Therefore, certain features could become hidden in the data (or even exacerbated) depending on the light curve.

To be clear, consider two bursts that are identical: one at $z = 4$ (Burst A), the other 'nearby' (Burst B). If Burst B is seen to have $\rm E_{peak} =$ 500 keV, then Burst A will have $\rm E_{peak} =$ 100 keV. If Burst A is shown to have $\tau_{\rm lag} = 1$ second between the 25- 50 and 100-300 keV bands, then Burst B measured in its rest frame (and corresponding energy bands 125-250 keV and 500-1500 keV) will already have a shorter lag time due to the higher energy bands, with perhaps a 0.5 second lag time. After time dilation, Burst B would be seen to have $\tau_{\rm lag} = 2.5$ seconds. In this case of lag times, one could easily make the mistake of *only* shifting for the time dilation, and would wrongly take the lag time to be 0.5 seconds (instead of it being 1 s as exemplified in Burst A). In doing this mistake, the worker would then assign a luminosity to Burst B twice that what it really is, which results in giving it a luminosity distance 1.4X too far. It is clear that a correction is required to allow for this relation to be used in a meaningful way.

Attempts have been made to fix these issues by crudely adding a correction factor of some power of $(1+z)$. Fenimore & Ramirez-Ruiz (2000) multiplies the variability by $(1+z)^{0.43}$, Firmani et al. (2006) corrected time scales by a factor of $(1+z)^{0.4}$, Norris corrected the lag time by $(1+z)^{0.33}$ (Gehrels et al. 2006). All of these attempts were done for reasonable cause, but have had limited success. A large problem with this kind of correction is that it treats all burst with a factor that is more suited for the general trend of bursts. Individual bursts vary too greatly for such a simple catch-all figure.

There is a much better way to correct these problems. The GRB light curves will be extracted with a constant energy band and time binning in the *rest frame of the burst*. This solution completely solves the problems of burst individuality. In addition, it makes for a simple means of answering the question of what the luminosity indicators are in the burst frame.

Light curves can be easily extracted with a time bin of 0.064 s and energy range of 100-400 keV in the burst rest frame. Specifically: a burst at $z = 0.5$ will have data that is binned in 0.096 s time intervals from 67-267 keV; a burst at $z = 3$, the binning will be 0.256 s and in the energy range of 25-100 keV; at $z = 6$, the time binning will be 0.448s and over the energy range 14-57 keV. This is easily done with modern satellites like *Swift* and *Fermi* for which data can be extracted for any bin size and energy band. Software is already readily available to perform these tasks with these missions. It will be considerably harder to do this for older bursts, for example those from BATSE will only provide energy bands which are close but not completely what is needed. This problem becomes even worse for the *HETE*-2 and *Konus* for which only specific energy band data are available. For these two cases, the closest energy bands will have to be combined to get a sort of best-estimate. As *Swift* has a combination of ease and quantity of bursts, it is the obvious sample to test these ideas on.

The fluence and peak flux from a burst should also be handled in a similar manner. The standard methodology at this time is to use the fitted spectrum for the burst (generally a smoothly broken power law; Band et al. 1993) to extrapolate to a very broad energy range, usually 1-10,000 keV in the burst rest frame. This transforms the brightness of a burst into a bolometric quantity, one free of issues that might arise due to the redshift of the burst. This solution is solid as, except for the most extremely distant bursts, most of the flux is not contained in the extrapolated regions. Nevertheless, a better solution might exist, such as always putting the brightnesses into some constant band like 100-1000 keV in the burst frame. To test this idea, a new set of burst brightnesses need to be calculated. From there, the scatter in the best fit of the luminosity relations can be derived and compared with the scatter using just the bolometric brightnesses.

In chapter 7, the promise of using individual pulses as luminosity indicators is explored. First, the Hakkila model is tested on a select sample of bursts with well separated pulses. This model is found to be volatile, with little to no robustness. In addition, the cross correlations between the parameters are far too great to make any accurate statements as to the best fit of the pulses. In order to reduce these issues, a simpler model is developed, a two sided gaussian. While the uncertainties are lower with this simpler model, no confident statements can be made about the burst parameters. As there is no reasonable way of confidently measuring the lag-time or rise-time in the Earth's frame, there is no hope of doing it in the burst's frame (where there are less photons), so the conclusion is that the *Swift* data can not use the luminosity relations on a pulse-by-pulse basis. The only parameter that is stable through fitting procedures is the amplitude of a pulse, for which the peak brightness could be extracted in the $E_{peak} - L_{iso}$ relation. Unfortunately, the E_{peak} values extracted from XSPEC show much of the same problems highlighted in Collazzi et al. (2011) in regards to

choices made by analysts. As such, the conclusion is that none of the luminosity relations can be used readily used on a pulse-by-pulse basis for the *Swift* data.

2.6 Conclusions and the Future

Finally, in chapter 8, there is a final discussion about the work presented in this thesis. The overall impact of the work is explored and the future of GRB luminosity relations is discussed. In particular, the possibility of new GRB luminosity relations , and possibly using existing ideas in different ways.

3. Generalized Tests for the Luminosity Relations[1]

3.1 Introduction

As of 2006, there were eight GRB luminosity relations, where a measured photometric or spectroscopic property is correlated with the burst's luminosity. Since then, the Firmani relation, $L_{iso} - E_{peak}\, T_{0.45}$, has been shown to be not good for cosmology (see Chapter 4). As was discussed in Chapter 1.4, many reasonable models have been put forth to explain the physics behind these relations, with some of them even been predicted by theory.

Nakar & Piran (2005) proposed a new test of one of these luminosity relations - the Amati relation, $E_{peak} - E_{\gamma,iso}$, (Amati et al. 2002; 2006). The relation connects the GRB isotropic γ-ray energy, $E_{\gamma,iso}$, and the observed photon energy of the peak in the νF_ν spectrum, E_{peak} . Their idea was to set up an equality between the energies based on the observed fluence as well as from the luminosity relation, move all the redshift dependent terms to one side and the observables to the other side of the equation. From here, a maximum can be found on the redshift side and compared with the quantity calculated from the observables for many GRBs. The Nakar & Piran test is then to see whether the derived quantities from the observables exceeds this maximum possible value (to within the error bars). When applied to a sample of BATSE bursts, they found that $\sim 48\%$ violated this simple requirement. Subsequently, Band & Preece (2005) found that 88% of their sample of BATSE bursts violated the Nakar & Piran test. This would be a serious blow against the validity of one of the luminosity

[1]This chapter is largely taken from an article that appeared in The Astrophysical Journal Letters, and is reproduced with permission of the AAS (see Appendix A for details).

relations. Amati (2006) has strongly defended this particular luminosity relation, mainly on the grounds that the luminosity relation is highly significant, broadly applicable, and fits a well-defined calibration. Ghirlanda et al. (2005) have explained the discrepancy as simply that Nakar & Piran used an old version of the Amati relation (based on just nine bursts) and did not allow for the real uncertainties.

Li (2007) has applied a similar analysis to the $E_{peak} - E_{\gamma,iso}$ Amati relation to demonstrate that the returned redshift for any burst is actually ambiguous with two possible values. Li finds the maximum to occur at a redshift of 3.8, such that, for example, a $z \sim 2.8$ burst has identical properties to a $z \sim 5$ burst. In addition, around the redshift of the maximum, the derived error bar should be very large. For realistic error bars, Li finds that the Amati relation will return redshifts with very large uncertainties for bursts with $z \gtrsim 1.4$.

With this, there is what can be perceived as a significant challenge to the reliability, uniqueness, and utility of one of the eight luminosity relations. The obvious task is to generalize this test to all eight of the luminosity relations. Indeed, Band & Preece have already applied the Nakar & Piran test to the $E_{peak} - E_{\gamma}$ relation of Ghirlanda et al. (2004), and found only a small fraction of violators (1.6%). In this chapter, generalized forms of the Nakar & Piran and Li tests are applied to all eight GRB luminosity relations. The importance of these tests is that they bear on the validity and accuracy of all the relations, and the utility of these relations is a prerequisite for getting cosmology from GRBs.

3.2 The Generalized Test

The first step to take is to generalize the Nakar and Piran (2005) test in a way that all eight of the luminosity relations can be tested.

The luminosity relations connect a measure of the burst's luminosity (notated as $\mathcal{L}$) with a luminosity indicator (notated as $\mathcal{I}$). The luminosity, $\mathcal{L}$, can be the isotropic luminosity, L_{iso} , the isotropic energy emitted in gamma rays, $E_{\gamma,iso}$, or the $E_{\gamma,iso}$ value corrected by the beaming factor ($F_{beaming}$) from the jet, E_{γ}. The luminosity indicator, $\mathcal{I}$, can be the spectral lag τ_{lag} (Norris et al. 2000), the variability V (Fenimore & Ramires-Ruiz 2000), the E_{peak} from the spectrum, the minimum rise time in the light curve τ_{RT}, or the number of peaks in the light curve N_{peak}. In addition, Firmani et al. (2006) take a particular combination involving E_{peak} and $T_{0.45}$ (the duration over which the brightest portion of the light curve emits 45% of the fluence) to be a luminosity indicator, as given by $E_{peak}^{1.62} T_{0.45}^{-0.49}$. All of these indicators have to be corrected from their observed values to the values in the GRB rest frame by multiplication by $(1+z)$ raised to a power Q. The relations are all simple power laws with indices m and constants $\mathcal{A}$. The luminosity relations can be expressed as

$$\mathcal{L} = \mathcal{A}[\mathcal{I}(1+z)^{Q}]^{m}. \tag{3.1}$$

The eight relations have their particular values for $\mathcal{L}$, $\mathcal{A}$, $\mathcal{I}$, Q, and m given in Table 3.1.

The $\mathcal{L}$ for each burst of known redshift can be determined from the observed brightness, $\mathcal{B}$. The $\mathcal{B}$ value will either be the bolometric peak flux, P_{bolo}, the bolometric fluence, S_{bolo} , or the beaming corrected fluence, $S_{bolo}F_{beaming}$, depending on the value for $\mathcal{L}$. The inverse square law of light can then be expressed as

$$\mathcal{L} = 4\pi \, d_L^2 \mathcal{B}(1+z)^{-B}. \tag{3.2}$$

The luminosity distance, d_L , is related to the redshift, z , through the usual integral,

$$d_L = c \, H_0^{-1} \int_0^z dz' \left[(1+z)^3 \, \Omega_M + \Omega_\Lambda\right]^{-1/2}. \tag{3.3}$$

Throughout this chapter, a flat universe with $\Omega_M = 0.27$ and an unchanging dark energy equation of state of $w = -1$ is assumed. When dealing with fluences and burst energies, a

factor of $(1+z)^{-1}$ is need to correct for time dilation. The corresponding values for $\mathcal{B}$ and B are presented in Table 3.1 for each luminosity relation.

From here, equation 3.1 and 3.2 are used to eliminate $\mathcal{L}$. With this, all the redshift-dependent terms onto the left side of the equation and all the observable quantities on the right side of the equation. Finally, both sides are multiplied by $(H_0/c)^2$ so as to make both sides dimensionless and of reasonable magnitude. Thus,

$$(\mathrm{H}_0/c)^2\,\mathrm{d}_\mathrm{L}^2(1+z)^{-Qm-B} = [(\mathrm{H}_0/c)^2/4\pi](\mathcal{A}\,\mathcal{I}^m/\mathcal{B}). \tag{3.4}$$

This chapter makes frequent reference to both the left and right sides of this equation separately, so the two sides will be notated here separately. This will be

$$\mathcal{F}(\mathcal{I},\mathcal{B}) = [(H_0/c)^2/4\pi](\mathcal{A}\,\mathcal{I}^m/\mathcal{B}), \tag{3.5}$$

$$\mathcal{F}(z) = (H_0/c)^2 d_L^2(1+z)^{-Qm-B}. \tag{3.6}$$

With this, it is expected that $\mathcal{F}(\mathcal{I},\mathcal{B}) = \mathcal{F}(z)$.

It is convenient to define a maximum value for $\mathcal{F}(z)$, which will be identified as $\mathcal{F}_{\max}$. For two of the relations, the $\mathcal{F}(z)$ comes to a simple maximum at some moderate redshift value, z_{peak} (see Table 3.1). For the other relations, the $\mathcal{F}(z)$ keeps rising as the redshift increases out past where any GRB might lie. In the spirit of this test, $\mathcal{F}(z)$ values for all observed bursts must be less that the value at the maximum GRB redshift. From Bromm & Loeb (2002), it is known that GRBs cannot be made at $z > 20$ or so. Thus, for the six relations with no z_{peak}, $\mathcal{F}_{\max}$ is taken to be the value of $\mathcal{F}(z = 20)$. The values of $\mathcal{F}_{\max}$ are given in Table 3.1. So in the most general terms, the Nakar & Piran test is whether $\mathcal{F}(\mathcal{I},\mathcal{B})/\mathcal{F}_{\max} > 1$ for observed GRBs, while the Li test is whether $z_{\mathrm{peak}} \lesssim 10$.

Table 3.1. Generalized Tests of the Luminosity Relations

Relation	$\mathcal{I}$	m	Q	$\mathcal{A}$	$\mathcal{B}$	B	$\mathcal{F}(z)_{max}$	$z_{\rm peak}$	$\sigma_{\log \mathcal{L}}$	Violators[a]
τ_{lag}-$L_{\rm iso}$	τ_{lag}	-1.01	-1	1.8×10^{51}	P_{bolo}	0	139	$\gg 20$	0.39	0%
V-$L_{\rm iso}$	V	1.77	1	3.2×10^{55}	P_{bolo}	0	13.7	$\gg 20$	0.40	4%[b]
E_{peak}-$L_{\rm iso}$	E_{peak}	1.68	1	1.1×10^{48}	P_{bolo}	0	18.0	$\gg 20$	0.36	3%[c]
E_{peak}-$E_{\gamma,iso}$	E_{peak}	2.04	1	8.5×10^{47}	S_{bolo}	1	0.56	3.8	0.15	44%[d]
E_{peak}-E_{γ}	E_{peak}	1.61	1	4.5×10^{46}	$S_{bolo}F_{beaming}$	1	1.23	7.4	0.16	19%[e]
τ_{RT}-$L_{\rm iso}$	τ_{RT}	-1.21	-1	2.1×10^{51}	P_{bolo}	0	75.4	$\gg 20$	0.47	0%
N_{peak}-$L_{\rm iso}$	N_{peak}	2	0	2.1×10^{50}	P_{bolo}	0	3002	$\gg 20$	0	0%
$E_{peak}T_{0.45}$-$L_{\rm iso}$	$E_{peak}^{1.62}T_{0.45}^{-0.49}$	1	1.91	3.2×10^{48}	P_{bolo}	0	8.95	$\gg 20$	0.16	4%[f]

[a] $\log[\mathcal{F}(\mathcal{I},\mathcal{B})/\mathcal{F}_{max}]$ values for the violators are given with footnotes.

[b] 0.46 ± 1.01 for GRB 050502 and 0.19 ± 1.17 for GRB 060526.

[c] 0.48 ± 0.93 for GRB 050904 and 0.10 ± 1.11 for GRB 060605.

[d] 1.22 ± 0.45 for GRB 970508, 0.49 ± 0.42 for GRB 971214, 0.57 ± 1.04 for GRB 980613, 0.29 ± 0.41 for GRB 980703, 0.02 ± 0.42 for GRB 990123, 0.13 ± 0.37 for GRB 000210, 0.62 ± 0.41 for GRB 000911, 0.04 ± 0.62 for GRB 020405, 0.16 ± 0.76 for GRB 021004, 0.24 ± 0.70 for GRB 030115, 0.46 ± 1.19 for GRB 050406, 0.37 ± 0.89 for GRB 050502, 0.55 ± 0.47 for GRB 050603, 1.16 ± 0.51 for GRB 050820, 0.92 ± 0.57 for GRB 050904, 0.06 ± 0.53 for GRB 050908, 0.80 ± 0.49 for GRB 050922, 0.51 ± 0.64 for GRB 051109, 0.61 ± 0.67 for GRB 060108, 0.43 ± 0.81 for GRB 060116, 0.16 ± 0.57 for GRB 060124, 0.40 ± 0.55 for GRB 060206, 0.43 ± 0.96 for GRB 060223, 0.25 ± 0.43 for GRB 060418, 0.52 ± 0.77 for GRB 060502, 0.61 ± 0.54 for GRB 060604, 1.27 ± 0.69 for GRB 060605, and 0.27 ± 0.57 for GRB 060607.

[e] 0.07 ± 0.62 for GRB 050318, 0.26 ± 0.88 for GRB 050505, 0.18 ± 0.58 for GRB 050904, 0.20 ± 0.55 for GRB 060124, and 0.70 ± 0.74 for GRB 060210.

[f] 0.19 ± 0.55 for GRB 050904 and 0.30 ± 0.82 for GRB 060605.

For this generalized Nakar & Piran test, a set of 69 GRBs with spectroscopic redshifts is used for which all the required data have already been extracted and reduced for purposes of making a GRB Hubble diagram. Complete details on the selection of these bursts, their redshifts, and all their observed properties are presented in Schaefer (2007). These bursts were the ones used to derive the best fit luminosity relations (Schaefer 2007) as expressed by equation 3.2 and the parameters in Table 3.1. The scatter of the observed $\mathcal{L}$ about the value derived from the observed $\mathcal{I}$ varies widely amongst the relations, with the scatter generally being larger than the error bars from measurement errors alone. To account for this systematic error, the values in Table 3.1 are added in quadrature. The result is that the combined redshifts (from all available luminosity indicators) have a one-sigma scatter of 26% when compared to the spectroscopic redshifts (see Figure 9 of Schaefer 2007). It is this analysis which validates the use of the luminosity relations to get burst redshifts which are reliable to within the quoted error bars (typically 26%).

3.3 Test for Ambiguity in Deriving Redshifts

The utility of the luminosity relations is that one can go from observed quantities to the distance. In more detail, the luminosity relations can be calibrated with GRBs of known redshift so as to derive $\mathcal{A}$ and m, measure $\mathcal{I}$ for each burst, calculate $\mathcal{F}(\mathcal{I},\mathcal{B})$, set $\mathcal{F}(z)$ as being equal to $\mathcal{F}(\mathcal{I},\mathcal{B})$, then determine the luminosity distance and redshift that produces the $\mathcal{F}(z)$. The problem that Li (2007) pointed out is that this procedure is ambiguous for the $E_{peak}-E_{\gamma,iso}$ Amati relation, because there are always *two* distances/redshifts that produce the observed value $\mathcal{F}(\mathcal{I},\mathcal{B})$. That is, there will always be a redshift below z_{peak} and a redshift above z_{peak} for which $\mathcal{F}(\mathcal{I},\mathcal{B}) = \mathcal{F}(z)$. To take a specific example, for the $E_{peak}-E_{\gamma,iso}$ Amati relation, a $z = 1.5$ burst could be confused with a $z = 10.6$ burst, and a $z = 1$ burst could

be confused for a $z = 18.5$ burst; at least in principle. More importantly, Li points out that the error bars on the derived redshift will be quite large when $z \sim z_{\rm peak}$, with the reason being that $\mathcal{F}(z)$ changes little with redshift. Again with the $\rm E_{peak} - E_{\gamma,iso}$ Amati relation, $\mathcal{F}(z)$ is within 10% of $\mathcal{F}_{\rm max}$ for $2.1 < z < 7.0$. Given a one-sigma uncertainty in $\log \mathcal{L}$ of ~ 0.15 (Amati 2006), any GRB with $z > 1.4$ will be within one-sigma of $z_{\rm peak}$. As such, the test of Li puts severe limits on the utility of one of the luminosity relations for purposes of deriving redshifts.

Amati (2006) defends his relation by pointing to the tight calibration curves over a large dynamic range of luminosities. This is indeed a strong defense if the question is about the existence and the fit parameters (i.e., $\mathcal{A}$ and m) for the $E_{\gamma,iso} - E_{peak}$ relation. This is because bursts with *known* redshifts will have a unique and well determined value for $\mathcal{F}(z)$. But this does not work in the other direction, as a known value of $\mathcal{F}(z)$ (from the observed $\mathcal{F}(\mathcal{I}, \mathcal{B})$) does not produce a unique or necessarily well-determined value for the redshift. So both sides appeared to be right; the $\rm E_{peak} - E_{\gamma,iso}$ relation appeared to exist (see Chapter 6), while the relation fails in practice for determining the redshift if $z \gtrsim 0.9$.

The test of Li shall now be expanded to all eight luminosity relations. This can be done by calculating the values of $\mathcal{F}(z)/\mathcal{F}_{\rm max}$ from $0 < z < 20$, as plotted in Figure 3.1. The curve that rises the fastest is for the $\rm E_{peak} - E_{\gamma,iso}$ Amati relation, and it is immediately clear why it runs trouble with the test of Li. The reason is that $z_{\rm peak}$ is in the range of redshift where many GRBs are seen, so that a horizontal line corresponding to $\mathcal{F}(\mathcal{I}, \mathcal{B})/\mathcal{F}_{\rm max}$ intersects the curve in two places. Also, the nearly flat part of the curve (around $z_{\rm peak}$ implies that a given measured value of $\mathcal{F}(\mathcal{I}, \mathcal{B})/\mathcal{F}_{\rm max}$ (with the usual uncertainties) will fit the curve over a large range of redshifts. With this, it is clear that a luminosity relation will have trouble with the test of Li only if it has $z_{\rm peak} \lesssim 10$ or if there is a near-flat portion.

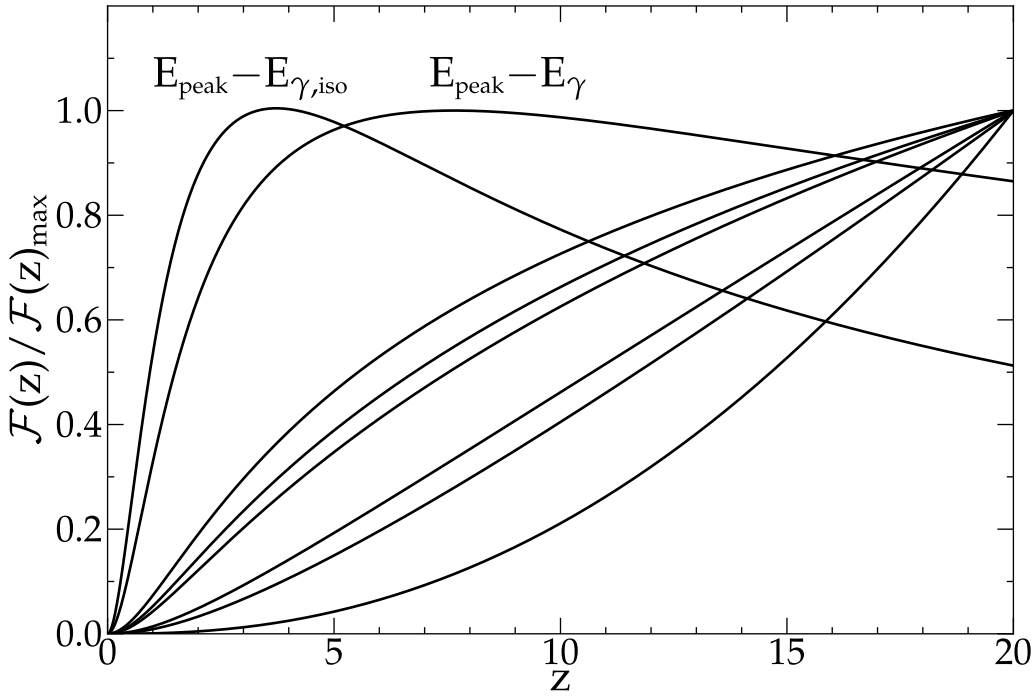

Figure 3.1 $\mathcal{F}(z)/\mathcal{F}_{\rm max}$ for the eight luminosity relations. The eight curves, from left to right where they intersect the horizontal line at 0.4 are for the $\rm E_{peak}-E_{\gamma,iso}$, $\rm E_{peak}-E_{\gamma}$, $\rm L_{iso}-E_{peak}\,T_{0.45}$, V−L , $\rm E_{peak}-L_{iso}$, $\tau_{\rm rise}-$ L , $\tau_{\rm lag}-$ L , and $\rm N_{peak}-$ L relations. The last six of these relations all meet at 1.0 for $z = 20$ as the $\mathcal{F}_{\rm max}$ value was taken at $z = 20$ for these relations with $z_{\rm peak} \gg 20$. When dealing with GRBs of *unknown* redshift, the value of $\mathcal{F}(\mathcal{I},\mathcal{B})/\mathcal{F}_{\rm max}$ is derived from the data, the $\mathcal{F}(z)/\mathcal{F}_{\rm max}$ is set equal to this, and then the plot is used to determine the redshift of the GRB. Li (2007) realized that the $\rm E_{peak}-E_{\gamma,iso}$ relation is ambiguous (in that two redshifts will both fit the observations) and that the uncertainty in the derived redshift will be large for bursts near the peak in the curve. With this generalized test, the $\rm E_{peak}-E_{\gamma}$ relation is shown to have the same problem, but at higher redshifts. Given the typical uncertainties, this means that the $\rm E_{peak}-E_{\gamma,iso}$ and $\rm E_{peak}-E_{\gamma}$ relations cannot be used with any accuracy to determine the redshifts of GRBs with $z \gtrsim 1.4$ and $z \gtrsim 3.4$ respectively. These problems arise due to the $\mathcal{F}(z)/\mathcal{F}_{\rm max}$ function having a maximum (at $z_{\rm peak}$) at redshifts below ~ 10. However, all other luminosity relations easily pass the test of Li. Also, when the GRB redshift is known from optical spectroscopy, the $\mathcal{F}(z)/\mathcal{F}_{\rm max}$ value will be uniquely and accurately determined, so all eight luminosity relations are fine for questions like the calibration of the relations and the construction of the GRB Hubble diagram.

Six of the relations have no problem with the test of Li, as they are monotonically rising fast out to high redshifts. Other than the $E_{peak} - E_{\gamma,iso}$ relation, only one relation has apparent problems, the $E_{peak} - E_{\gamma}$ relation of Ghirlanda et al. (2004). In this case, $z_{peak} = 7.4$. So, for example, one might be in danger of confusing a $z = 3.2$ burst for a $z = 20$ burst. More importantly, high redshift bursts must have a large uncertainty in any derived redshift. For a one-sigma scatter in $\log \mathcal{L}$ of ~ 0.06 (Ghirlanda et al. 2004), all bursts with redshift $z \gtrsim 3.4$ will be within one-sigma of each other.

In general, the ambiguities in derived redshifts for the $E_{peak} - E_{\gamma,iso}$ and $E_{peak} - E_{\gamma}$ relations can always be resolved. For example, with the $E_{peak} - E_{\gamma}$ relation, the high redshift branch will return z values that can be rejected due to afterglow being seen at optical wavelengths (as required to observe a jet break) which would be shorter than the Lyman limit. Also, the lower possible redshift will always be much more likely than the higher possible redshift simply due to the rarity of very high luminosity events in the GRB luminosity function. But the general solution is to have multiple luminosity indicators, for which the various indicators will overlap for only one solution. In all, even though there is formally an ambiguity for two of the relations, the ambiguities will always be resolved in practice.

One of the uses of the luminosity indicators is in the construction of a GRB Hubble diagram from bursts with known redshifts. The problems noted by Li are not relevant in this case, as the *known* redshifts allow us to derive a unique and well-determined value of $\mathcal{F}(z)$ (for the given cosmology).

In summary: (a) Li's test is easily passed for six of the relations for all questions, (b) the redshift ambiguity will always be resolved in practice for the other two relations, (c) the $E_{peak} - E_{\gamma,iso}$ and $E_{peak} - E_{\gamma}$ relations cannot return accurate derived redshifts for $z \gtrsim 1.4$

and $z \gtrsim 3.4$ respectively, (d) all eight luminosity relations have no problems for questions (such as the GRB Hubble diagram) involving bursts of *known* redshifts.

3.4 Test for Violators

Nakar & Piran (2005) and Band & Preece (2005) report that a large fraction of GRBs violate the idealized requirement that $\mathcal{F}(\mathcal{I},\mathcal{B})/\mathcal{F}_{\rm max} \leq 1$ for the $\rm E_{peak}-E_{\gamma,iso}$ relation. Ghirlanda et al. (2005) argue that these violations arise only due to the use of an old calibration of the Amati relation and due to unrealistically small adopted error bars. For whatever resolution, this test should be extended to all eight luminosity relations.

For the 69 GRBs, $\mathcal{F}(\mathcal{I},\mathcal{B})/\mathcal{F}_{\rm max}$ is calculated for each burst. The number of bursts that have this value above unity, and thus are violators of the Nakar and Piran test, are tallied. For each luminosity relation, the fraction of violators are given in the last column of Table 3.1. Three of the relations have zero violators. Three other relations each have only two bursts that are just barely in violation, where the violators are all within 0.6-sigma of the expected value of $\mathcal{F}(z)/\mathcal{F}_{\rm max}$. Thus, these six relations pass the Nakar & Piran test. But two relations (the $\rm E_{peak}-E_{\gamma,iso}$ and $\rm E_{peak}-E_{\gamma}$ relations) have substantial fractions of violators, and it is no coincidence that these are the same relations that have $z_{\rm peak} \lesssim 10$.

For the two relations with the most violators, a plot is provided of $\mathcal{F}(\mathcal{I},\mathcal{B})/\mathcal{F}_{\rm max}$ and the theoretical $\mathcal{F}(z)/\mathcal{F}_{\rm max}$ as a function of redshift (see Figure 3.2). If the luminosity indicators were perfect, then all the observed points would fall along the smooth curve. The plotted error bars as well as the apparent scatter about the model curve illustrate the typical scatter that arises in each relation. Violators of the Nakar & Piran test are those GRBs that are higher than zero on this log-scale.

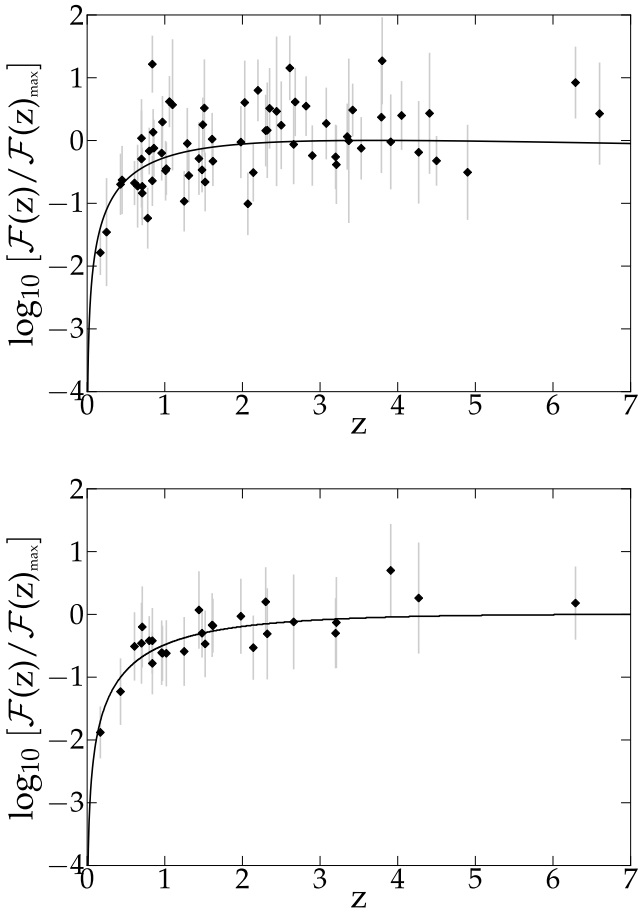

Figure 3.2 $\mathcal{F}/\mathcal{F}_{\rm max}$ for two relations. The observed $\mathcal{F}(\mathcal{I},\mathcal{B})/\mathcal{F}_{\rm max}$ values for each burst are over-plotted on the theoretical $\mathcal{F}(z)/\mathcal{F}_{\rm max}$ curve for the $\mathrm{E_{peak}}-\mathrm{E_{\gamma,iso}}$ Amati relation (top panel) and the $\mathrm{E_{peak}}-\mathrm{E_{\gamma}}$ relation of Ghirlanda et al. (bottom panel). Bursts which violate the Nakar & Piran test are those with $\log[\mathcal{F}(\mathcal{I},\mathcal{B})/\mathcal{F}_{\rm max}] > 0$ on this plot. For these two relations only, the theoretical curve is close to the limit over much of the redshift range of observed bursts. With the normal scatter apparent in these plots, roughly half the GRBs are expected to be violators when the curve is near the limit. These plots indicate that the violators are caused by normal scatter about the relation.

By using a sample of bursts with spectroscopic redshifts, it is easier to see what is going on. In particular, most of the GRBs have redshifts where $\log[\mathcal{F}(z)/\mathcal{F}_{\rm max}] \approx 0$, and so the normal scatter in the relation naturally creates many violators. At $z_{\rm peak}$, half of the bursts are expected to be violators. And for redshifts of $z > 1.4$, one has $\mathcal{F}(z)/\mathcal{F}_{\rm max}$ close to unity, so somewhat less than 50% of the bursts should be violators. Figure 3.2 shows that the violators are simply the upper tail of a normal distribution, and hence do not significantly violate the $\rm E_{peak} - E_{\gamma,iso}$ relation.

For the $\rm E_{peak} - E_{\gamma}$ relation of Ghirlanda et al. (2004), Figure 3.2 shows a similar situation with only five violators, all with $< 1 - \sigma$ deviations. The curve is near zero for the higher redshifts, the violators are all at high redshift, and the scatter about the curve is normally distributed. Again, the existence of violators appears to be a simple consequence of the expected scatter from both systematic and observational errors.

In summary of the generalized Nakar & Piran test, all eight luminosity relations are found to have passed the test. In particular, while some bursts have $\mathcal{F}(\mathcal{I}, \mathcal{B})/\mathcal{F}_{\rm max} > 1$, this is an expected consequence of ordinary scatter about the best fit relation.

4. Does the Addition of a Duration Improve the $E_{peak} - L_{iso}$ Relation for Gamma-Ray Bursts? - An Examination of the 'Firmani Relation'[1]

4.1 Introduction

Following the generalized tests of the GRB luminosity relations (Chapter 3), eight luminosity relations were commonly accepted. One of these eight relations is the $L_{iso} - E_{peak}\, T_{0.45}$ relation proposed by Firmani et al. (2006, hereafter named the Firmani relation). Here, E_{peak} describes the peak of the E×F(E) curve (proportional to νF_ν), which is the photon energy of the peak spectral flux; L_{iso} is the isotropic luminosity of the burst measured bolometrically (1-10,000 kev in the burst rest frame). $T_{0.45}$ is the Reichart definition of a GRB time duration (Reichart et al. 2001) where the duration is the total time interval of the brightest bins in the light curve that contains 45% of the burst fluence. The Firmani relation was presented as an improvement over the $E_{peak} - L_{iso}$ relation. Nineteen GRBs were used to demonstrate a tight correlation with a reduced chi-square of 0.7 over 16 degrees of freedom; the resulting luminosity relation being $L_{iso} \propto E_{peak}^{1.62}\, T_{0.45}^{-0.49}$. The reported scatter in the Firmani relation is substantially smaller than those of most other GRB luminosity relations. This result offers the hope of substantial improvement in the accuracy of GRBs for cosmological distance measures.

[1]This chapter is largely taken from an article that appeared in The Astrophysical Journal, and is reproduced with permission of the AAS(see Appendix A for details).

There is no physical reason to expect that the addition of a duration should make for a tighter relation. Nonetheless, it is reasonable to investigate whether a tighter luminosity relation can be obtained from duration definitions other than $T_{0.45}$, as $T_{0.45}$ may not be the optimal duration to use. There is no physical reason to expect that any one definition of duration is best, while the particular choice of the Reichart definition was used only for historical reasons no longer of any relevance. For example, use the Reichart definition, but measure the duration over a different percentage of the burst fluence. So perhaps the use of a duration based on 30% or 60% ($T_{0.30}$ or $T_{0.60}$) might be better. Alternative definitions of duration can be considered instead of the Reichart formulation. For example, the duration can be defined as equalling the total fluence divided by the peak flux to get a sort of equivalent width; alternatively, use the familiar T_{90} or T_{50} durations. The T_{90} and T_{50} duration definitions are a practical means to identify effective start and stop times, but with the disadvantage of counting perhaps long intervals in the middle with little or no flux as part of the duration. They are defined as the central 90% and 50% of the burst light curve. A wide variety of alternative durations can be defined, and there is no way to know which one is optimal.

This chapter tests the Firmani relation for its potential as a GRB luminosity relation. First, the Firmani relation is reproduced for the original data of Firmani et al. (2006) as a test that identical fitting procedures are being used. Then the Firmani relation is tested with a set of independent data for the same 19 bursts. A further test of the Firmani relation is made with a much larger sample of 60 bursts. In section 4.3, many duration definitions are tested in a Firmani-like relation to see which produces the 'tightest' correlation. Section 4.4 contains a simple and forced derivation of the Firmani relation from two other luminosity relations.

4.2 Testing the Firmani Relation

First, start with the model as stated in Firmani et al. (2006):

$$\mathrm{L_{iso}} = 10^{52.11\pm0.03}\left(\frac{\mathrm{E_{peak}}}{10^{2.37}\,\mathrm{keV}}\right)^{1.62\pm0.08}\left(\frac{\mathrm{T_{0.45}}}{10^{0.46}\,\mathrm{s}}\right)^{-0.49\pm0.07}\frac{\mathrm{erg}}{\mathrm{s}}. \tag{4.1}$$

This equation is then generalized, and put into logarithmic form:

$$\log_{10}(\,\mathrm{L_{iso}}) = \gamma + \xi\log_{10}\left(\frac{\mathrm{E_{peak}}}{10^{2.37}\,\mathrm{keV}}\right) + \eta\log_{10}\left(\frac{\mathrm{T_{0.45}}}{10^{0.46}\,\mathrm{s}}\right). \tag{4.2}$$

Here γ, ξ, and η are the fit parameters derived from fitting a set of GRB data, which can then predict model values of $\log_{10}(\,\mathrm{L_{iso}})$. For the one-sigma uncertainty used in evaluating the chi-square, an elliptical error box was used to account for the errors in the measured quantities on both axes. Specifically,

$$\sigma^2_{\mathrm{combined}} = \sigma^2_{\log_{10}(\,\mathrm{L_{iso}})} + \left(\frac{\xi\,0.434\,\sigma_{\,\mathrm{E_{peak}}}}{\mathrm{E_{peak}}}\right)^2 + \left(\frac{\eta\,0.434\,\sigma_{\,\mathrm{T_{0.45}}}}{\mathrm{T_{0.45}}}\right)^2. \tag{4.3}$$

This formulation of the combined error box comes from simple error propagation as shown below.

$$\begin{aligned}
\sigma^2_{\mathrm{combined}} &= \sigma^2_{\log_{10}(\,\mathrm{L_{iso}})} + \sigma^2_{\mathrm{model}} \\
\sigma^2_{\mathrm{combined}} &= \sigma^2_{\log_{10}(\,\mathrm{L_{iso}})} + \sigma^2_{\gamma} + \sigma^2_{\xi*\log_{10}\left(\frac{\mathrm{E_{peak}}}{10^{2.37}\,\mathrm{keV}}\right)} + \sigma^2_{\eta*\log_{10}\left(\frac{\mathrm{T_{0.45}}}{10^{0.46}\,\mathrm{s}}\right)} \\
\sigma^2_{\mathrm{combined}} &= \sigma^2_{\log_{10}(\,\mathrm{L_{iso}})} + \sigma^2_{\xi*\log_{10}\left(\,\mathrm{E_{peak}}\right)} - \sigma^2_{\xi*\log_{10}(10^{2.37}\,\mathrm{keV})} + \sigma^2_{\eta*\log_{10}(\,\mathrm{T_{0.45}})} - \sigma^2_{\eta*\log_{10}(10^{0.46}\,\mathrm{s})} \\
\sigma^2_{\mathrm{combined}} &= \sigma^2_{\log_{10}(\,\mathrm{L_{iso}})} + \left(\frac{\xi\,0.434\,\sigma_{\,\mathrm{E_{peak}}}}{\mathrm{E_{peak}}}\right)^2 + \left(\frac{\eta\,0.434\,\sigma_{\,\mathrm{T_{0.45}}}}{\mathrm{T_{0.45}}}\right)^2
\end{aligned}$$

With the model values for the luminosity and its uncertainty as well as the observed luminosity (all in logarithmic space), the reduced-chi-square for the model fit can now be calculated.

To perform this test on the 19 bursts, the data as reported in Firmani et al. (2006) was used: Their values for $T_{0.45}$ were the observed durations, and thus needed to be corrected for time dilation into the burst frame via dividing by $(1+z)$. Their values of E_{peak} were already in the burst frame, and did not need to be corrected. L_{iso} was obtained by taking their value of L_{iso} / E_{iso} and multiplying it by their value E_{iso}. Firmani's reported redshift values were also used. This fit was done manually in Microsoft Excel.

The best fit had a ${\chi_r}^2 = 0.7$ with an root-mean-square (RMS) scatter of the observed values of $\log_{10}(L_{iso})$ about the best fit model equal to 0.14. With 19 bursts and 3 fit parameters, there are 16 degrees of freedom. This is in agreement with the reported value of $\chi_r^2 = 0.7$ reported by Firmani et. al. (2006). The best fit parameters and their uncertainties as reported by Firmani et al. (2006) and as given in Equation 4.1 are also confirmed. Thus, the result has been reproduced, and and these procedures will be used for all subsequent fits.

Given the nature of observational data, there are inevitably differences in the various published values of all these burst properties. For instance, Firmani et al. (2006) report $E_{peak} = 685 \pm 133$ keV for GRB971214 , while Jimenez et al. (2001) reports a value of 840 $\pm$ 88 keV. For the same burst, the peak flux is slightly different for different detectors, so Fimani et al. (2006) report $\log_{10}(L_{iso})$ equals 52.86 $\pm$ 0.08, while Schaefer (2007) derives a value of 52.92 $\pm$ 0.01. The Firmani relation should be robust on the use of independent measures from different published sources, so the same result should be obtained with these different values. For this test, independent measures for the luminosity, peak energy, and $T_{0.45}$ from various published reports were collected. There is no reason to think that either set of values for these 19 GRBs is better or worse in accuracy. The independent quantities for these burst qualities are in Table 4.1. Column 1 is the GRB designation; column 2 is the redshift; column 3 is the log of the isotropic bolometric luminosity; column 4 is the photon

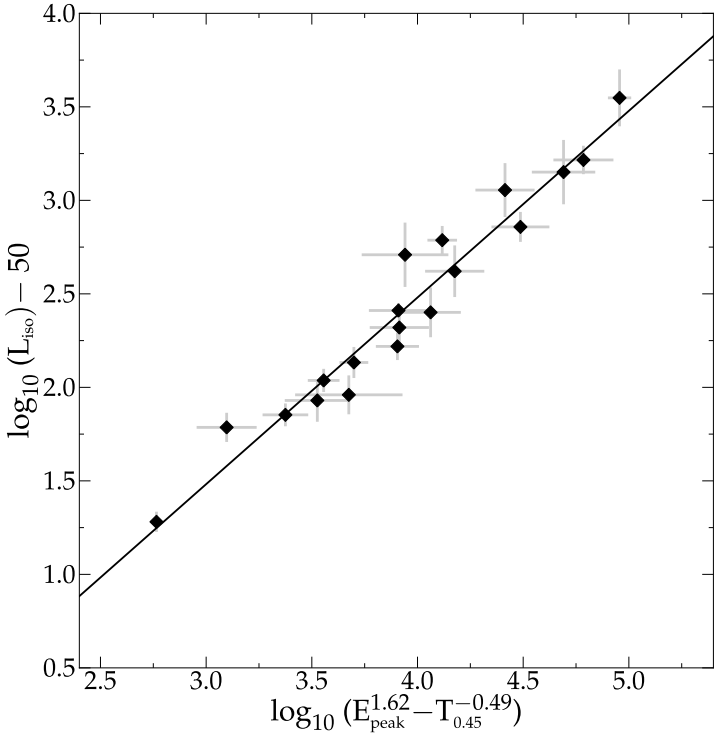

Figure 4.1 The Firmani relation with Firmani's data. Here all burst properties as reported by Firmani et al., (2006) have been used. Because the scatter was so small, this result is potentially important as it would offer a means to substantially improve the calibration of distances to many GRBs. Here, the y-axis is the logarithm of the luminosity which is in ergs per second. The subtraction of 50 is for easier comparison to the graph as shown in Firmani et al., (2006). This y-axis convention is used on all subsequent plots for ease of comparing the results.

energy of the observed peak spectral energy (which needed to be blueshifted into the bursts' frame); and column 5 is the Reichart duration $T_{0.45}$. The values and their references for the luminosities, peak energies, and redshifts can be found in Schaefer (2007). Durations for $T_{0.45}$ were measured from light curves directly using Excel.

The formal measurement error bars quoted for the $T_{0.45}$ values in Table 4.1 are fairly small, but the real total uncertainties are substantially larger. This is evident because various groups have reported measures of $T_{0.45}$ for many of the same GRBs and the scatter is much larger than anyone's quoted error bars. In particular, independent measures have been collected as reported by Guidorzi (2005), Firmani et al. (2006), Rizzuto et al. (2007), Rossi et al. (2008), Table 4.1 of this paper, and independent calculations made by others at LSU, with an average of five values for each of the bursts in Table 4.1. The median scatter of these measurements is 17%. This value changes little between bursts measured with one satellite (*Swift*) alone and only the results from within the LSU GRB group. It is likely that variation arises from relatively small changes resulting from differing time bin sizes and time intervals for the calculation. (Similar scatter is found for other duration measures, see for example Koshut et al. 1996 and Norris et al. 1995.) This additional systematic error contributes a small fraction of the extra scatter observed in the Firmani relation. The reason for this small contribution is that the extra systematic error on $T_{0.45}$ is $\sim$12% and the values are included nearly as a square root (see Eq. 4.1), so the extra contribution to $\sigma_{\rm combined}$ is 0.026 (see Eq. 4.3). All this is to say that the systematic errors in measuring $T_{0.45}$ are much larger than has ever been realized, yet even these additional uncertainties are negligibly small.

Table 4.1. Burst Properties Used Throughout This Chapter

BURST	z[a]	$Log(\mathrm{L_{iso}})$[a] (erg/s)	$\mathrm{E_{peak}}$[a] (keV)	$\mathrm{T_{0.45}}$ [b] (s)
(1)	(2)	(3)	(4)	(5)
970228[c]	0.70	52.20 ± 0.03	115^{+38}_{-38}	2.37 ± 0.44
970508	0.84	52.04 ± 0.04	$389^{+[40]}_{-[40]}$	4.03 ± 0.24
970828[c]	0.96	52.68 ± 0.05	$298^{+[30]}_{-[30]}$	10.50 ± 0.45
971214[c]	3.42	52.92 ± 0.01	$190^{+[20]}_{-[20]}$	6.72 ± 0.09
980703[c]	0.97	51.78 ± 0.01	$254^{+[25]}_{-[25]}$	18.00 ± 1.80[e]
990123[c]	1.61	53.36 ± 0.02	$604^{+[60]}_{-[60]}$	16.58 ± 0.05
990506[c]	1.31	53.05 ± 0.01	$283^{+[30]}_{-[30]}$	12.67 ± 0.63[d]
990510[c]	1.62	52.76 ± 0.02	$126^{+[10]}_{-[10]}$	5.06 ± 0.25[d]
990705[c]	0.84	52.36 ± 0.02	189^{+15}_{-15}	9.54 ± 0.27
991208	0.71	52.67 ± 0.04	$190^{+[20]}_{-[20]}$	4.80 ± 0.24[d]
991216[c]	1.02	53.36 ± 0.01	$318^{+[30]}_{-[30]}$	3.58 ± 0.05
000131[c]	4.5	53.20 ± 0.05	163^{+13}_{-13}	4.54 ± 0.09
000210	0.85	52.85 ± 0.04	408^{+14}_{-14}	1.73 ± 0.06
000911[c]	1.06	53.05 ± 0.04	$986^{+[100]}_{-[100]}$	6.46 ± 0.32[d]
000926	2.07	52.97 ± 0.04	100^{+7}_{-7}	4.67 ± 0.45
010222	1.48	53.51 ± 0.01	309^{+12}_{-12}	6.46 ± 0.14
010921	0.45	51.14 ± 0.04	$89^{+21}_{-13.8}$	5.74 ± 0.58
020124[c]	3.2	52.76 ± 0.07	87^{+18}_{-12}	12.14 ± 0.58
020405	0.7	52.20 ± 0.02	364^{+90}_{-90}	10.18 ± 0.38
020813[c]	1.25	52.56 ± 0.03	142^{+14}_{-13}	17.36 ± 0.23
021004	2.32	52.00 ± 0.10	80^{+53}_{-23}	6.89 ± 0.41
021211[c]	1.01	52.08 ± 0.03	46^{+8}_{-6}	0.66 ± 0.12
030115	2.5	52.22 ± 0.07	83^{+53}_{-22}	4.26 ± 0.30
030226[c]	1.98	51.89 ± 0.08	97^{+27}_{-17}	8.86 ± 0.87
030323	3.37	52.11 ± 0.22	44^{+90}_{-26}	6.89 ± 0.70
030328[c]	1.52	52.38 ± 0.03	126^{+14}_{-13}	20.83 ± 0.70
030329[c]	0.17	51.14 ± 0.02	$68^{+2.3}_{-2.2}$	4.43 ± 0.23
030429	2.66	52.08 ± 0.12	35^{+12}_{-8}	2.13 ± 0.35
030528	0.78	50.66 ± 0.09	$32^{+4.7}_{-5}$	9.99 ± 0.93
040924[c]	0.86	51.97 ± 0.05	67^{+6}_{-6}	0.49 ± 0.02[d]
041006[c]	0.71	51.76 ± 0.03	63^{+13}_{-13}	4.26 ± 0.12
050126	1.29	51.03 ± 0.05	47^{+27}_{-8}	6.59 ± 0.32
050318	1.44	51.85 ± 0.05	47^{+15}_{-8}	2.88 ± 0.20
050401	2.9	53.19 ± 0.05	118^{+18}_{-18}	4.61 ± 0.23
050406	2.44	51.32 ± 0.11	25^{+35}_{-13}	1.92 ± 0.18
050416	0.65	50.99 ± 0.07	$15^{+2.3}_{-2.7}$	0.58 ± 0.07
050502	3.79	52.79 ± 0.12	93^{+55}_{-35}	4.60 ± 0.28
050505	4.27	52.79 ± 0.07	70^{+140}_{-24}	9.02 ± 0.41
050525	0.61	51.90 ± 0.01	$81^{+1.4}_{-1.4}$	2.24 ± 0.11[d]
050603	2.82	53.84 ± 0.03	344^{+52}_{-52}	1.47 ± 0.12
050820	2.61	52.28 ± 0.07	246^{+76}_{-40}	6.46 ± 0.41
050904	6.29	53.08 ± 0.06	436^{+200}_{-90}	59.46 ± 2.97[d]
050908	3.35	52.02 ± 0.07	41^{+9}_{-5}	4.86 ± 0.14
050922	2.2	52.88 ± 0.02	198^{+38}_{-22}	1.15 ± 0.05
051022	0.8	52.53 ± 0.03	510^{+22}_{-20}	10.30 ± 0.23

Table 4.1—Continued

BURST	z[a]	$Log(L_{iso})$[a] (erg/s)	E_{peak}[f] (keV)	$T_{0.45}$ [b] (s)
(1)	(2)	(3)	(4)	(5)
051109	2.35	52.54 ± 0.05	161^{+130}_{-35}	3.78 ± 0.35
060108	2.03	51.54 ± 0.43	65^{+600}_{-10}	3.20 ± 0.14
060115	3.53	52.21 ± 0.05	62^{+19}_{-6}	15.42 ± 0.54
060116	6.6	53.03 ± 0.24	139^{+400}_{-36}	21.76 ± 1.15
060124	2.3	52.66 ± 0.05	237^{+76}_{-51}	5.12 ± 0.18
060206	4.05	52.86 ± 0.02	75^{+12}_{-12}	1.86 ± 0.09
060210	3.91	52.93 ± 0.02	149^{+400}_{-35}	23.62 ± 1.00
060223	4.41	52.64 ± 0.08	71^{+100}_{-10}	2.82 ± 0.18
060418	1.49	52.35 ± 0.02	$230^{+[20]}_{-[20]}$	12.48 ± 0.59
060502	1.51	51.75 ± 0.19	156^{+400}_{-33}	7.42 ± 0.28
060510	4.9	52.42 ± 0.07	$95^{+[60]}_{-[30]}$	70.21 ± 1.63
060526	3.21	52.36 ± 0.06	$25^{+[5]}_{-[5]}$	9.54 ± 1.03
060604	2.68	51.75 ± 0.08	$40^{+[5]}_{-[5]}$	9.28 ± 0.63
060605	3.8	52.25 ± 0.19	$169^{+[30]}_{-[30]}$	8.83 ± 0.22
060607	3.08	52.36 ± 0.13	120^{+190}_{-17}	13.12 ± 0.54

[a]These values were obtained from Schaefer (2007); all appropriate references are located in that paper.

[b]These values were calculated from light curves from BATSE, *HETE*-2 , *Swift* and *Konus* websites.

[c]These bursts were used by Firmani et al. (2006) to obtain the Firmani relation.

[d]Indicates where an estimate of 5% error was used.

[e]Indicates where an estimate of 10% error was used.

[f]Values in square brackets indicate an estimate based on typical values (see Schaefer 2007).

Upon optimizing the fit with the independent values, the equation for the best fit is:

$$L_{iso} = 10^{52.09\pm0.02} \left(\frac{E_{peak}}{10^{2.37}\,keV}\right)^{1.90\pm0.05} \left(\frac{T_{0.45}}{10^{0.46}\,s}\right)^{-0.52\pm0.05} \frac{erg}{s}. \quad (4.4)$$

A comparison with Eq. 4.1 shows that the two best fits are similar, with the exponent for the E_{peak} being moderately different. The Firmani relation for this independent data is displayed in Figure 4.2. The obvious difference between Figures 4.1 and 4.2 is that Figure 4.2 has a much larger scatter than in Figure 4.1. The RMS value for the independent data was 0.35,

whereas the RMS for the data from Firmani et al. (2006) is 0.14. The reduced chi-square for the 19 bursts about this best fit model is $\chi^2_{\rm r} = 14.50$ for the independent data. This is greatly larger than the value of $\chi^2_{\rm r} = 0.7$ obtained from the data from Firmani et al. (2006). With this large reduced chi-square, the realization is that there must be some additional source of systematic uncertainty that is beyond that from ordinary measurement errors.

An additional figure of merit can be introduced which quantifies the scatter about the best fit Firmani relation. This is the systematic error required to be added in quadrature to the measurement error such that the resulting reduced chi-square equals unity. A desirable fit with little scatter will have a small required systematic contribution to the uncertainties, whereas a poor fit with large scatter will have a large required systematic contribution. For this, the systematic error is assumed to be a constant, even though the reality is likely more complex in ways that are unseen. In essence, the uncertainty in the chi-square calculation is calculated as

$$\sigma^2_{\rm total} = \sigma^2_{\rm sys} + \sigma^2_{\rm combined}. \tag{4.5}$$

For the case of Firmani's 19 GRBs with his data, there is no required additional systematic uncertainty (as indicated by the reduced chi-square being less than unity). But for the independent data for the same bursts, a systematic error of 0.34 (in logarithmic units) is required be added in quadrature so as to get an acceptable fit with a reduced chi-square of unity. So in all, the quality of the Firmani relation for any data set can be quantified by three parameters, $\chi^2_{\rm r}$, RMS, and $\sigma_{\rm sys}$. Table 4.2 summarizes these parameters for the Firmani relations with various data sets.

The next step was to add more bursts. That is, the Firmani relation should be robust when applied to a much larger sample of bursts. Specifically, 60 of the bursts as given in Table 4.1 were used, with the observed burst properties as collected in Schaefer (2007) based

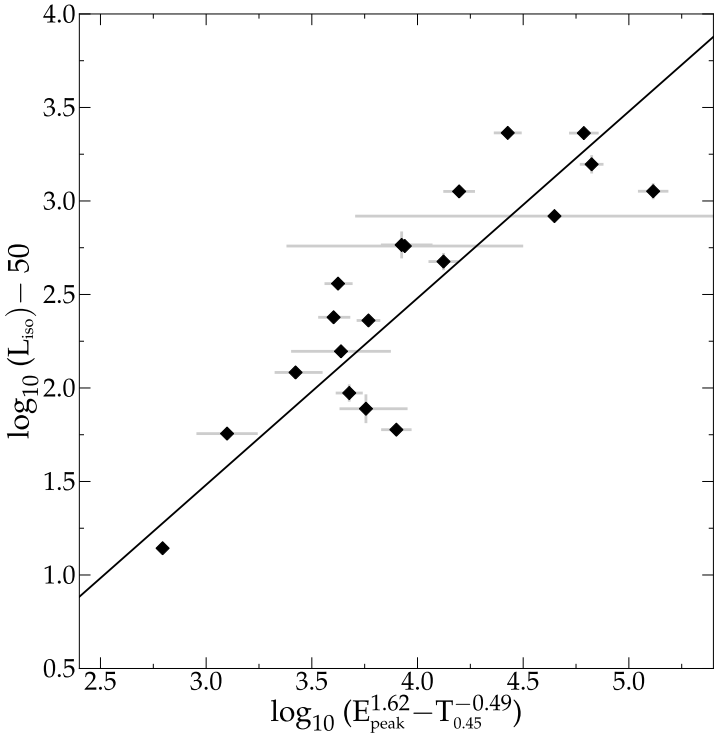

Figure 4.2 The Firmani relation with independent data for the same 19 GRBs. The main point from this figure is that the scatter is much greater than in Figure 4.1. The chart area is matched to the previous one to make better comparison of the relations. The line in this figure is identical with the line in Figure 4.1 (i.e., the original Firmani relation) as another aid for comparison. The two best fits for the first two figures have slightly different exponents (see Eqs 1 and 4) so Figure 4.2 is slightly non-optimal in representing the best fit.

Table 4.2. Expanding the Firmani Relation.

Relation	γ^{a}	ξ^{a}	η^{a}	χ^2_r	RMS	σ_{sys}
19 Bursts, Firmani's Data	52.11±0.03	1.62±0.08	-0.49±0.07	0.74	0.14	0.00
19 Bursts, Independent Data	52.09±0.02	1.90±0.05	-0.52±0.05	14.50	0.35	0.34
60 Bursts, Independent Data	52.09±0.01	1.91±0.03	-0.67±0.03	15.89	0.41	0.38

[a]Fit parameters in accordance with equation 4.2. γ refers to a constant, ξ refers to the power on E_{peak} , and η is the power on $T_{0.45}$.

on references reported therein. Schaefer (2007) tabulates 69 bursts in all, but several had to be omitted for various reasons. GRB 980613, GRB 990712, GRB 011211, and GRB 020903 were not used due to inability to obtain the light curves for duration calculations. GRB 050824 was omitted because the value of E_{peak} is only an upper limit. GRB 050319, GRB 050408, GRB 050802, and GRB 051111 were omitted due to the reported value of E_{peak} in Schaefer 2007 not having been directly measured.

To remain consistent, only data reported in Schaefer (2007) for the peak energy and redshift were used. The values for both L_{iso} and $\sigma_{L_{iso}}$ were derived from values for the bolometric peak flux (P_{bolo}) reported by Schaefer (2007). With the standard inverse square law, one gets

$$L_{iso} = P_{bolo}\, 4\pi\, d_L^2. \tag{4.6}$$

The luminosity distance (d_L) to the GRB is calculated with the measured spectroscopic redshift, assuming the concordance cosmology (Ω_M=0.27 in a flat universe with $w = -1$).

With this independent data set for 60 GRBs, the model Eq. 4.2 is fitted manually (again in Excel). The equation for the best fit for this extended sample is:

$$L_{iso} = 10^{52.09\pm0.01} \left(\frac{E_{peak}}{10^{2.37}\,\mathrm{keV}}\right)^{1.91\pm0.03} \left(\frac{T_{0.45}}{10^{0.46}\,\mathrm{s}}\right)^{-0.67\pm0.03} \frac{\mathrm{erg}}{\mathrm{s}}. \tag{4.7}$$

This best fit model is similar to the best fits with the 19 GRB subsample (cf. Eqs 4.1 and 4.4). The resulting Firmani relation is plotted in Figure 4.3. Again, the immediate reaction is that the figure displays a lot of scatter, and much more scatter than in either Figures 4.1 or 4.2. Quantitatively, the comparisons are presented in Table 4.2. One sees that the RMS scatter has risen to 0.41, which is greatly larger than in the earlier figures. The reduced chi-square of the fit is $\chi_r^2 = 15.89$, which shows that there is some source of scatter that is much

larger than produced by the simple measurement uncertainties in the input parameters. The systematic error for the 60 burst sample is 0.38, which is substantially larger than for either data set in the 19 burst subsample.

The primary result from this section is that the Firmani relation is neither robust to the use of independent data nor robust to the extension to many more bursts.

4.3 Seeking the Optimal Duration

In the previous section, the behavior of the Firmani relation for a sample of 60 GRBs was identified. The next step would be to try the same test procedures for various different duration definitions. For this, start with a generalized form of Eq. 4.2:

$$\log_{10}(\mathrm{L_{iso}}) = \gamma + \xi \log_{10}\left(\frac{\mathrm{E_{peak}}}{<\mathrm{E_{peak}}>}\right) + \eta \log_{10}\left(\frac{\tau}{<\tau>}\right). \tag{4.8}$$

Here, the duration has been generically labeled as τ, and the denominators inside the logarithms are constants equal to the average τ and $\mathrm{E_{peak}} - \mathrm{L_{iso}}$ values for the data set. The reason to have these averages in the denominator is to improve the convergences of the fits by avoiding long thin error regions with strong correlations between fit parameters.

There are many alternative ways to measure duration. For example, start with the Reichart definition, but use a different percentage of the total fluence to take the duration over. In other words, expand the Reichart definition of duration out to say $\mathrm{T_{0.60}}$, or contract it to $\mathrm{T_{0.30}}$. Again, there is no reason to believe that using the exact duration as proposed by Reichart ($\mathrm{T_{0.45}}$) would be any more effective than the others. Other duration definitions are reasonable, and indeed much easier to calculate. Or, adopt a duration defined as the time a burst spends above $x\%$ of the peak flux of the burst ($\mathcal{T}_{\mathrm{x}}$). The well-known definitions of duration, $\mathrm{T_{90}}$ and $\mathrm{T_{50}}$, should also be included. Here, the two durations are the time interval containing the central 90 or 50 percent of the fluence of the burst, respectively. Another

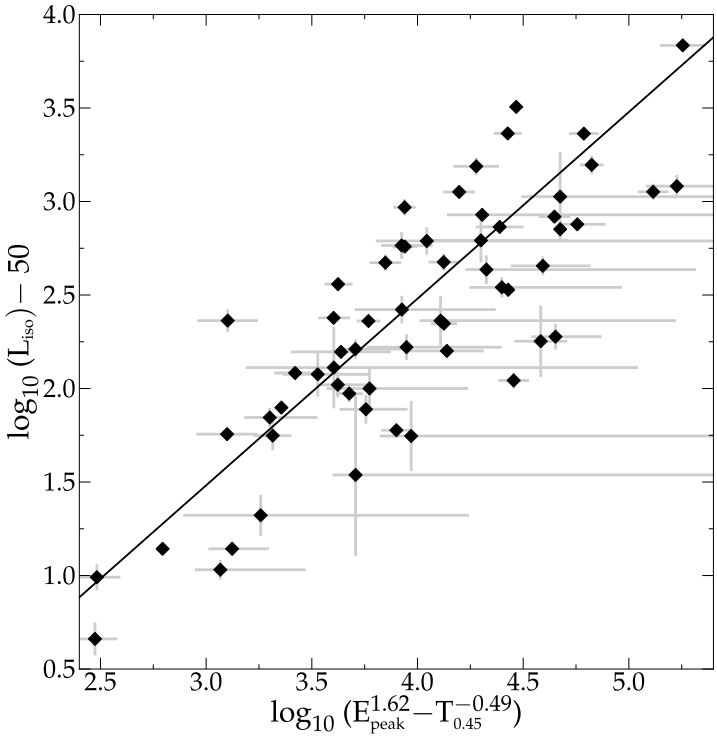

Figure 4.3 The Firmani relation when extended to 60 GRBs. The main point from this figure is that the scatter is much greater than in Figure 4.1, and is also significantly larger than in Figure 4.2. This figure is given with identical axes and fit line (from Eq. 4.1) as the other figures to allow simple comparisons. This scatter is comparable to that for the older $E_{peak} - L_{iso}$ relation, and this points to the main conclusion that the Firmani relation is not an improvement.

option is take the bolometric fluence S_{bolo} and divide it by the bolometric peak flux P_{bolo} to get a sort of 'equivalent width'.

A control timescale is also needed, so a case was adopted where all the burst durations are set equal to a constant, which is arbitrarily taken to be τ=10 seconds. The chosen value does not matter, as different choices will merely result in a different γ value that will not change the quality of the fit. By taking a constant duration, the Firmani relation ($L_{iso} - E_{peak}\, T_{0.45}$) is transformed into the old $E_{peak} - L_{iso}$ relation. A comparison of the scatter in the τ=10 seconds relation versus the generalized Firmani relations will tell us whether the addition of a time scale has substantially improved the quality of the luminosity indicator.

So far, the alternative durations have all been measures of the total duration of the burst. However, the physics of the luminosity relations points to the correlations as being with the individual peak pulse and not the overall set of pulses that make up the entire light curve (Schaefer 2003; 2004). So the individual pulse duration measures should be considered. A simple and reasonable means of doing this is to take all of the overall-burst-duration measures and divide by the number of pulses in the light curve (N_{peak} , as defined in Schaefer 2007). This immediately doubles the number of trial definitions considered. The final tally is then 32 different measurements of duration, all of which are listed in Table 4.3.

For all 60 bursts in the sample, the durations according to all 32 definitions have been measured (all in Excel). These durations have been calculated from the light curves as given from the light curves as given on the BATSE, *HETE*-2 , *Konus* , and *Swift* websites as well as the values reported in Schaefer (2007). For T_{90} and T_{50}, the derived values in Excel almost always in agreement with values as reported by the instrument teams (see Schaefer 2007 for references).

Table 4.3. RMS and Systematic Errors Values For Durations.

Duration Definition	RMS	$\sigma_{\rm sys}$
$T_{0.15}$	0.41	0.37
$T_{0.30}$	0.40	0.36
$T_{0.45}$ (Firmani Relation)	0.41	0.38
$T_{0.50}$	0.41	0.37
$T_{0.60}$	0.41	0.37
$T_{0.75}$	0.41	0.38
$\mathcal{T}_{15}$	0.46	0.39
$\mathcal{T}_{30}$	0.41	0.38
$\mathcal{T}_{45}$	0.37	0.33
$\mathcal{T}_{50}$	0.38	0.38
$\mathcal{T}_{60}$	0.41	0.36
$\mathcal{T}_{75}$	0.40	0.36
$S_{\rm bolo}/P_{\rm bolo}$	0.56	0.49
T_{90}	0.46	0.41
T_{50}	0.47	0.43
10 s ($E_{\rm peak} - L_{\rm iso}$)	0.50	0.46
$T_{0.15}/N_{\rm peak}$	0.33	0.29
$T_{0.30}/N_{\rm peak}$	0.35	0.30
$T_{0.45}/N_{\rm peak}$	0.34	0.30
$T_{0.50}/N_{\rm peak}$	0.34	0.30
$T_{0.60}/N_{\rm peak}$	0.35	0.31
$T_{0.75}/N_{\rm peak}$	0.35	0.31
$\mathcal{T}_{15}/N_{\rm peak}$	0.37	0.30
$\mathcal{T}_{30}/N_{\rm peak}$	0.31	0.27
$\mathcal{T}_{45}/N_{\rm peak}$	0.32	0.28
$\mathcal{T}_{50}/N_{\rm peak}$	0.35	0.30
$\mathcal{T}_{60}/N_{\rm peak}$	0.38	0.34
$\mathcal{T}_{75}/N_{\rm peak}$	0.38	0.35
$S_{\rm bolo}/P_{\rm bolo}/N_{\rm peak}$	0.41	0.33
$T_{90}/N_{\rm peak}$	0.42	0.38
$T_{50}/N_{\rm peak}$	0.41	0.37
$10\,{\rm s}/N_{\rm peak}$	0.52	0.51

Equation 4.8 is fitted for all 60 GRBs for all 32 duration measures. For each best fit relation, the RMS and $\sigma_{\rm sys}$ values are calculated as quantitative figures of merit. These are summarized in Table 4.3.

The results indicate that while there are certainly differences between duration definitions, the differences tend to be small. The smallest values of RMS and $\sigma_{\rm sys}$ occurs for durations defined as $\mathcal{T}_{30}/N_{\rm peak}$. The scatter in this best relation is somewhat smaller than for the original Firmani relation (with $T_{0.45}$ in the third line of Table 3). However, these

differences do not appear to be significant. The reason being that there will be noise in the figures of merit which will inevitably produce one duration definition as being the best even if the values were uncorrelated or random, and the scale for such variations can be seen by comparing the values in Table 4.2. That is, the variations of the figures of merit in Table 4.3 are consistent with the case where duration information is not correlated with L_{iso} , and a different set of 60 GRBs would randomly produce a different 'best' definition. As such, the Firmani relation should not be replaced with a luminosity relation involving $\mathcal{T}_{30}/N_{peak}$.

A particularly important comparison is between the Firmani relation and the $E_{peak} - L_{iso}$ relation (represented by the line with the durations all taken to be a constant of 10 seconds). One sees that the $E_{peak} - L_{iso}$ relation is the third poorest relation in the table. Nevertheless, the difference is not large enough to evaluate as being significant. That is, the differences in the figures of merit (0.09 in the RMS and 0.08 in σ_{sys}) are too small to view as necessarily arising from a physical effect in the bursts. This is evident because the variation caused by simple sampling effects (see the last two lines of Table 4.2) are of order 0.06 in the RMS and 0.04 in σ_{sys}. As such, the Firmani relation should be viewed as having a similar scatter as the $E_{peak} - L_{iso}$ relation.

4.4 Discussion

In a recent independent study, Rossi et al. (2008) also examined the Firmani relation, in particular with a comparison to the Amati relation. They use an extended sample of 40 *Beppo-Sax* and *Swift* bursts, with little overlap with the sample of 60 GRBs. Their best fit is somewhat different from those in Eqs 4.1, 4.4, or 4.7; with their fitted Firmani relation scaling as $L_{iso} \propto E_{peak}^2 T_{0.45}^{-1}$. They realized that this Firmani relation is essentially identical to the Amati relation (Amati et al. 2002), which gives the isotropic energy emitted in gamma

radiation over the whole burst duration as $E_{\gamma,iso} \propto E_{peak}^2$. With the reasonable approximation that the total energy in the light curve equals the peak luminosity times the duration ($E_{\gamma,iso} \approx L_{iso} T_{0.45}$), the Amati relation ($E_{\gamma,iso} \propto E_{peak}^2$) is transformed into their Firmani relation ($L_{iso} \propto E_{peak}^2 T_{0.45}^{-1}$). While the exponents in the Firmani relation are somewhat different from those derived in this work, the Rossi derivation demonstrates that the Firmani relation has a physical basis that is close to that of the Amati relation. Rossi et al. (2008) further go on to show that the scatter in their Firmani relation is comparable to that in the Amati relation, which is another way of saying that the two relations are not independent.

In this section, the Firmani relation will be derived from *both* the $E_{peak} - L_{iso}$ and Amati relations. First, start with the relation $L_{iso} \propto E_{peak}^{1.68}$ as given in Schaefer (2007). This can be rearranged as $L_{iso} \propto E_{peak}^{1.9} (E_{peak}^2 / L_{iso})^{-0.69}$. The Amati relation ($E_{\gamma,iso} \propto E_{peak}^2$) can be inserted to get $L_{iso} \propto E_{peak}^{1.9} (E_{\gamma,iso} / L_{iso})^{-0.69}$. Next, select one of the duration definitions with $\tau = S_{bolo}/P_{bolo}$. The ratio of fluence to peak flux will equal to the ratio of the burst energy and the peak luminosity, leaving $\tau = E_{\gamma,iso}/L_{iso}$. This can now be substituted to obtain $L_{iso} \propto E_{peak}^{1.9} \tau^{-0.69}$. The resulting equation is simply Eq 4.8 $\xi = 1.9$ and $\eta = -0.69$, values which are characteristic of the fitted Firmani relation (cf. Eq. 4.7). With this, one sees that the Firmani relation has no independent existence because it is only a combination of two simpler relations.

Thus, given any two of these three relations, the third can be derived. A question is which of these is more fundamental. The inherent problem with making this assessment is that it comes down to how one identifies the more fundamental of relations that really address different physics. By Occam's Razor, the more fundamental relation would be one that has the fewest parameters, while accurately and efficiently yielding a luminosity. Thus, the Firmani relation is less fundamental as it uses more parameters for the fit. Of the two

relations that remain, the one that has the most 'utility' will be the one with the least amount of scatter in its calibration curve.

In this chapter, Firmani's results over his small sample of 19 bursts were successfully reproduced. However, when independent values for L_{iso}, E_{peak} and $T_{0.45}$ were substituted in, a substantial broadening occurs around the model. That is, the Firmani relation is not robust on the use of alternative input data. In addition, when the test is extended to a larger sample of 60 bursts, the scatter becomes substantially larger again. Indeed, this scatter is comparable to the scatter in the original $E_{peak} - L_{iso}$ relation. That is, the Firmani relation is not robust for the use of additional bursts. These failures of the Firmani relation have dashed the hopes raised by the tight calibration curves displayed in Firmani et al. (2006). It also suggests that the addition of a duration does not significantly improve the $E_{peak} - L_{iso}$ relation. The larger point of interest is that no duration shows a significant advantage over the $E_{peak} - L_{iso}$. While it might be possible that that a relation involving $\mathcal{T}_{30}/N_{peak}$ might really have a smaller scatter than the Firmani relation, the improvements are small and not significant. This leads to the conclusion that the addition of a duration is not doing enough to improve the $E_{peak} - L_{iso}$ relation to be considered to be a separate luminosity relation.

The conclusion is, therefore, that the Firmani relation is not useful for several reasons: First, the Firmani relation is simply derived by putting together two well-known, simpler, and independent luminosity relations, and thus it has no separate existence. Second, it is not robust for the inclusion of independent input data or for the extension to many more GRBs. Third, the real scatter for the Firmani relation does not live up to the hope generated by the original report, with the scatter being comparable to those of the luminosity relations

from which it is derived. In all, no utility or advantage can be gained in using the Firmani relation.

5. How Accurately Is E_{peak} Being Measured?[1]

5.1 Introduction

E_{peak} , the peak of the νF_ν power spectrum from the prompt emission of a long-duration GRB, is one of the most important quantities measured from a GRB. GRB spectra are essentially smoothly broken power laws with no sharp features (Band et al. 1993),

$$\frac{dN}{dE} = \begin{cases} A \left(\frac{E}{100\,keV}\right)^{\alpha} e^{\frac{-E(2+\alpha)}{E_{peak}}} & : E \leq \frac{\alpha-\beta}{2+\alpha} E_{peak} \\ A \left(\frac{(\alpha-\beta) E_{peak}}{100\,keV(2+\alpha)}\right)^{\alpha-\beta} e^{\beta-\alpha} \left(\frac{E}{100\,keV}\right)^{\beta} & : E \geq \frac{\alpha-\beta}{2+\alpha} E_{peak} \end{cases} . \quad (5.1)$$

Where A is a constant, and α and β are the low and high energy spectral indices respectively. Thus, the E_{peak} value is the primary description of the entire spectrum. Observed E_{peak} values typically range from a few keV to over a few MeV (e.g. Barraud et al. 2003; Kippen et al. 2003; Schaefer 2003a; Sakamoto et al. 2005; Sakamoto et al. 2008a). This distribution is single-peaked (from 20-2000 keV) and fairly narrow (Mallozzi et al. 1995). It is unclear how X-Ray Flashes (XRFs) fit into this distribution. Two good examples of XRFs contribution to the distribution can be seen in Figure 7 of Sakamoto et al. (2005) and Figure 4 of Pélangeon et al. (2008). In both these figures, there is a small marginally-significant secondary peak composed of XRFs. It is not yet clear whether this is a separate peak or merely an extended tail from the originally found GRB distribution (as seen in Mallozzi et al. 1995).

Through the luminosity relations, the distances of GRBs can be determined without relying on spectroscopic redshifts, which offers a means for estimating the luminosity and hence

[1]This chapter is largely taken from an article that appeared in The Astrophysical Journal, and is reproduced with permission of the AAS(see Appendix A for details).

redshift for the $\sim 70\%$ of bursts with no measured spectroscopic redshift. In comparison with spectroscopic redshifts, the GRB luminosity relations have the big disadvantage of providing relatively poor accuracy, but they have the big advantages of providing unbiased redshifts for almost all bursts for demographic purposes (Xiao & Schaefer 2011) and of providing independent luminosity distances for Hubble Diagram purposes (Schaefer 2007).

A variety of different problems have been raised regarding the luminosity relations, many of which focus on one specific relation or another. For example, the Amati relation has an ambiguity when the measured properties are used to determine the redshift (Li 2007; Schaefer & Collazzi 2007; Chapter 3), the Ghirlanda relation can only be applied to the small fraction of bursts with a known jet break, the identification of jet breaks has become confused when the X-ray afterglow light curves are considered (Melandri et al. 2008), the 'variability' relation suffers from issues tied to how variability is defined (Schaefer 2007), and the number-of-peaks relation only provides a limit on the luminosity (Schaefer 2007). Another proposed luminosity relation (Firmani et al. 2006) has been shown to provide no improvement upon previously existing ones, and indeed can be directly derived from the prior luminosity relations (Collazzi & Schaefer 2008; Chapter 4). In addition, a variety of new luminosity relations have been proposed and have yet to be extensively tested (e.g. Dainotti et al. 2008; 2010; 2010). These various problems can be well handled, mainly by the careful use of the relations and their input.

By far the greatest problem with all the luminosity relations is accuracy. The most accurate of the luminosity relations (the Ghirlanda relation, $E_{peak} - E_{\gamma}$) has an RMS scatter about its calibration line of 0.15 in the log of the luminosity. Meanwhile, the weakest of the luminosity relations (the variability and rise-time relations) have an RMS scatter about their calibration lines of 0.45 in the log of their luminosity. When the resultant luminosities for the

relations for a single burst are combined as a weighted average, the average uncertainty is 0.26 in log-luminosity (Schaefer 2007). This translates into an average one-sigma error in distance modulus (σ_μ) of 0.65 mag. This error is greatly larger than those from optical spectroscopy, yet this poorer accuracy is fine for many GRB demographic studies. For Hubble diagram work, the community will compare the $\sigma_\mu = 0.65$ mag accuracy for GRBs with those of the Type Ia supernovae. For comparison, supernovae have $\sigma_\mu = 0.36$ mag (Perlmutter et al. 1999), $\sigma_\mu = 0.29$ mag even after heavy selection to create the 'gold sample' (Riess et al. 2004) and $\sigma_\mu > 0.25$ mag from the Supernova Legacy Survey (Astier et al. 2006). For some sort of an average of $\sigma_\mu \approx 0.30$ mag for supernovae, one can see that a single GRB has an accuracy that is 2.1× worse than that of a single supernova. This is much better than some people might expect. For Hubble diagram work, GRBs provide unique information on the expansion history of the Universe for redshifts from 1.7 to 8.2.

A primary task for the GRB community is to substantially improve the accuracy of the luminosity relations. Some of the scatter in the current calibration might be caused by apparently random fluctuations in the source resulting in variations of the burst luminosity even for bursts with identical measured indicators. Another source of scatter might be that the luminosities and the indicators cannot (or have not) been measured with sufficient accuracy. That is, the scatter in the luminosity relations might owe part of its scatter to systematic uncertainties in the luminosity indicators. However, it is not entirely clear how scatter in E_{peak} will effect the scatter in the associated luminosity relations. This is largely because a error in finding E_{peak} will also result in a mis-calculation of the factors used in the associated luminosities, E_γ, L_{iso} and E_{peak} Therefore, it is difficult to quantify just how much the scatter in finding E_{peak} will scatter the luminosity relations. Nonetheless, it is clear that

understanding just how much scatter there is in the measurement of E_{peak} is important to work on luminosity relations.

The LSU GRB group has been closely evaluating and optimizing the various luminosity relations (e.g., Schaefer & Collazzi 2007; Collazzi & Schaefer 2008, Xiao & Schaefer 2009), so a program has been started to evaluate the real total uncertainties in the various luminosity relations. The E_{peak} quantity is the most prominent luminosity indicator (and of high importance for many other applications), so it will be the focus of this study. The chapter begins by studying the sources of uncertainty that arise in measuring E_{peak}. This goes beyond the usual measurement errors derived from Poisson statistics as reported in all papers, and all the various sources of systematic errors must be looked at. Three sources of uncertainty are quantified overall, with the primary tool being the comparison of multiple independent published values of E_{peak} reported for the same bursts.

5.2 Types of Uncertainty in E_{peak}

When a burst occurs, there are a variety of ways in which uncertainty is added. The most familiar source of uncertainty is the ordinary Poisson variations in the number of photons that appear in each energy bin, resulting in random variations in the measured E_{peak}. This statistical error ($\sigma_{Poisson}$) is what is reported in the literature when values of E_{peak} are given.

A second issue that arises in determining E_{peak} is the various choices that are made by the analyst. These choices include the exact time and form of the background light curve, the exact time interval over which to accumulate the spectrum, the energy range for the spectral analysis (which is often smaller than the full range of the instrument), and even the convergence criteria for the fit. Identical burst data can be fit by two independent analysts with two entirely different (yet reasonable) sets of choices, resulting in different E_{peak} values.

Neither of these values can be identified as being right or wrong, nor can one know which one is better. Therefore, this difference between the two is a type of uncertainty, $\sigma_{\rm Choice}$.

A third source of uncertainty comes from not knowing the detector response perfectly, which can be characterized as imperfect calibration of the detector response matrix. These errors will be identified as $\sigma_{\rm Det}$. Another component of $\sigma_{\rm Det}$ is the energy range of different detectors. Two satellites can yield different values for $\rm E_{peak}$ merely as a result of covering different energy ranges. This would occur when one satellite gets a better profile of the 'turnover' of the spectral profile than another.

The final source of uncertainty is related to the specific definition of $\rm E_{peak}$. While, at first glance, the $\rm E_{peak}$ has a simple definition, there are actually a variety of alternatives that are commonly used. Each of these definitions produces a different value, and this appears as a systematic uncertainty, which is labeled $\sigma_{\rm Def}$. Four alternative definitions can be pointed to: (1) The GRB spectrum can be fit either to the Band model, a smoothly broken power law (Band et al. 1993) or to the 'Comptonized Power Law' model, a power law times an exponential cutoff. (2) The GRB spectrum can be extracted for the entire burst (a 'fluence spectrum') or for just the time of the peak flux. The fluence spectrum is relevant to the Amati and Ghirlanda relations (which use the burst fluence), while the peak flux is relevant for the other relations (which use the burst peak luminosity). Problems with the use of the peak spectrum are that the number of photons are usually low (leading to poor accuracy) and that the time range for extracting the spectrum is not defined (leading to variations due to the choice of interval). $\rm E_{peak}$ varies substantially throughout most bursts (e.g. Ford et al. 1995), so the choice of the time interval makes for large uncertainty. (3) The high -energy and low-energy power law indices for the Band function can either be fitted to the spectrum or they can be set to average values. When the spectrum does not extend much

above E_{peak}, many analysts will simply set the high-energy index equal to some average. This common practice leads to systematically different E_{peak} values. (4) The analyst might define the E_{peak} value based on traditional frequentist method, or they might impose various priors within a Bayesian method. Depending on the adopted priors, the Bayesian method can give greatly different values than the frequentist method.

The luminosity relations are all expressed as power laws, which is appropriate for the physical derivations of the relations, and the various errors are multiplicative. Therefore it is best to consider the logarithm of the relevant quantities, for example, $\log(E_{peak})$. The *total* measurement uncertainty of $\log(E_{peak})$ will be labeled as σ_{Total}. Therefore, as the individual errors are additive on a logarithmic scale, the total error will be:

$$\sigma^2_{Total} = \sigma^2_{Poisson} + \sigma^2_{Det} + \sigma^2_{Choice} + \sigma^2_{Def}. \tag{5.2}$$

The task is now to derive σ_{Total} by determining the remaining three sources of individual errors (as $\sigma_{Poisson}$ is already reported in the literature).

The general procedure for isolating the various sources of errors will be to compare two measured E_{peak} values, $E_{peak,1}$ and $E_{peak,2}$, that have identical conditions except for some difference. This difference is quantified as:

$$\Delta = \log_{10}(E_{peak,1}) - \log_{10}(E_{peak,2}). \tag{5.3}$$

In general, Δ will be evaluated for various sets of bursts, for example with the values from one source all being denoted with the subscript '1' and some other source being denoted with the subscript '2'. With many measures of Δ, the average will generally be near zero and there will be some RMS scatter, denoted as σ_Δ. The scatter of the Δ values will be a measure of the uncertainty arising from the differences in the input.

5.3 Specific Examples

The essence of the problem and of this method comes from a comparison of E_{peak} values as reported for many different satellites, analysts, and models. In this chapter, the analysis will highlight abstract statistics for which it is easy to lose the real picture that the published E_{peak} values have much larger scatter than expected from statistical errors alone. Below, four specific examples of GRBs are provided. In some cases, e.g. Butler et al. (2007), the reported error bars had to be converted from their stated 90% confidence values into their standard one-sigma values. Therefore, all uncertainties below are at the one-sigma level.

GRB 910503 (BATSE trigger 143) was one of the brightest bursts seen by BATSE. Independent reports on E_{peak} give 466 ± 4 keV (Band et al. 1993), 741± keV (Schaefer et al. 1994), 621 ± 11 (Yonetoku et al. 2004), and 586 ± 28 (Kaneko et al. 2006). All of these values have small statistical error bars, and all are separated from each other by much more than these error bars. All these measures use identical data and models, so the wide divergence must be due to specific choices made by the individual analyst. The $\log_{10}(E_{peak})$ values are 2.668 ± 0.004, 2.87, 2.793 ± 0.008, and 2.768 ± 0.021. The RMS scatter is 0.083 (which is greatly larger than all the $\sigma_{\rm Poisson}$ values), which should equal to $\sigma_{\rm Choice}$ for this one burst.

GRB 911109 (BATSE trigger 1025) is a burst near the BATSE median brightness level for which five independent measures of E_{peak} are found. Band et al. (1993) give 114 ± 3 keV, Schaefer et al. (1994) give 125 keV, Yonetoku et al. (2004) give $153.2^{+7.5}_{-7.1}$ keV, Kaneko et al. (2006) give 131 ± 6 keV, and Nava et al. (2008) give 117 ± 74 keV. Again,a scatter greatly larger than the quoted error bars is seen. For this one burst, the RMS scatter gives $\sigma_{\rm Choice} = 0.05$.

GRB 050525A was a very bright burst detected by four instruments. *Swift* data gives $78.8^{+2.4}_{-1.8}$ keV (Blustin et al. 2006), $82^{+2.4}_{-1.8}$ (Sakamoto et al. 2008a), $82^{+2.4}_{-1.8}$ keV (Butler et al.

2007), 81 ± 3 keV with a Bayesian analysis (Butler et al. 2007), and $102.4^{+4.8}_{-4.0}$ keV for a time interval including only the peak of the burst (Blustin et al. 2006). The first three of these values from *Swift* are found using identical models and data, so the variations can only arise from analyst choices, which for a very bright burst will have relatively small effect on the spectrum. (In particular, it does not really matter what the choices for the background fit are because the background is so small compared to the burst flux. Also, with a very bright burst, the start and stop times are well defined so that analyst choices will be very close.) Nevertheless, two separate analyses of the identical data from INTEGRAL IBIS data gives either 69 ± 72 (Foley et al. 2008) or 58^{+29}_{-21} keV (Vianello et al. (2009), with these values not being so close. For measures with other instruments, INTEGRAL SPI data gives 80 ± 28 keV (Foley et al. 2008), and *Konus* data gives 84.1 ± 1.7 keV (Golenetskii et al. 2005a).

GRB 070508 was a bright burst detected by four satellites. *Konus* data gives 188 ± 5 keV (Golenetskii et al. 2007), *Suzaku* data gives 233 ± 7 keV (Uehara et al. 2007), and RHESSI data gives 254^{+43}_{-27} keV (Bellm et al. 2007). These values are inconsistent with any constant, implying that there must be additional systematic uncertainties past the reported statistical error bars. E_{peak} values have also been reported many times for *Swift* data, with the first circular giving 258 ± 80 keV (Barthelmy et al. 2007), the Sakamoto et al. (2008a) catalog giving 260^{+122}_{-41} keV, an independent analysis giving 210^{+48}_{-24} keV (Butler et al. 2007), a Bayesian analysis giving 208^{+46}_{-25} keV (Butler et al. 2007), while a joint fit of the *Swift*-plus-*Suzaku* data gives 235 ± 12 keV for the Band function or 238 ± 11 for the CPL (Comptonized Power Law) function (Krimm et al. 2009). The first four *Swift* values all use identical data and models, yet still the uncertainty for this bright burst runs from 210-260 keV. Looking at all the reports, if there were a 'vote on the truth' with an average, the guess would be $E_{peak} \sim 230$, with this being dominated by the three 'votes' controlled by the *Suzaku* data.

For all nine published values, a realistic analysis could take the E_{peak} to be anywhere from roughly 190 to 260 keV. And this is for a *bright* burst where all the problems are minimized.

5.4 Typical $\sigma_{\rm Poisson}$

Ordinary Poisson fluctuations of the counts in each spectral energy bin result in an apparently random noise, which will somewhat shift the fitted E_{peak} value. This statistical uncertainty can be reliably calculated by keeping track of the counts and applying Poisson statistics, with the resulting uncertainties confidently propagated. Most of the reported E_{peak} values in the literature have reported error bars, and these are always from Poisson statistics alone. These reported error bars are cast into log-base-10 and are labeled $\sigma_{\rm Poisson}$.

The Poisson errors change greatly from burst to burst. At one extreme for a very bright burst, GRB050525A has $E_{peak} = 82^{+2.4}_{-1.8}$ keV (Sakamoto et al. 2008a), with this being converted to $\log_{10}(E_{peak}) = 1.91 \pm 0.01$. At the other extreme are faint bursts with only poor constraints, for example BATSE trigger 658 with $E_{peak} = 70 \pm 56$ keV (Nava et al. 2008), with this being converted to $\log_{10}(E_{peak}) = 1.85 \pm 0.35$. This chapter uses error bars on the log-base-10 of E_{peak}, where ± 0.01 corresponds to a 2.3% error in E_{peak}, ± 0.10 corresponds to a 23% error, and ± 0.30 corresponds to a factor of two error.

Collections of bursts with a wide range of individual error bars will have a much more restricted range of average error bars. From 306 BATSE bursts, Kaneko et al. (2006) have error bars with average $\sigma_{\rm Poisson} = 0.04$. From 37 *HETE*-2 bursts, Sakamoto et al. (2005) have the average $\sigma_{\rm Poisson} = 0.17$. From 9 INTEGRAL bursts (after excluding two with very large quoted error bars), Foley et al. (2008) have the average $\sigma_{\rm Poisson} = 0.35$. From 32 *Swift* bursts, Sakamoto et al. (2008a) have the average $\sigma_{\rm Poisson} = 0.08$.

An annoying problem is that recently some satellite programs have taken to reporting 90% error bars rather than the universal standard one-sigma error bars. This creates a problem when comparing the error bars with standard results or in doing any sort of statistical analyses. The general solution is to assume that the error distribution is Gaussian in shape and to multiply the quoted error bars by 0.61 so as to produce one-sigma values. Nevertheless, this practice still has to be remembered every time, and occasionally the writer (e.g., Krimm et al. 2009) does not tell the reader that 90% error bars are used.

A complexity arises with many measured E_{peak} values having asymmetric error bars, usually with the uncertainty towards high energy being much larger than the uncertainty towards lower energy. This arises when E_{peak} is near the upper end of the spectrum. To illustrate this with an extreme example, consider a spectrum that shows a power law with a small amount of curvature up to a cutoff of 300 keV, in which case one can say that the E_{peak} value is near 300 keV with a small uncertainty to low energies and an unlimited uncertainty to high energies. This case arises frequently for the *Swift* satellite due to its fairly low energy cutoff. The general solution is the tedious one of carrying asymmetric error bars for all quantities derived from the E_{peak} values.

5.5 Quantifying $\sigma_{\rm Choice}$

If two separate analysts independently report their E_{peak} values, for the same burst as measured from the same satellite, with the exact same Poisson noise, using the same model, then the only difference is from the choices made by the analysts, $\sigma_{\rm Choice}$. Once a pairing of this kind is identified, for each burst the two analysts have in common, Δ is the logarithmic difference in the values the two analysts measured the burst. The result of this will be a list of Δ values for the comparison pairs. From here, a simple calculation of the standard

deviation of the Δ values will equal σ_Δ. This scatter of Δ arises from the differences in the two individual sets of choices, so the uncertainty due to a single set of choices would simply be given by:

$$\sigma_{\rm Choice} = \frac{\sigma_\Delta}{\sqrt{2}}. \tag{5.4}$$

The procedure is then to find published analyses which report $E_{\rm peak}$ values for many identical bursts all using the exact same data from some satellite, to calculate a list of Δ values, and finally to calculate $\sigma_{\rm Choice}$ from equation 5.3. With this, the ordinary variations in $E_{\rm peak}$ caused by analysis choices will be attributed equally between the two analysts.

For the BATSE era, values from Band et al. (1993), Yonetoku et al. (2004), Kaneko et al. (2006), and Nava et al. (2008) can be compared. For example, BATSE trigger 1025 has reported $E_{\rm peak}$ values of 114, 153, 131, and 117 keV for the four sources, while trigger 451 has 40, 134, and 143 keV for the first three sources respectively. For the BATSE era, the results are presented in Table 5.1. The Kaneko-Yonetoku pair has the lowest scatter, which is about half that of the Band-Kaneko pairing and about a quarter of that of the Band-Nava pairing. This indicates that the choices made by Kaneko and Yonetoku are typically more alike than the choices made by any other pair. No one analyst can be identified as producing better be results.

For the *Swift* era, there is just the one pairing to consider, the published values of Sakamoto et al. (2008a) and Butler et al. (2007). Here, the Butler values of $E_{\rm peak}$ that were derived from frequentist statistics were used, as that is what Sakamoto used in obtaining his values. 23 common bursts are found for use in this pairing, resulting in $\sigma_{\rm Choice} = 0.04$. One possible reason for this *Swift* $\sigma_{\rm Choice}$ being much smaller than the BATSE values (see Table 5.1) is that the coded mask of *Swift* eliminates the uncertainties in the background subtraction.

Table 5.1. $\sigma_{\rm Choice}$ in the BATSE Era [a]

	Yonetoku[c]	Band[d]	Nava[e]
Kaneko[b]	0.07 (75)	0.15 (11)	—
Yonetoku[c]	—	0.21 (34)	0.14 (62)
Band[d]	—	—	0.29 (5)

[a]The values reported in this table are $\sigma_{\rm Choice}$, which are the uncertainties in $\log_{10}{\rm E_{peak}}$ due to the particular choices made by *one* analyst. The following number in parentheses is the number of common bursts that were used for the calculation.

[b]Kaneko et al. (2006)

[c]Yonetoku et al. (2004)

[d]Band et al. (1993)

[e]Nava et al. (2008)

To further illustrate the effects of $\sigma_{\rm Choice}$, see Figures 5.1 and 5.2, which display two of the comparison sets with the BATSE data. Figure 5.1 plots $E_{\rm peak}$ from Yonetoku et al. (2004) vs. Kaneko et al. (2006). Figure 5.2 plots $E_{\rm peak}$ from Yonetoku et al. (2004) vs. Nava et al. (2008). In both cases, bursts are represented with a diamond with their associated error bars. A solid line is plotted in each of these figures to represent where the bursts should lie in an ideal world (i.e. in total agreement). As described earlier, in these data pairs the only difference in the analysis is the choices made by the analysts.

There is a significant scatter on the value of $E_{\rm peak}$ that can be attributed purely to the choices analysts make in deriving these values. Six different values of $\sigma_{\rm Choice}$ have now been calculated; 0.07, 0.15, 0.21, 0.14, 0.29, and 0.04. The $\sigma_{\rm Choice}$ can vary by up to a factor of six. For any analyst, only the average can be used. A simple average is 0.15. Likely, a better representation is the weighted average where the weights equal the number of bursts, for which the result is $\sigma_{\rm Choice} = 0.12$. This typical value of $\sigma_{\rm Choice}$ is daunting in size. For an example with $E_{\rm peak} = 100$ keV, the one-sigma range (from $\sigma_{\rm Choice}$ alone) would be from 76-132 keV, which is nearly a factor of two in total size.

5.6 Measuring $\sigma_{\rm Det}$

$\sigma_{\rm Det}$ is the uncertainty associated with three particular problems related to the detector response. The first of these issues is associated with imperfect knowledge of the detector response. The second issue is how the energy ranges of various detectors are different and thus could yield different values for $E_{\rm peak}$. A third issue lies in the detector thresholds in that bursts for which the peak energy is just above the detector threshold will have ill defined spectral indices and therefore will not be well measured. In principle, this can be measured by comparing $E_{\rm peak}$ values for measures of individual bursts with different detectors. Care

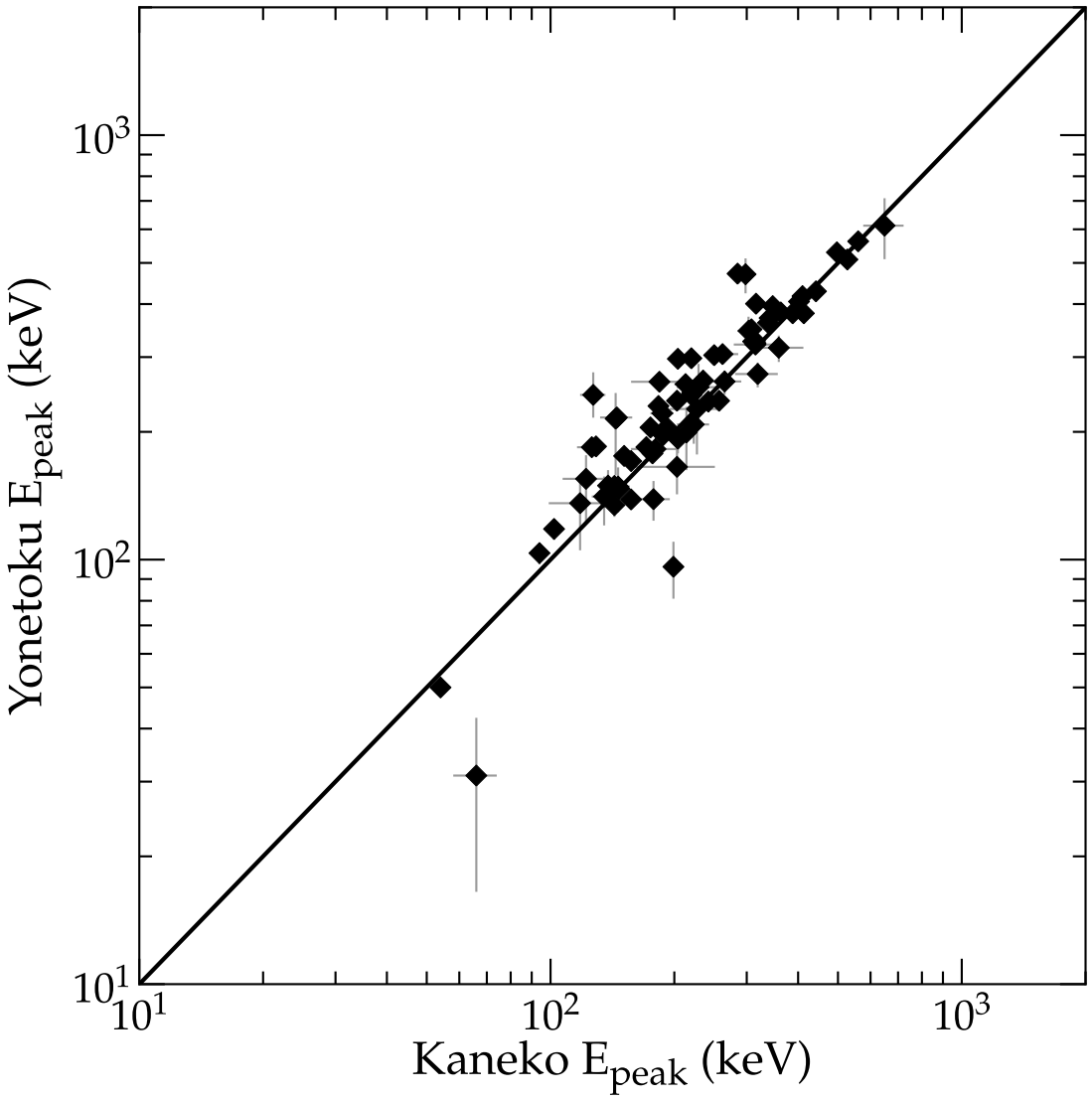

Figure 5.1 A visualization of the scatter in E_{peak} due to σ_{Choice} alone. Plotted are BATSE bursts (diamonds) as measured by two groups of analysts - Yonetoku et al. (2004) vs. Kaneko et al. (2006). The solid line denotes the ideal case where both groups would be in complete agreement. The scatter about the diagonal line is σ_{Choice}, and the point of this figure is that there is significant scatter even for identical bursts, identical Poisson noise, and identical data.

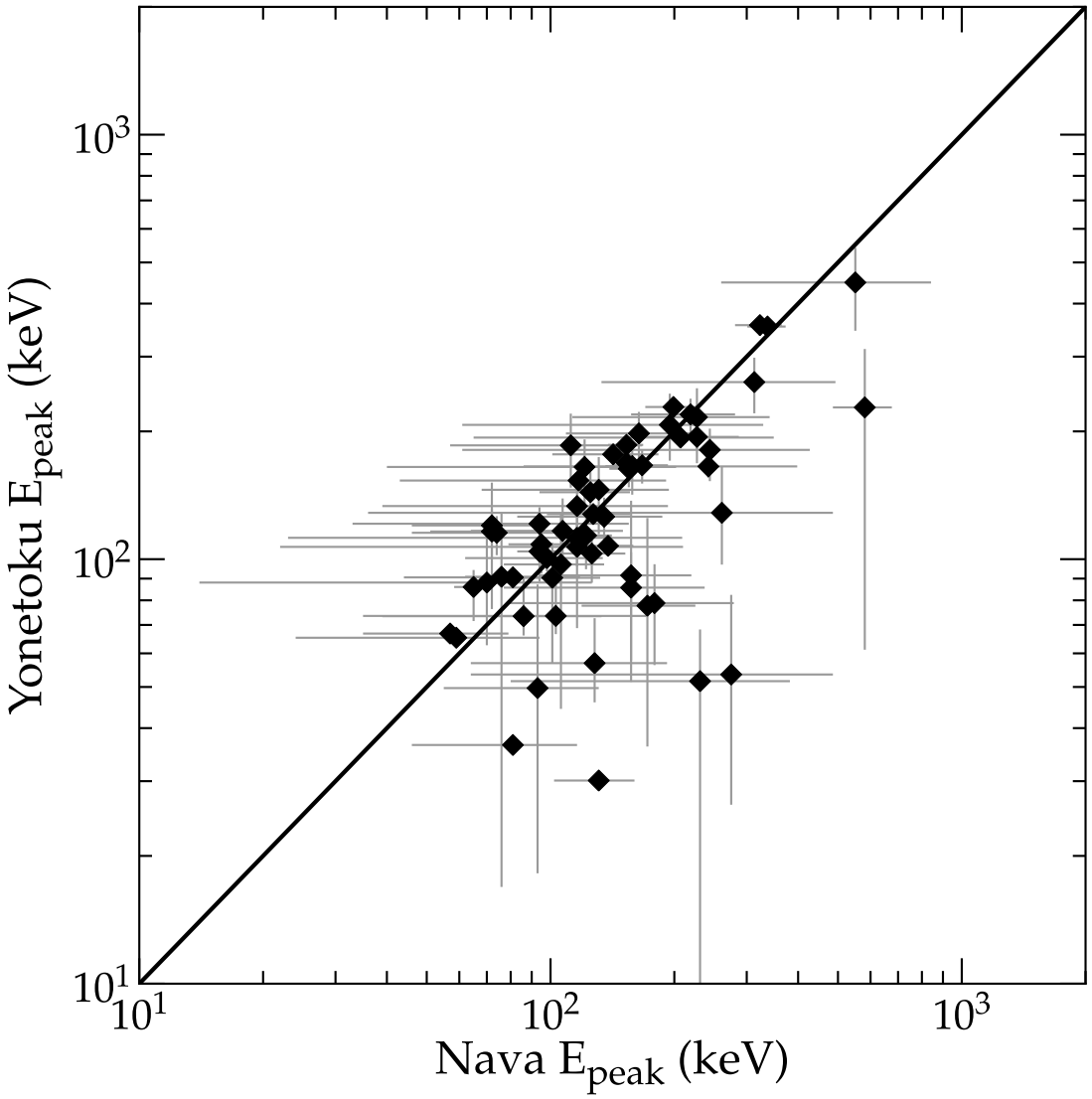

Figure 5.2 Another visualization of the scatter in E_{peak} due to σ_{Choice} alone. Plotted are compare BATSE bursts (diamonds) as measured by two groups of analysts - Yonetoku et al. (2004) vs. Nava et al. (2008). The solid line denotes the ideal case where both groups would be in complete agreement. The two analysts compared identical bursts, with identical data, and with identical models; so the large scatter about the diagonal proves that individual unrecorded choices by the analysts have a large effect on the reported E_{peak} .

must be taken that these compared values were made over the whole time interval of the burst and with an identical model. The procedure is to tabulate Δ values for many bursts observed with pairs of satellites, with the RMS scatter of Δ being related to $\sigma_{\rm Det}$. The statistical error bars ($\sigma_{\rm Poisson}$) for each measure are known and can be accounted for. In principle however, the effects of $\sigma_{\rm Choice}$ and $\sigma_{\rm Det}$ cannot be separated out. So what can be taken from this comparison of $\rm E_{peak}$ values from different detectors is just the combined uncertainty, $\sigma_{\rm Sat} = \sqrt{\sigma^2_{\rm Choice} + \sigma^2_{\rm Det}}$.

The uncertainty in each Δ comes from the statistical uncertainty for each satellite and the σ_{Sat} for each satellite;

$$\sigma^2_{\Delta} = \sigma^2_{\rm Poisson,1} + \sigma^2_{\rm Poisson,2} + \sigma^2_{\rm Sat,1} + \sigma^2_{\rm Sat,2} \tag{5.5}$$

Where the numbers in the subscripts identify the two satellites. In practice, the separate systematic effects of the two detectors can not be distinguished, so all that can be done is to take $\sigma_{\rm Sat}$ as the average of the two satellites.

The Δ values will be for bursts with a wide range of statistical errors, with each individual value being a Gaussian distribution with standard deviation of

$$\sigma_{\Delta} = \sqrt{\sigma^2_{\rm Poisson,1} + \sigma^2_{\rm Poisson,2} + 2\sigma^2_{\rm Sat}}. \tag{5.6}$$

So the quantity Δ/σ_{Δ} should be distributed as a Gaussian with a standard deviation of unity. The procedure is to vary $\sigma_{\rm Sat}$ until the RMS scatter of Δ/σ_{Δ} equals 1.

Published $\rm E_{peak}$ values for many bursts as measured by many satellites that were collected. Pairs of measures for individual GRBs that have identical models and that cover the entire time interval of the burst were identified. For each pair of satellites, $\sigma_{\rm Sat}$ was calculated such that the Δ/σ_{Δ} values have an RMS of unity. These values are given in Table 5.2. Two effects should be considered when viewing these results. First, the entire second column,

involving *Swift* - *Suzaku* and either *Swift* or *Suzaku* , involves joint data in the comparison, so the differences in the two E_{peak} values will be smaller than if the two spectra were totally independent. Thus these two values will not be used in evaluating an overall average σ_{Sat}. Second, whenever a small number of bursts are involved, random fluctuations in E_{peak} will lead to large variations in σ_{Sat}. To take an extreme example, if only one burst is considered and the two measures are randomly close together, then the σ_{Sat} value will be near zero. Indeed, for the entire right-hand column of Table 5.2, with all entries coming from 2-4 GRBs, all entries are at the extremes of the range. These three entries have a total of 9 comparisons, which when combined, form a single σ_{Sat} involving RHESSI versus other satellites, with this value being 0.14.

So there are now a number of values for σ_{Sat}, one from the *Suzaku* column, three from the *Konus* column, and one combined value for RHESSI. These values range over a factor of two, from 0.08 to 0.16. A straight average of these five measures is 0.13. A weighted average involving the number of bursts in each measure yields 0.12. This last value is taken to be characteristic and average for a wide range of detectors and analysts.

Therefore, the conclusion is that the global average $\sigma_{Sat} = 0.12$ and $\sigma_{Choice} = 0.12$. Formally, this implies that $\sigma_{Det} = 0$, but the only readily available conclusion is that σ_{Det} is negligibly small. This provides confidence that the detector calibrations are well done. In other words, the systematic differences from satellite to satellite are negligible, whereas the often-large differences from satellite to satellite are apparently caused simply by the ordinary choices made by the individual analysts.

Table 5.2. $\sigma_{\rm Sat}$ in the *Swift* Era[a]

	Suzaku[c]	*Swift* - *Suzaku*[d]	*Konus* -Wind[c]	RHESSI[c]
Swift[b]	0.15 (7)	0.04[e](8)	0.16 (13)	—
Suzaku[c]	—	0.03[e](11)	0.08 (23)	0.18 (3)[f]
Swift - *Suzaku*[d]	—	—	0.12 (23)	0.02 (2)[f]
Konus -Wind[c]	—	—	—	0.18 (4)[f]

[a]The values reported in this table are $\sigma_{\rm Sat}$, which are the one-sigma uncertainty of $\log_{10}(\rm E_{peak})$ for the combined causes of uncertainties in one detector response and one analyst's choices. The following number in parentheses is the number of common bursts that were used for the calculation.

[b]Sakamoto et al. (2008) and Butler et al. (2010)

[c]Multiple GCNs

[d]Krimm et al. (2009)

[e]This entry is a comparison between composite spectra from *Swift* -plus- *Suzaku* versus spectra from one part of that composite. So the resulting $\rm E_{peak}$ values are not independent, as the joint part will share identical data, identical Poisson noise, and identical detector response measures. As such, the Δ values will be systematically smaller, and hence $\sigma_{\rm Sat}$ will be smaller than expected for the case where the input data was completely independent.

[f]RHESSI comparisons have small number statistics, so the three measurements are combined in a weighted average to get one singular measurement of $\sigma_{\rm Sat} = 0.14$ (9).

5.7 Measuring $\sigma_{\rm Def}$

Previous workers have defined $E_{\rm peak}$ in a variety of different ways, with the resultant variations leading to an uncertainty labeled $\sigma_{\rm Def}$. This definitional uncertainty can be broken into four components: $\sigma_{\rm Model}$ for whether the Band model or the Comptonized power law model is adopted, $\sigma_{\rm Peak?}$ for whether the spectrum is extracted for the entire burst or just the time interval around the peak flux, $\sigma_{{\rm Fixed}\alpha\beta}$ for whether the analyst systematically fixes the high-energy and low-energy power law slopes in the Band function (α and β respectively) to some average value, and $\sigma_{\rm F/B}$ for whether the analyst uses frequentist fitting or uses Bayesian analysis with some set of adopted priors. For each of these, the same approach is taken as was taken with $\sigma_{\rm Choice}$ and divide σ_Δ by a factor of $\sqrt{2}$. The overall uncertainty from these definition issues ($\sigma_{\rm Def}$) will be just the addition in quadrature of the four components as applicable for the question in hand.

The definition of $E_{\rm peak}$ (i.e., the photon energy for the maximum of νF_ν) requires a fit to the spectrum, but it has not specified the functional form for this fit. Most published values are roughly evenly divided between the Band function or the Comptonized power law (CPL). There is a systematic offset in how $E_{\rm peak}$ is measured in that the CPL model consistently predicts a higher $E_{\rm peak}$ than the Band model (see Figure 6 of Krimm et al. 2009). This offset is expected, because the CPL falls off much faster than the Band function at high energies, so the CPL fit must push $E_{\rm peak}$ to higher energies to match the observed spectra. To measure this difference in $E_{\rm peak}$ for a typical ensemble of GRBs, the results from Krimm et al. (2009) are used, where the *Swift*-plus-*Suzaku* spectra are fitted to both the Band function and the CPL. In all, Δ values is calculated for 67 bursts. The average Δ is 0.14, while $\sigma_{\rm Model} = 0.12$.

The definition of $E_{\rm peak}$ does not state the time interval over which the spectrum is to be extracted. Indeed, the $E_{\rm peak}$ values change fast throughout the entire burst, so there is a

big problem in knowing what interval to use. A unique solution is to take the entire burst. This has the advantage of getting the best signal-to-noise ratio for the spectrum (unless the burst is not sufficiently above the background). A spectrum from the entire burst (the fluence spectrum) makes logical sense for use with the Amati and Ghirlanda relations, both of which connect with the burst fluence. An alternative solution is to use the E_{peak} value for the time interval around the time of the peak flux in the burst light curve. This solution is logical for all the other luminosity relations that connect with the burst peak luminosity, as then both the E_{peak} and luminosity will correspond to the same time and physics. An ambiguity arises in specifying the duration of the interval, where this interval might be constant, scale with the (perhaps unknown) redshift, or scale with the burst or pulse duration. The point is that alternative solutions will lead to a systematic variation in E_{peak} , and this uncertainty will be labeled as $\sigma_{\rm Peak?}$. To evaluate this, the results taken by Krimm et al. (2009) are taken for 28 GRBs as measured by *Swift* -plus- *Suzaku* . For these bursts, they report E_{peak} for the Band function for both the entire burst as well as a tight interval centered on the peak in the light curve, and for these the Δ and total $\sigma_{\rm Poisson}$ values were calculated. As in section 5.6, one calculates $\sigma_{\rm Peak?}$=0.06.

The definition of E_{peak} can use the Band model with or without fixed high-energy and low-energy power law slopes, and this change of definition will lead to a variation labeled as $\sigma_{{\rm Fixed}\alpha\beta}$. In general, the Band function is fitted with both α and β as free parameters. However, in practice, spectra rarely extend far past E_{peak} which provides little constraint on β. This is often solved by simply setting the power law slope equal to some average value. The original paper on the Band function (Band et al. 1993) provides 53 bursts with alternative fits where the slopes are allowed to vary freely or are fixed at $\alpha = -1$ and $\beta = -2$. The values of Δ were calculated for these bursts. The average Δ is -0.07 while the RMS

scatter is 0.21. This average is marginally different from zero in the sense that the fixed-slope values are larger than the values with freely-fitted-slopes. In all, $\sigma_{\mathrm{Fixed}\alpha\beta} = 0.15$.

The usual definition of $\mathrm{E_{peak}}$ relies on frequentist methods (i.e, chi-square minimization of spectral models), whereas another possibility is to use Bayesian methods. The Bayesian approach explicitly assumes sets of priors, where each prior quantifies the likely distribution of values. This Bayesian method has been used in only one paper (Butler et al. 2007), and unfortunately, this paper made a variety of poor assumptions for the priors. Most importantly, they assumed that the probability of the $\mathrm{E_{peak}}$ values above 300 keV falls off fast as a log-normal distribution, and this means that the bursts with high $\mathrm{E_{peak}}$ values will have their values pushed to greatly lower energy. The fallacy of this assumption is demonstrated by a comparison of their $\mathrm{E_{peak}}$ values with those from *Suzaku* , *Konus* and RHESSI. For example, GRB 051008 has a measure of $\mathrm{E_{peak}} = 266^{+349}_{-80}$ keV from Butler et al. (2007), while *Konus* reports 865^{+107}_{-81} keV (Golenetskii et al. 2005b), *Suzaku* reports 1167^{+1078}_{-427} keV (Ohno et al. 2005), and *Swift* -plus- *Suzaku* reports 815^{+54}_{-47} keV (Krimm et al. 2009). Of the 11 *Konus* GRBs with $\mathrm{E_{peak}} > 600$ keV, all 11 Butler et al. (2007) values are smaller (whereas only half should be smaller if the Bayesian prior was reasonable), with typical errors of a factor of 2. Another mistaken prior is that they assume the β values to follow a simple exponential distribution, with the result being to push the β values greatly negative (making for a claimed high-energy cutoff that is too sharp hence pushing $\mathrm{E_{peak}}$ to larger values). Butler et al. (2007) give fitted $\mathrm{E_{peak}}$ values by both frequentist and Bayesian methods for the exact same data for many bursts, and for each of these there is a calculated Δ value. For 75 bursts for which the frequentist methods return a value instead of a limit (i.e., the case where the troubles with the priors are minimized), the RMS of Δ is 0.07, and this is the value of $\sigma_{\mathrm{F/B}}$.

Measures of $\sigma_{\rm Model} = 0.12$, $\sigma_{\rm Peak?} = 0.06$, $\sigma_{\rm Fixed\alpha\beta} = 0.15$, and $\sigma_{\rm F/B} = 0.07$ are now in hand. In a situation where all four uncertainties are operating fully, the total uncertainty caused by the variations in the definition would be the sum in quadrature of the four components, with $\sigma_{\rm Def} = 0.21$. This would correspond to a one-sigma uncertainty of a factor of 1.62.

Which of these uncertainties are applicable depends critically on the situation. Here are four typical situations, each with different answers: (1) If one is trying to compare an observed $\rm E_{peak}$ value with some measure of a particle energy distribution, then it is completely unclear how to connect the two, so a full $\sigma_{\rm Def} = 0.21$ is appropriate. That is, the Band function is a completely empirical description of the turnover in the spectrum, so it is unknown what part of the spectrum corresponds with any point in a calculated theoretical particle distribution. (2) If a Hubble diagram is constructed using luminosity relations where the calibration and bursts all use exactly the same definition, then $\sigma_{\rm Def} = 0$. This might be the case if all the $\rm E_{peak}$ values are pulled from a single paper, or the case if one is anticipating some future program designed for the purpose. (3) If the luminosity function is calibrated with a particular definition but then applied to a set of $\rm E_{peak}$ values with a mixed set of definitions, then the contribution will be only a fraction of its full value. For a data set that involves a fraction 'f' of values made with the alternative definition, the σ value will be $\sqrt{f}$ times the full value. For example, the BATSE $\rm E_{peak}$ values presented in Nava et al. (2008) have $f = 0.31$ of the bursts with fixed α or β, so the result would be $\sigma_{\rm Def} = \sqrt{0.31}\sigma_{\rm Fixed\alpha\beta} \approx 0.08$. (4) If the Amati relation is evaluated with bursts from a wide array of detectors, then the mixed sets of definitions will lead to a partial contributions from the various alternative definitions used. Schaefer (2007) has calibrated the Ghirlanda and

$E_{peak} - L_{iso}$ relations with bursts from BATSE, *Beppo-Sax* , *Konus* , INTEGRAL, and *Swift*, with the estimate being $\sigma_{Def} \approx 0.15$.

The contributions to σ_{Def} change greatly with the question being asked. The contributions will also change substantially with the data set being used. Not only will the fractions 'f' change, but the size of the unmixed contribution will change. For example, $\sigma_{F/B}$ will change greatly with the adopted priors, while $\sigma_{Fixed\alpha\beta}$ will change greatly depending on the adopted power law slopes. In practice, it is impossible to evaluate meaningful error bars for the various contributions, because they change for every circumstance. Therefore, the quantitative measures of the contributions to σ_{Def} in this section can only be taken as approximate or maybe as typical, and each of the definitional alternatives leads to variation with an RMS scatter of roughly 0.1-0.2 (i.e., 23% to 46% errors). Depending on the situation, the resulting σ_{Def} might vary anywhere from 0.0-0.2.

5.8 Are GRBs Thermostated?

The distribution of E_{peak} for GRBs has been observed to be fairly narrow (Mallozzi et al 1995), and thus the intrinsic scatter of E_{peak} must be narrow as well. The observed and intrinsic values of E_{peak} can be related by a simple equation:

$$E_{peak,Obs} = E_{peak,Int} \, (1+z)^{-1} \, \eta \tag{5.7}$$

The observed E_{peak} is related to the intrinsic E_{peak} by the cosmological redshift factor of $(1+z)$. The factor η encompasses all the various effects that lend to the imperfect measure of E_{peak} , with the RMS scatter of $\log \eta$ equaling σ_{Total}. Since these factors are multiplicative, it is more appropriate to evaluate this equation in log space. Therefore, the expression for

the distribution of E_{peak} in log space can be given as:

$$\sigma^2_{\log \mathrm{Ep,Obs}} = \sigma^2_{\log \mathrm{Ep,Int}} + \sigma^2_{\log (1+z)} + \sigma^2_{\mathrm{Total}} \tag{5.8}$$

Many of these values can be quantified from data already in hand. The *Swift* website provides a list of confirmed spectroscopic redshifts from a list can be comprised of $\log_{10}(1+z)$, for which the RMS scatter is 0.19, which is taken to be the typical value of $\sigma_{\log(1+z)}$. Likewise, published data sets can be used to get an estimate for $\sigma_{\log \mathrm{Ep,Obs}}$. The scatter in the log of the observed E_{peak} can be found from Brainerd et al. (1999). In this paper, the authors found the full width half-maximum of the BATSE E_{peak} distribution to be 0.796 in log of the E_{peak} , which equates to a one-sigma scatter of ~ 0.34, which can be used as the value of $\sigma_{\mathrm{Ep,Obs}}$. Putting all these values together yields:

$$\sigma^2_{\log \mathrm{Ep,Int}} = 0.08 - \sigma^2_{\mathrm{Total}}. \tag{5.9}$$

So $\sigma^2_{\mathrm{Total}}$ needs to be 0.08 in order for the intrinsic scatter of E_{peak} to be zero. This equates to a $\sigma_{\mathrm{Total}} \sim 0.28$.

In previous sections, the values that go into σ_{Total} were identified, so expected values for σ_{Total} can be easily calculated and compared to what kinds of σ_{Total} are needed for a 'zero' distribution of E_{peak} in the burst rest frame. $\sigma_{\mathrm{Poisson}}$ is found to have typical values near 0.15 for collections of bursts (with the values for individual bursts varying greatly with the detector and the burst brightness), with an extreme range of 0.04 to 0.35. The average value of σ_{Choice} is found to be 0.12 and σ_{Sat} is found to be 0.12 (so that σ_{Det} is near zero), with extreme values of 0.08 and 0.16. σ_{Def} depends critically on the application, but typical applications might have values of 0.15, with extremes of 0.0 to 0.2. These sources of error are independent, so they should be added in quadrature. For these typical values, the $\sigma_{\mathrm{Total}} = 0.24$, with an extreme range of 0.09 to 0.43. So the σ_{Total} needed for $\sigma_{\log \mathrm{Ep,Int}}$ to

be zero is not only within the expected range of $\sigma_{\rm Total}$, it is a typical value for $\sigma_{\rm Total}$. The value of $\sigma_{\log {\rm Ep,Int}}$ will be small for any realistic value of $\sigma_{\rm Total}$. Even if one were to take a the lowest estimate of $\sigma_{\rm Total} = 0.09$, there would still be a small value of $\sigma_{\log {\rm Ep,Int}} = 0.28$. This means that for the observed distribution of $E_{\rm peak}$ to be as narrow as observed, the intrinsic rest frame distribution of $E_{\rm peak}$ must also be narrow in all cases.

In order to be sure that the choice of $E_{\rm peak,Obs}$ is appropriate, one must be certain that selection effects are not causing a perceived distribution. An example of this is in Sakamoto et al. (2008b), where there are clear cutoffs for different instruments depending on the energy range of a detector's energy threshold. This is why exclusively BATSE data is used to determine this value. In Brainerd et al. (1999), the authors found that the BATSE trigger thresholds did not cause the observed distributions. The X-Ray flashes (e.g. Sakamoto et al., 2005; Pélangeon et al., 2008) are just the tail of the observed classical burst distribution, or at most a small excess out on the tail. Another important part of the findings of Brainerd et al. (1999) is that the detector thresholds are not causing an artificial distribution in the detected bursts. Figure 5.3 of Brainerd et al. (1999) shows a simulated histogram for the detection of bursts for a given power-law distribution of $E_{\rm peak}$. The results show that the distribution of the detection of $E_{\rm peak}$ has roughly the same efficiency on either side. This implies that the narrowness of the BATSE distribution is not being artificially cut off by some sort of systematic effects on the part of the detector threshold. It is for this reason that is reasonable to believe that the BATSE data at the very least shows a real distribution for $E_{\rm peak}$, not an artifact of selection effects. Therefore, the finding of no scatter in the intrinsic $E_{\rm peak}$ distribution is sound.

Another method for showing that the distribution of $E_{\rm peak,Int}$ is small is to use a large sample of data for which there are known bursts across a wide range of known redshifts.

Using the known redshifts, the scatter of $E_{peak,Obs}(1+z)$ can be found directly. In doing this, one of the terms from the earlier method can be, in a sense, removed. The uncertainty found by finding the standard deviation of $E_{peak,Obs}(1+z)$ will instead be quantified as:

$$\sigma^2_{Epeak,Obs(1+z)} = \sigma^2_{Ep,Int} + \sigma^2_{Total}. \tag{5.10}$$

For this purpose, the large data set available in Schaefer (2007) can be used. The RMS scatter of $E_{peak,Obs}(1+z)$ of the whole data set to be 0.47. Adopting a typical value of $\sigma_{Total} = 0.30$, the resulting scatter is found to be $\sigma_{Ep,Int} = 0.37$, which is still a fairly narrow distribution. While it is not as small as the first test showed, it is nonetheless narrow, showing that the one sigma scatter of E_{peak} is merely a factor of ~ 2.

There is also the possibility of mixing bursts from widely different redshifts in the sample. To check this, the Schaefer data are binned up by redshift ranges of 0-1, 1-2, 2-3, and 3-5. The RMS scatter of $E_{peak,Obs}(1+z)$ for these bins is 0.62, 0.40, 0.35 and 0.27 respectively. In addition, a similar test of *Swift* - *Suzaku* data (Krimm et al. 2009) is also applied. For these data, bursts are binned by redshifts 0-1, 1-2, and 2-4. The RMS scatter of $E_{peak,Obs}(1+z)$ for these bins is 0.42, 0.44, 0.24 respectively. With seven different bins, the median value is 0.40. Using the Schaefer (2007) data, that the average value of the log of $E_{peak,Obs}(1+z)$ is found to be 2.23, 2.58, 2.52 and 2.60 for their respective bins, and for the Krimm et al. (2009) data the average value is found to be 2.66, 3.03, 2.89 respectively. Therefore, there are no visible trends with redshift. Indeed, this shows that the average value of $E_{peak,Obs}(1+z)$ is close to 511 keV. This implies that the narrowness of E_{peak} is therefore physical and not the result of selection effects.

With this finding, the obvious question is what is the mechanism driving *all GRBs* to have the same (or essentially the same) intrinsic E_{peak}. With the rest frame E_{peak} values being like the effective temperature of the gamma-ray emitting region, the nearly constant

temperature requires some mechanism to act as a thermostat, holding the temperature at a fixed value. The realization that the rest frame E_{peak} is nearly a constant is new, with this conclusion being simple and forced. The task for the community is now to understand the physical mechanism for this thermostat effect.

The typical values of $E_{peak,Obs}(1+z)$ is nearly comparable to the electron rest-mass energy ($m_e c^2$) of 511 keV. This suggests that the thermostat mechanism involves an equilibrium between electron-positron pair creation and annihilation.

5.9 Implications

The various sources of scatter on E_{peak} have now been identified. $\sigma_{Poisson}$ was found to have typical values near 0.15, although this has a large range of 0.04 to 0.35. The reason for this range is mostly due to the detector and the brightness of the burst. σ_{Choice} is found to be on the same order of σ_{Sat}, 0.12. This indicates that the scatter due to the detector itself, σ_{Det} is small. There is an extreme range of 0.08 and 0.16 for the error due to analyst choices. The uncertainty associated with the definition of E_{peak} depends on the application and a range of 0.0 to 0.2 for σ_{Def}, with a typical value of 0.15. Finally, if these are all put together, σ_{Total} has a range of 0.09 to 0.43. For the typical values, a value of $\sigma_{Total} = 0.24$ should be expected.

One important implication is that there is a real limit on the accuracy with which any E_{peak} can be measured. Even for a very bright burst with a well placed E_{peak}, say with $\sigma_{Poisson} = 0.01$, and some agreed-upon definition (so $\sigma_{Def} = 0$), there will still always be $\sigma_{Total} = \sigma_{Choice} = 0.12$. There is no realistic way to dictate or legislate or even define the 'best' choices by analysts, so this limit cannot be improved. This means that all GRBs must have at least a 28% error in E_{peak}.

A second implication that can come from this result is that E_{peak} has accuracy limits as a luminosity indicator. On an individual basis, this is a valid limitation. Supernovae have a similar limitation, although their real systematic uncertainty for an individual event is 2.1× better than for GRBs. The accuracy limitation can be overcome in the same way as for supernovae by using large numbers of bursts. Therefore, the uncertainty can be brought down by a factor of the square root of the number of bursts. Again, while Gamma-Ray Bursts have less accuracy than supernovae, they make up for it in their unique coverage at high redshifts.

A third important implication is that collections of bursts have a greatly larger average error than is realized in the community. All collections of E_{peak} values have mixed definitions and few bright bursts, so $\sigma_{Total} \approx 0.24$ is the norm. This corresponds to a 55% error. For a burst claimed to be $E_{peak} = 100$ keV, the real total 1-sigma error region will be like 58-174 keV, regardless of the published statistical error bar.

An important implication of this work is that it implies that GRBs have their emission region effectively held to a constant temperature by some thermostat mechanism. That is the observed E_{peak} distribution is already fairly narrow, so the intrinsic distribution of E_{peak} in the burst rest frame must be very narrow. There is no conclusive mechanism to cause this, but one such explanation is that electron-positron annihilation may be acting as a thermostat for GRB emission.

A final important implication is to that the community can improve the measurement of E_{peak} for many purposes. There is no obvious realistic or effective way to legislate the analyst's choices. But the community can make sure that all the E_{peak} values being used have only one definition. This will require a uniform analysis, which might be accomplished by having one analyst processing all the bursts used in the sample. Or it might require that

multiple analysts agree to adopt some standard definition. For this, the suggested standard would be to use the Band function with freely varying α and β and a frequentist chi-square minimization for the entire burst time interval.

6. A Significant Problem with Using the Amati Relation for Cosmological Purposes[1]

6.1 Background

In the last chapter, an exhaustive study was performed on the sources of error on E_{peak}. This study showed a considerable amount of scatter was hidden in how E_{peak} is measured, which was much larger than that from the reported Poisson errors alone. The sources of this scatter included the choices of different analysts, which E_{peak} is measured, and the detector response matrix, all in addition to the regular Poisson statistical error. This scatter can be as large as 0.43 in log space and has a typical value of 0.24. This scatter can explain the scatter seen in the luminosity relations that use E_{peak}.

Recall that the currently accepted luminosity relations have their drawbacks. The best (i.e. the tightest) of these relations, the Ghirlanda relation, can only be applied if there is an observed jet break. Jet breaks are a well understood phenomena (Rhoads 1997; Sari et al. 1999). This is fairly difficult for a variety of reasons, and has only been observed in a small percentage of bursts. Melandri et al. (2008) and Kocevski & Butler (2008) have pointed out problems in identifying these jet breaks with the X-ray data.

Most notably, the Amati relation has been criticized for several reasons. Refer back to chapters 2 and 3 for the legacy of these tests. As a quick reminder, the tests of Nakar and Piran (2005) have been generalized in several independent investigations (e.g. Band &

[1]The following work has been submitted to the Astrophysical Journal for review. As such, this work may appear in whole or in parts in a submitted academic journal article (as a Collazzi et al. 2011b). Co-Authors for this future article are Bradley E Schaefer of LSU, along with Adam Goldstein and Robert Preece of University of Alabama at Huntsville.

Preece 2005; Schaefer & Collazzi 2007; Goldstein et al. 2010; Chapter 3). They combined the Amati relation (equation 6.1) with the inverse square law for fluences (equation 6.2) to eliminate $E_{\gamma,iso}$ (equation 6.3).

$$E_{\gamma,iso} = (9.2 \times 10^{47}\,\mathrm{erg\ keV^{-2.04}})\,[\,E_{peak}\,(1+z)]^{2.04} \tag{6.1}$$

$$E_{\gamma,iso} = \frac{4\pi\, d_L^2\, S_{bolo}}{1+z} \tag{6.2}$$

$$\frac{E_{peak}^{2.04}}{S_{bolo}} = \frac{4\pi d_L^2}{(1+z)^{3.04}(9.2 \times 10^{47}\,\mathrm{erg\ keV^{-2.04}})} \tag{6.3}$$

Here, $E_{\gamma,iso}$ is the isotropic gamma ray energy, d_L is the luminosity distance as derived with the concordance cosmology ($\Omega_\Lambda = 0.7$, $\Omega_m = 0.3$, $H_0 = 74$ km/s/Mpc), S_{bolo} is the bolometric fluence (the fluence over the burst rest frame 1-10,000 keV range), and z is the redshift of the burst. The quantity $\frac{E_{peak}^{2.04}}{S_{bolo}}$ has been called the 'energy ratio' for the Amati relation (e.g. Band & Preece 2005). The left side of equation 6.3 uses only directly observable quantities (albeit, they are model dependent), while the right side is only a function of distance. As the distance rises, ${d_L}^2$ gets larger and $(1+z)^{-3.04}$ gets smaller, which gives a maximum value for the right side. When the concordance cosmology is used, the function peaks at $z \sim 3.6$. Specifically, the right side of the equation cannot exceed $1.13 \times 10^9\,\mathrm{keV^{2.04}\ erg^{-1}\ cm^2}$ and, therefore,

$$\frac{E_{peak,obs}^{2.04}}{S_{bolo}} \leq 1.13 \times 10^9\,\mathrm{keV^2\ erg^{-1}\ cm^2}. \tag{6.4}$$

This becomes a simple way to test the Amati relation even for bursts without redshifts.

Similarly, for the Ghirlanda relation,

$$E_\gamma = (1.35 \times 10^{47}\,\mathrm{erg\ keV^{-1.43}})\,[\,E_{peak}\,(1+z)]^{1.43} \tag{6.5}$$

$$E_\gamma = \frac{4\pi\, d_L^2\, S_{bolo}\, F_{beam}}{1+z} \tag{6.6}$$

$$\frac{\mathrm{E}_{\mathrm{peak}}^{1.43}}{\mathrm{S}_{\mathrm{bolo}}} = \frac{4\pi\,\mathrm{d}_{\mathrm{L}}^{2}\,\mathrm{F}_{\mathrm{beam}}}{(1+z)^{2.43}(1.35\times10^{47}\,\mathrm{erg\,keV^{-1.43}})} \tag{6.7}$$

The beaming factor, $\mathrm{F}_{\mathrm{beam}}$, is defined as $(1-\cos\theta_{\mathrm{jet}})$, where θ_{jet} is the opening angle of the jet of the burst. The right hand side has a maximum value at $z_{\mathrm{max}} = 12.6$ with a value of $2.7\times10^{10}\,\mathrm{keV}^{1.43}\,\mathrm{erg}^{-1}\,\mathrm{cm}^{2}$ for $\mathrm{F}_{\mathrm{beam}} = 1$. Thus, the Ghirlanda relation forces the limit,

$$\frac{\mathrm{E}_{\mathrm{peak,obs}}^{1.43}}{\mathrm{S}_{\mathrm{bolo}}} \leq 2.7\times10^{10}\,\mathrm{keV}^{1.43}\ \mathrm{erg}^{-1}\ \mathrm{cm}^{2}. \tag{6.8}$$

This results in a simple observational test for compliance with the Ghirlanda relation. This also reproduces the result that the 'energy ratio' for the Ghirlanda differs from the Amati relation (e.g. Band & Preece 2005).

In this chapter, the Nakar and Piran test is revistited, which following Band & Preece (2005), is extended by considering bursts in a plot of their $\mathrm{S}_{\mathrm{bolo}}$ versus $\mathrm{E}_{\mathrm{peak,obs}}$. In addition, an explanation is provided as to why a certain amount of violators are expected, and what the observed distributions of bursts indicate should be expected. This is followed by presenting gathered data from various detectors and providing a comprehensive examination of how each detector's data performs under the Nakar and Piran test. Following this, an explanation is provided for why the vast majority of the data sets have too many violators of the Amati limit, and therefore the Amati relation is not good as a luminosity relation. Finally, an examination is provided of several sources of systematic offsets that are actually the cause of the Amati relation in the first place, which only further condemns the Amati relation's usefulness.

6.2 The $\mathrm{S}_{\mathrm{bolo}}-\mathrm{E}_{\mathrm{peak}}$ Diagram and the Amati Relation

One way to visualize bursts under the Nakar and Piran test is to plot them on a $\mathrm{S}_{\mathrm{bolo}}-\mathrm{E}_{\mathrm{peak,obs}}$ diagram. In doing this, one can not only easily see how a certain group

of bursts fares on the Nakar and Piran test, but also determine if there is a systematic offset between different detectors. As an example, one can determine whether different detectors are pre-disposed towards different regions on the diagram. In addition to plotting points for individual bursts, the Amati limit (equation 6.4) and the Ghirlanda limit (equation 6.8) are plotted for easier visualization of where the limits lie. Figure 6.1 shows the basic idea behind the plots, with three zones for whether the burst violates no limit, the Amati limit only, or both limits.

To illustrate the Amati limit, Figure 6.2 presents a created Monte Carlo simulation of 1000 bursts where the Amati relation is adopted. There are no measurement errors, no selection effects for satellite detectors, and the burst luminosity and distance distributions are a reasonable model of the real Universe. This simulation for each burst starts with the random selection of $E_{peak,obs}$ as based on a log-normal distribution like in Mallozzi et al. (1995). In addition, the redshift of the burst is randomly selected from a reasonable cosmological distribution, in this case, a log normal distribution with z=2 and a standard deviation of 1. With these two values, an intrinsic E_{peak} is found by simply applying the redshift correction: $E_{peak,int} = E_{peak,obs}(1 + z)$. The Amati relation is then used to derive $E_{\gamma,iso}$, and use equation 6.2 to get the observed S_{bolo}. As such, the figure shows a realistic distribution, or at least for no measurement uncertainties. In the figure, one sees that there are no violators (i.e., bursts appearing below the Amati limit), with most bursts appearing close to the limit line. This figure is a central illustration of the Nakar & Piran test, which will be extended in this chapter.

Once one allows for ordinary scatter caused by measurement errors in $E_{peak,obs}$ and S_{bolo}, then the tight scatter in Figure 6.2 is lost. This is shown in Figure 6.3, where suddenly somewhat less than half of the bursts become violators. For this simulation, the measurement

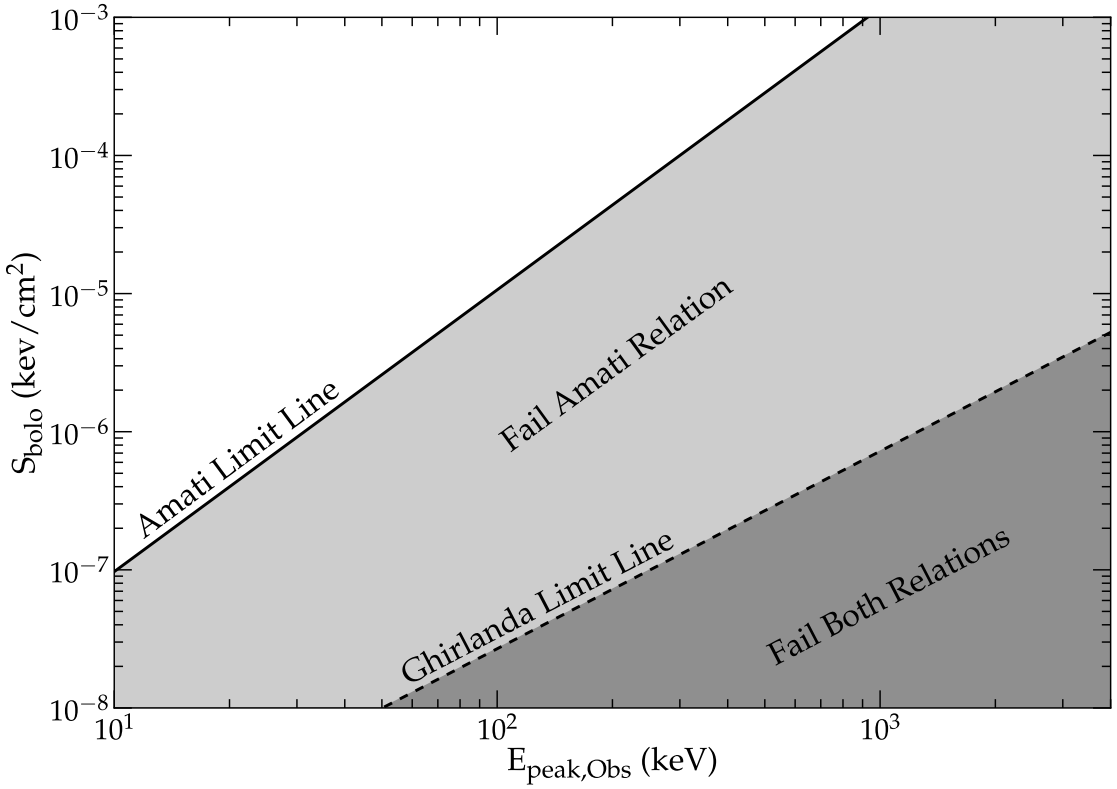

Figure 6.1 The basics of the Nakar and Piran test in graphical form. Any burst (even without a known redshift) can be plotted on this diagram. If the Amati relation is correct, then any burst must lie above the solid line (from equation 6.4), although normal scatter from measurement error will put somewhat less than half of the bursts just below the limit line. If the Ghirlanda relation is correct, then any burst must lie above the dashed line (from equation 6.8), although normal scatter from measurement error can put a small fraction of the bursts just below the limit line. If a burst lies below one of the lines, then it is called a 'violator' of that relation.

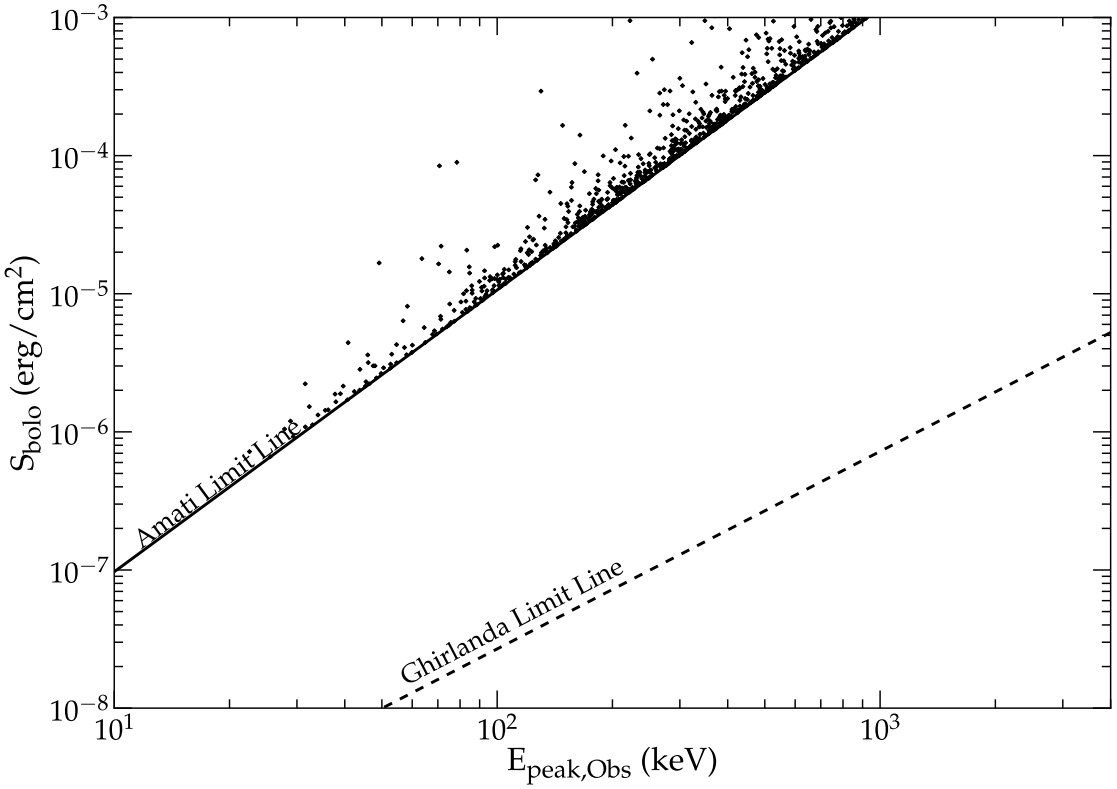

Figure 6.2 1,000 simulated bursts based on the Amati relation with no measurement errors. This simulation assumes that the Amati relation is exact. In the Monte Carlo simulation, each burst had a redshift chosen randomly from a reasonable cosmological model for bursts, an $E_{peak,obs}$ value chosen randomly from the log-normal distribution of Mallozzi et al. (1995), the burst energy calculated from the Amati relation, then the observed S_{bolo} calculated from the burst energy and redshift. The simulated bursts are usually close to the Amati limit line, and there are no violators.

errors were assumed to have a log-normal distribution with a one-sigma width of 0.25 (Collazzi et al. 2011; Chapter 5). The exact fraction of violators will depend on the size of the observational scatter. In this realistic simulation, ∼40% of the bursts are below the Amati limit line. The point of this figure is that normal and expected observational measurement errors will lead to nearly half the bursts being apparent violators. Importantly, this scatter does not explain the high violator rates reported by Band & Preece (2005) and Goldstein et al. (2010). This discrepancy is the main topic of this chapter.

For comparison, consider how the $S_{bolo}-E_{peak,obs}$ diagram would look if neither the Amati or Ghirlanda relations were valid. For this, another Monte Carlo simulation was constructed (see Figure 6.4). As in Figure 6.2, no assumptions were made about measurement errors and selection by satellite detectors. Realistic luminosity and distance distributions were assumed, but no constraints were made from either the Amati or Ghirlanda relations. To do this, start by selecting burst distances and energies in the 100-500 keV such that they reproduce the observed $\log(\mathrm{N}) - \log(\mathrm{P})$ curves for BATSE (Fenimore et al. 1993, Fishman & Meegan 1995). E_{peak} is then generated based on a log normal distribution with some loose connection to the brightness of the burst (as seen in Mallozzi et al. 1995). A bolometric correction is then appled with ($\alpha = -1.0$ and $\beta = -2.0$). The result is an in illustration of the intrinsic distribution of bursts on the sky. The simulation of 10,000 bursts has approximate edges at 20 and 3000 keV, plus lower and upper edges simply where the $\log(\mathrm{N}) - \log(\mathrm{P})$ curve was cut off. The key point is that Figures 6.2 and 6.4 are greatly different, because low-fluence bursts will dominate unless some law/correlation forces these low-fluence events to have low-$E_{peak,obs}$. So there are now two extreme cases that produce greatly different distributions in the $S_{bolo}-E_{peak,obs}$ diagram.

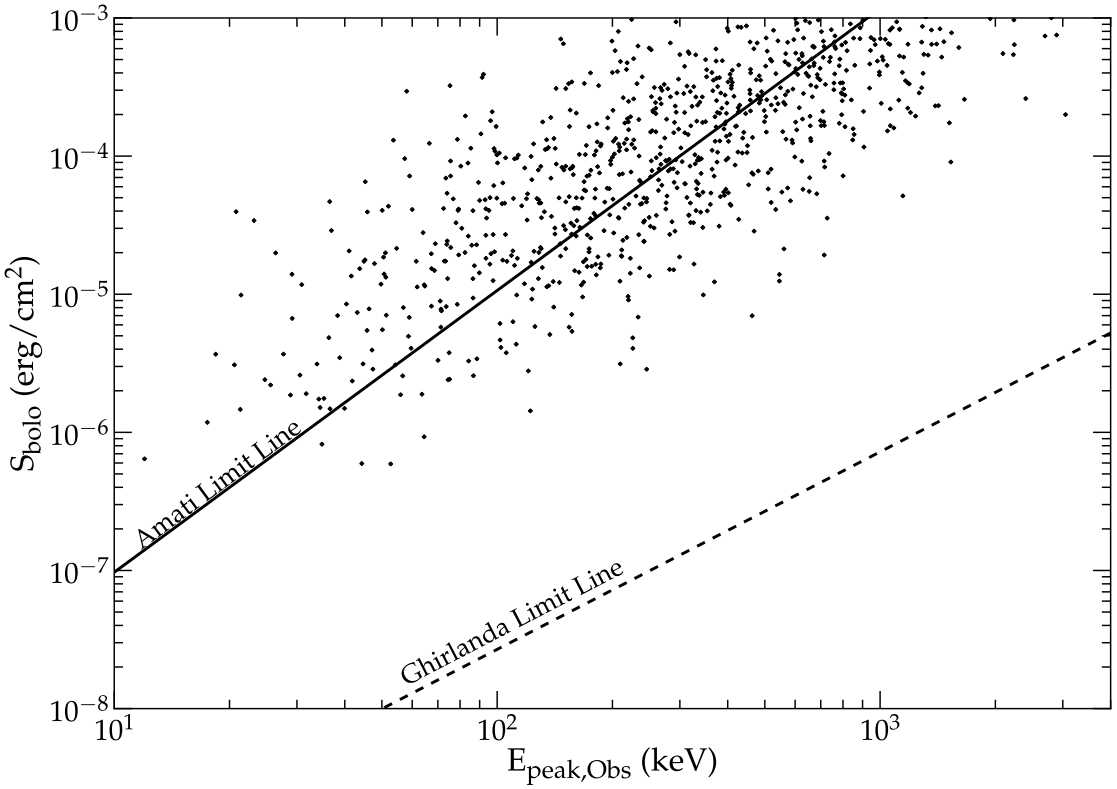

Figure 6.3 1,000 simulated bursts based on the Amati relation with realistic measurement errors. These 1,000 bursts are identical with the bursts in the previous figure, except that a statistical scatter has been added to the intrinsic values. For this Monte Carlo simulation, the measurement error is taken from a log-normal distribution where the one-sigma scatter in $\log(E_{peak,obs})$ is 0.25 (c.f., Collazzi et al. 2011; Chapter 5). With this, the fraction of burst that violate the Amati limit rises from zero to $\sim 40\%$.

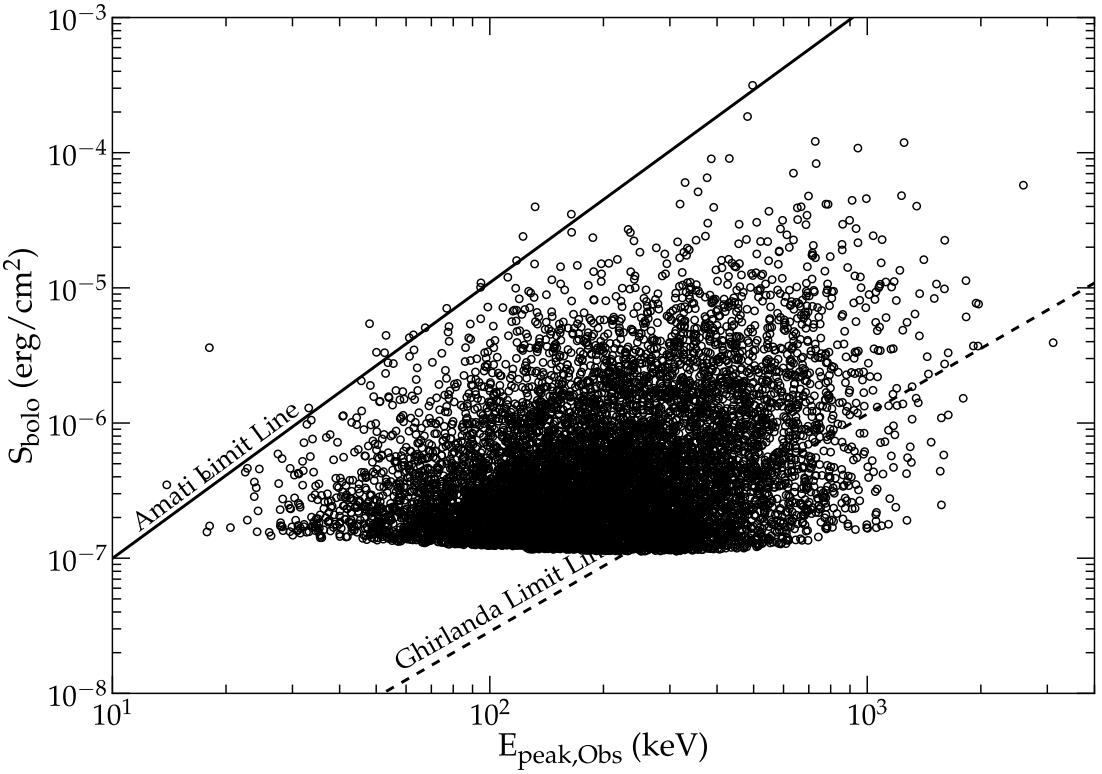

Figure 6.4 10,000 simulated bursts without the Amati relation. First, a flux in the 100-500 keV range is generated using the BATSE $\log[N(>\mathrm{P})]-\log[\mathrm{P}]$ relation (Fenimore et al. 1993, Fishman and Meegan, 1995). $\mathrm{E_{peak}}$ is then generated based on a log normal distribution, with a dependence on the brightness of the burst (as seen in Mallozzi et al. 1995). Finally, the generated $\mathrm{E_{peak}}$ is used to apply an appropriate bolometric correction based on the band function with ($\alpha = -1.0$ and $\beta = -2.0$). This bolometric correction ranges from a factor of ~ 3.5 to ~ 7.1. The result is an *illustration* of the intrinsic distribution of the population of bursts on the sky. The point of this Figure is that the distribution covers a large area without the Amati relation.

Both Figures 6.2 and 6.4 are for the intrinsic distributions of GRBs in a realistic case with no effects of detector thresholds or measurement uncertainties. From a comparison of Figures 6.2 and 6.3, one sees that the realistic measurement errors will substantially smear the underlying distribution. Detector thresholds will also force a fuzzy cutoff roughly running along some horizontal curve. For a detector with a high threshold, the many violators in Figure 6.4 will never be detected and the violator fraction might appear acceptable. For a detector with a low threshold, it should be easy to determine whether the Amati relation is valid.

6.3 Generalizing the Test to Many Detectors

So far, the Nakar & Piran test has only been applied to BATSE bursts (Nakar & Piran 2005, Band & Preece 2005; Goldstein et al. 2010) and to a collection of bursts with redshifts as detected by a range of many satellites (Amati 2002; 2006; Schaefer & Collazzi 2007; Chapter 3). But this test can be extended to many satellites, because all that is needed are values of S_{bolo} and $E_{peak,obs}$, with both of these being commonly reported for many bursts. The essence is to find the fraction of violators, ξ, for each sample. The quantity $\langle \log \frac{E_{peak}^{2.04}}{S_{bolo}} \rangle$ will be also tracked for each sample, as this can be directly compared to 1.13×10^9 (in units of $keV^{2.04}$ erg^{-1} cm^2) so as to test the Amati limit (cf. equation 6.4). These statistics will be tracked for both bursts with spectroscopically determined redshifts (Greiner 2010) and those with no known redshift. The samples and their statistics are presented in Table 6.1, with some discussion in Sections 6.3.1 to 6.3.8. The $S_{bolo}-E_{peak,obs}$ diagrams for each sample are presented in Figures 6.5-6.13.

Table 6.1. Demographics of the Data Samples

Data Set	$\#_{w/z}$	$\xi_{w/z}$[a]	$\langle \log \frac{E^{2.04}_{peak}}{S_{bolo}} \rangle_{w/z}$[b]	$\#_{w/o\ z}$	$\xi_{w/o\ z}$[a]	$\langle \log \frac{E^{2.04}_{peak}}{S_{bolo}} \rangle_{w/o\ z}$[b]
Ideal, no scatter	...	0%	8.92±0.24	...	0%	8.92±0.24
Ideal, with scatter	...	∼40%	8.91±0.64	...	∼40%	8.91±0.64
Amati et al. 2006	50	34%	8.90±0.56	0	...	...
Schaefer 2007	27	41%	8.95±0.57	0	...	...
BATSE	0	...	...	1654	93%	10.18±0.88
HETE-2	12	33%	8.67±0.62	24	54%	9.05±0.84
Swift	25	76%	9.42±0.47	46	85%	9.46±0.45
Suzaku	7	100%	9.77±0.74	25	92%	10.28±0.87
Swift - *Suzaku*	28	86%	10.01±1.01	38	74%	9.63±0.85
Konus	33	73%	9.42±0.58	64	78%	9.68±0.87
Beppo-Sax	10	90%	9.36±0.39	119	90%	9.51±0.39

[a] ξ is the fraction of bursts that violate the 'Amati limit' of $1.13 \times 10^9\,\mathrm{keV^2\,erg^{-1}\,cm^2}$ for the Amati energy ratio E^2_{peak}/S_{bolo}.

[b] For the Amati relation, the quantity $E^{2.04}_{peak}/S_{bolo}$ should never exceed $1.1 \times 10^9\,\mathrm{keV^{2.04}\,erg^{-1}\,cm^2}$, so even with normal observational scatter a sample of GRBs should not have $\langle \log \frac{E^{2.04}_{peak}}{S_{bolo}} \rangle > 9.05$ in appropriate units. With a reasonable distribution of burst distances, the limit will be even smaller. So this column provides a measure of the disagreement with the Amati limit for a sample of bursts. The RMS scatter for $\log \frac{E^{2.04}_{peak}}{S_{bolo}}$ is given after the average value, so this can give a measure of the scatter of the distribution.

6.3.1 Amati et al. (2006) Data

The first task is to use the compilation of data from Tables 1 and 2 of Amati et al. (2006). These bursts all have redshifts and come from *Beppo-Sax* , *Konus* , *HETE*-2 , BATSE, and *Swift* . Using the Amati relation, S_{bolo} is calculated from the given spectral data. Bursts 050315, 050824, 050904, 981226, 000214 and 030723 are excluded because only limits to $E_{peak,obs}$ are provided, and therefore are not useful. Bursts 980329 also had to be excluded because a redshift range is given, and therefore an accurate measurement of d_L could not be obtained for converting E_{iso} into S_{bolo} . The results are in Figure 6.5.

This sample of GRBs was largely the same as used by Amati (2002) to discover and calibrate the Amati relation, so it is no surprise that the bursts are spread out along the Amati limit line. The violator fraction is $\xi = 34\%$, which is as expected given the usual scatter due to measurement errors. The sample has $\langle \log \frac{E_{peak}^{2.04}}{S_{bolo}} \rangle = 8.90$ which is close to the limit of $\log(1.13 \times 10^9) = 9.05$ (in appropriate units). The RMS scatter of $\log \frac{E_{peak}^{2.04}}{S_{bolo}}$ is 0.56, which is a measure of how tight the Amati relation is for the sample.

6.3.2 Schaefer (2007) Data

Next, another compilation set, this time from Schaefer (2007). This data set also takes its burst sample from a variety of different detectors: *Konus* , *Beppo-Sax* , *HETE*-2 , BATSE, and *Swift* bursts were included for this sample. While the paper studies 69 GRBs with known redshift, only 27 have the bolometric fluence reported and thus are the ones that are used (see Figure 6.6).

Of the 27 bursts, 11 fail the Nakar and Piran test (ξ=41%). This is an expected failure rate for the Amati relation and is in agreement with previous analysis on this data (see Schaefer and Collazzi 2007; Chapter 3). The average value for the log of $\langle \log \frac{E_{peak}^{2.04}}{S_{bolo}} \rangle$ is

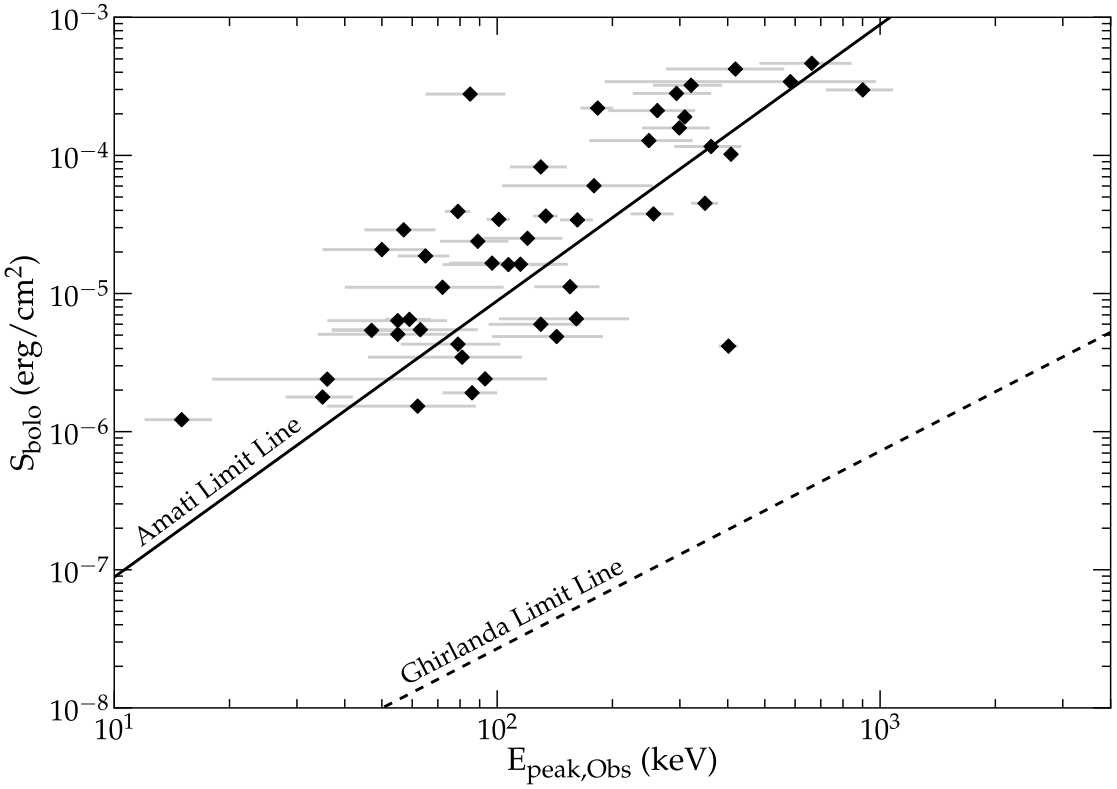

Figure 6.5 The Nakar and Piran test for 50 bursts from Amati et al. (2006). This data came from a variety of different detectors, including *Beppo-Sax* , *Konus* , BATSE, *HETE*-2 , and *Swift* . All bursts in this sample have known associated spectroscopic redshifts. Of the 50 bursts, 34% fail the test. This is within the expected failure rate of the Amati relation.

8.95±0.57. So this data is similar to the previous data set (which is not surprising as they share some of the same bursts).

The two samples which contain exclusively bursts with known redshifts both agree well with the Amati relation, and this has long been the primary justification for accepting the Amati relation as a physical relation for GRBs. However, other samples (see below) do not agree with the Amati limit, and this suggests that bursts with redshifts might be a significantly different sample from those without redshift. This is the reason why bursts with and without redshifts are distinguished in Table 6.1 and in the figures.

6.3.3 BATSE Data

Data used from BATSE is a part of the upcoming 5B catalog (Goldstein et al. 2011). Values of E_{peak} and S_{bolo} are presented for the most statistically preferred fitting model, CPL or Band. Only bursts for which there is 40% relative error or better is used. After applying these selection criteria, there are 1654 bursts, which are plotted in Figure 6.7. In the figure, two new curved lines are introduced, which represent *illustrative thresholds* for the trigger (dotted) and the ability to detect E_{peak} (dot-dashed). These are explained in detail in Section 6.4.

The BATSE bursts fail at an extreme rate, with 93% violators. In addition, the BATSE bursts cover a large region of the disallowed zone, with very few bursts above the limit. One finds that $\langle \log \frac{E_{peak}^{2.04}}{S_{bolo}} \rangle$ to have a value of 10.18±0.88. The failure rate is consistent with that observed in the past of BATSE bursts in previous works. The spread of BATSE bursts is so large, it hints that almost any future changes to the Amati relation (e.g. as more *Swift* bursts are detected with redshifts) will result in a high failure rate.

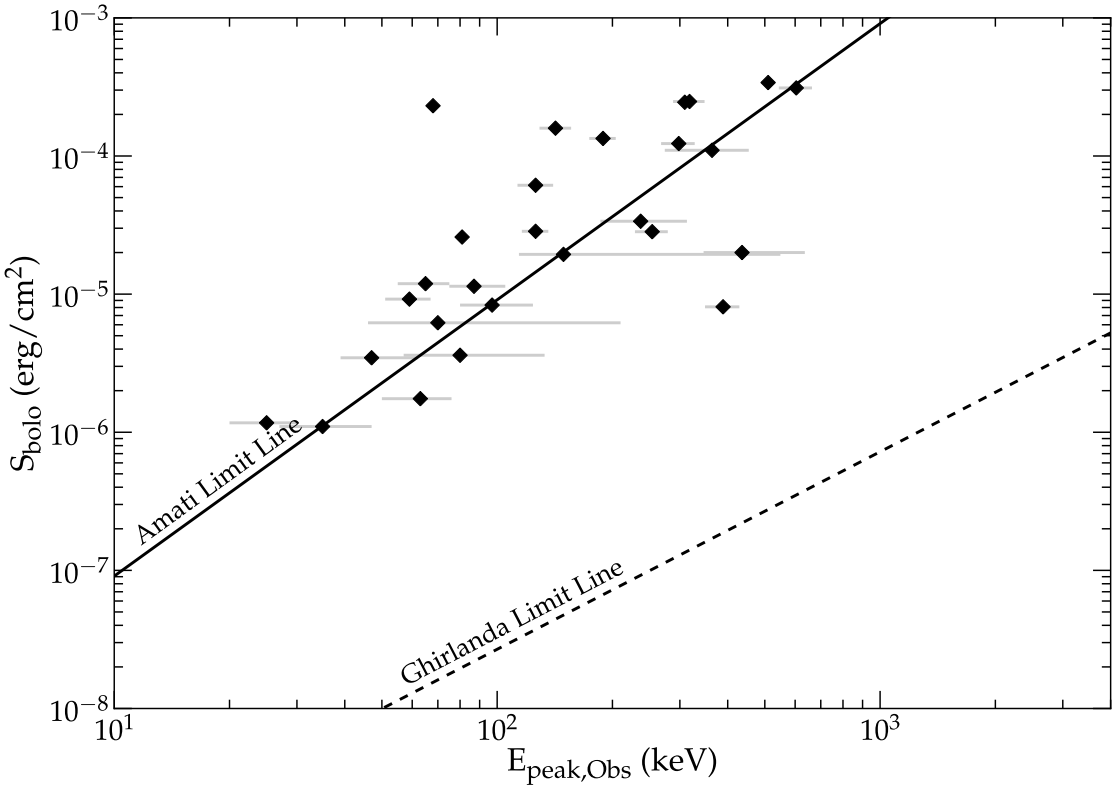

Figure 6.6 The Nakar and Piran test for 27 bursts from Schaefer (2007). This data came from a variety of different detectors, including *Beppo-Sax* , *Konus*, *HETE*-2 , BATSE, and *Swift*. All bursts in this ample have known associated spectroscopic redshifts. Of the 27 bursts, 41% fail the test. This is in within the expected failure rate of the Amati relation and in agreement with previous tests on this data (see Schaefer and Collazzi 2007; Chapter 3).

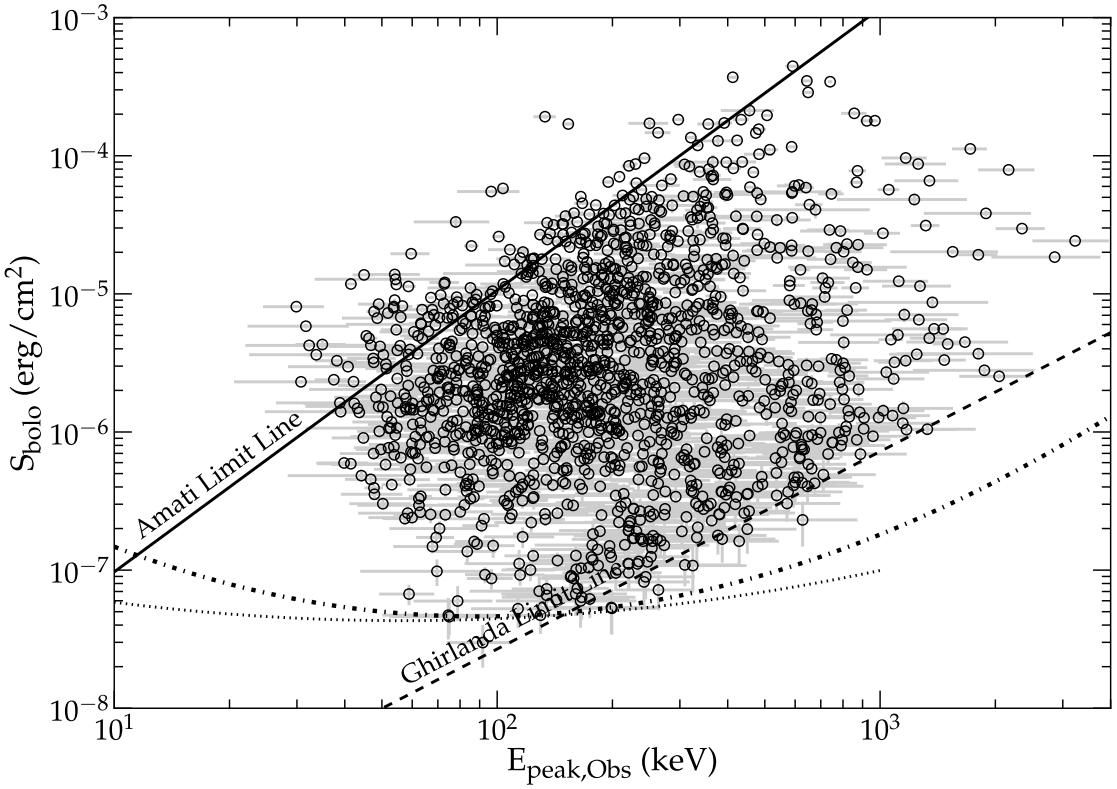

Figure 6.7 1654 BATSE bursts from the future 5B BATSE catalog (Goldstein et al. 2011). The E_{peak} and S_{bolo} data come from the best fit of either a CPL or Band model, whichever was significantly better. In addition, only the bursts for which the relative error on the measurements are 40% or better are used. This selection fails at a very high rate, with 93% violators. The zone covered by the BATSE sample has a very large coverage area, but still only a very few bursts are passing. This is particularly condemning, as it hints that any future Amati relation will also fail for the BATSE sample. The dotted line represents an *illustrative* line for the trigger threshold and the dot-dashed line represents an *illustrative* model of the E_{peak} detection threshold (see Section 6.4).

6.3.4 *HETE*-2 Data

The sample of *HETE*-2 bursts comes from Sakamoto et al. (2005). The quoted values for S_{bolo} only cover the 2-400 keV range, and had to be converted into bolometric fluences. This was done by using the given parameters for the spectral model (Band or Cut-off Power Law (CPL)) to extrapolate a bolometric correction. This was generally a small correction, while even the large corrections are still small compared to scatter in Figure 6.8. The quoted error bars for both E_{peak} and S_{bolo} are given for the 90% level, so they had to be converted into standard one sigma confidence level error bars ($\sigma_{90\%} = 1.645\,\sigma_{1-sigma}$). The figure also has *illustrative* lines to represent trigger thresholds (dotted line) and the E_{peak} detection threshold (dot-dashed line). Again, these will be explained in detail in Section 6.4.

The *HETE*-2 bursts have $\xi = 33\%$ and $\langle \log \frac{E_{peak}^{2.04}}{S_{bolo}} \rangle$ similar to that of the original Amati sample, so it appears that these bursts are consistent with the Amati relation. Nevertheless, the scatter apparent in Figure 6.8 is so large that there is little utility in applying the Amati relation to these bursts. The difference is insignificant for $\langle \log \frac{E_{peak}^{2.04}}{S_{bolo}} \rangle$ between bursts with and without redshifts. Of all the single-satellite data sets that are considered, the *HETE*-2 data is the only one that apparently obeys the Amati relation, although its large scatter limits its usefulness.

6.3.5 *Swift* Data

For the *Swift* data, the catalog in Butler et al. (2007) is used. Their values of E_{peak} as derived from frequentist statistics are used as it is the most common approach to finding E_{peak}. (Their Bayesian values were made with unreasonable priors that significantly skew the results.) The *Swift* burst detector only goes up to ~ 150 keV, so the reported values of $E_{peak,obs}$ are almost all lower than 200 keV. Their bolometric fluences have been adopted and

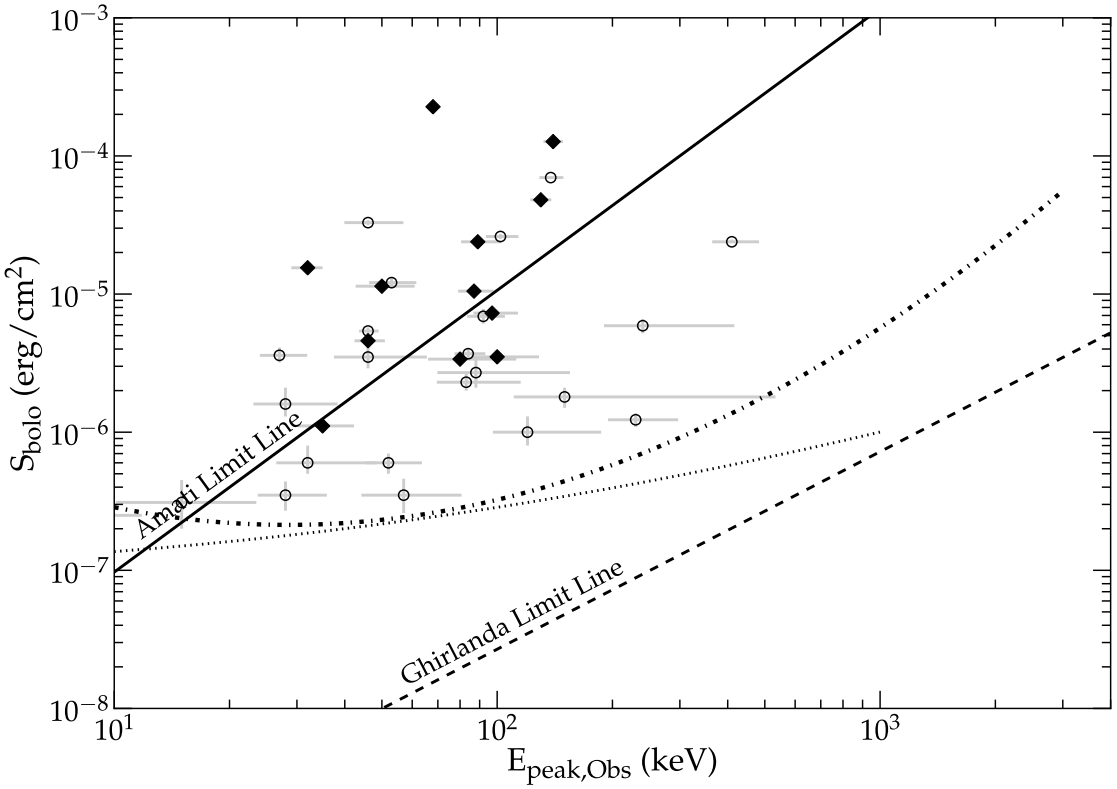

Figure 6.8 *HETE*-2 data from Sakamoto et al. (2005). In total, 44% of the 36 bursts fail below the Amati limit line, which is within the expected failure rate. Likewise, 33% of the 12 bursts with associated spectroscopic redshift are violators (which again, is within the expected failure rate). The bursts with redshift do not appear to be significantly different from those without. The *HETE*-2 data is unique in that it seems to most resemble the original data from Amati, even though the scatter around the Amati limit line is very large. The dotted line represents an *illustrative* line for the trigger threshold and the dot-dashed line represents an *illustrative* model of the E_{peak} detection threshold (see Section 6.4). Filled diamonds represent bursts for which there is a measured redshift, unfilled circles are bursts for which there is no redshift.

these have been converted their non-standard 90% error bars into standard one-sigma error bars. Figure 6.9 plots the results; bursts without known redshifts are represented as empty circles and bursts with known redshift are represented by a filled diamond. This will be true for all future plots. This is the last of the three plots in which *illustrative* lines representing trigger (dashed line) and E_{peak} detection thresholds (dot-dashed line) were plotted, which again, are detailed in Section 6.4.

The *Swift* bursts violate the Amati limit at a rate of 76% to 82%. That is, the Amati relation does not work for *Swift* . This result is not the result of small number statistics, and it is clear to see that the distribution that the disagreement is highly significant. This is another version of the same conclusion first reported by Butler et al. (2007).

When first confronted with the discrepancy that bursts with redshifts agreed with the Amati relation (see Figures 6.5 and 6.6) while bursts without redshifts disagreed with the Amati relation (Band & Preece 2005), the initial thought was that the bursts with redshifts might be somehow selected from a separate population for which the Amati relation applied. However, with this large sample of well-measured bursts from *Swift* , the distributions of bursts with and without redshifts is essentially identical. Thus, this is a proof that the success or failure of the Amati relation does not depend on some selection effect that correlates with the measuring of spectroscopic redshifts. Another thing to remember is that since *Swift* bursts are the bursts that account for a majority of the bursts with known redshifts, there is a built-in selection effect that will eventually develop that will bias future iterations of the Amati limit towards the area *Swift* bursts cover.

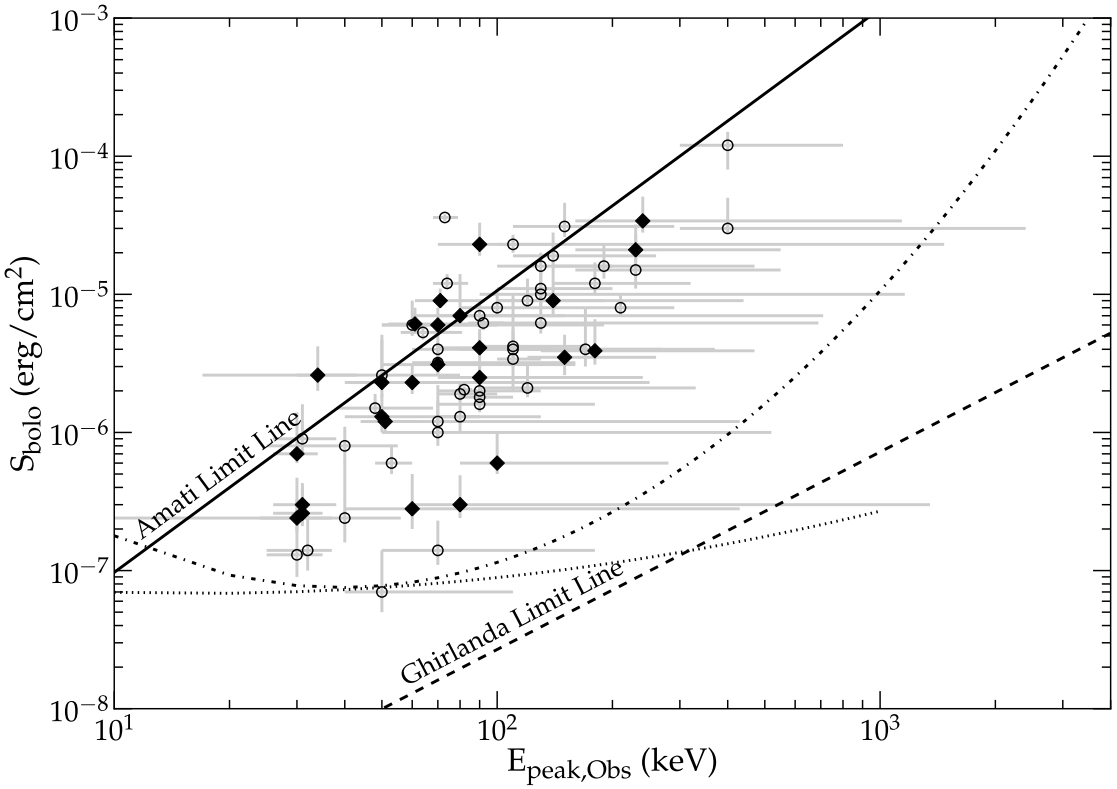

Figure 6.9 *Swift* data from Butler et al. (2007). In total, there are 71 bursts, 82% of which violate the Amati limit. This is far beyond the expected value, and thus the Amati relation fails for the *Swift* data. The same conclusion is reached when looking just at the bursts with known spectroscopic data, with 76% of those 25 bursts being violators.The bursts with known redshift are not different from those without known redshift (see Table 6.1). The dotted line represents an *illustrative* line for the trigger threshold and the dot-dashed line represents an *illustrative* model of the E_{peak} detection threshold (see Section 6.4). Filled diamonds represent bursts for which there is a measured redshift, unfilled circles are bursts for which there is no redshift.

6.3.6 *Suzaku* Data

Suzaku data for long GRBs are available through the GCN circulars[2]. Typically, the reported fluence covers the 100 keV to the 1 MeV range, so a bolometric correction is applied based on the reported spectral fit. A typical bolometric correction value is a factor of ∼1.7. The $E_{peak,obs}$ and fluence values reported in the circulars are preliminary and made soon after the burst, yet any likely changes to get to the final best fits are greatly smaller than the scatter shown in Figure 6.10 and are thus not important. The Suzaku bursts all have $E_{peak,obs} > 200$ keV, a result of the relatively high energy range of sensitivity of the detector.

Most of the Suzaku bursts violate the Amati limit, usually by a large factor ($\xi \sim, 94\%$) and the small fraction that are not violators are very close to the limit (Figure 6.10). Therefore, the Amati relation does not work for Suzaku bursts. This is true for both bursts with redshifts and without.

6.3.7 *Swift* - *Suzaku* Data

Krimm et al. (2009) presented a catalog of bursts for which there was both *Swift* and *Suzaku* data. The expanded energy range gave better fits to the spectra, with *Swift* covering the lower energies and *Suzaku* covering the higher energies. With the joint spectral fits over a very wide range of photon energies, the sample has a wide range of $E_{peak,obs}$ values from 30 keV to 2000 keV. The catalog lists the best fit for the three major spectral models (power law, power law with an exponential cutoff, and Band model) for the majority of the listed bursts, while the used $E_{peak,obs}$ values from just the Band function.

[2]http://gcn.gsfc.nasa.gov

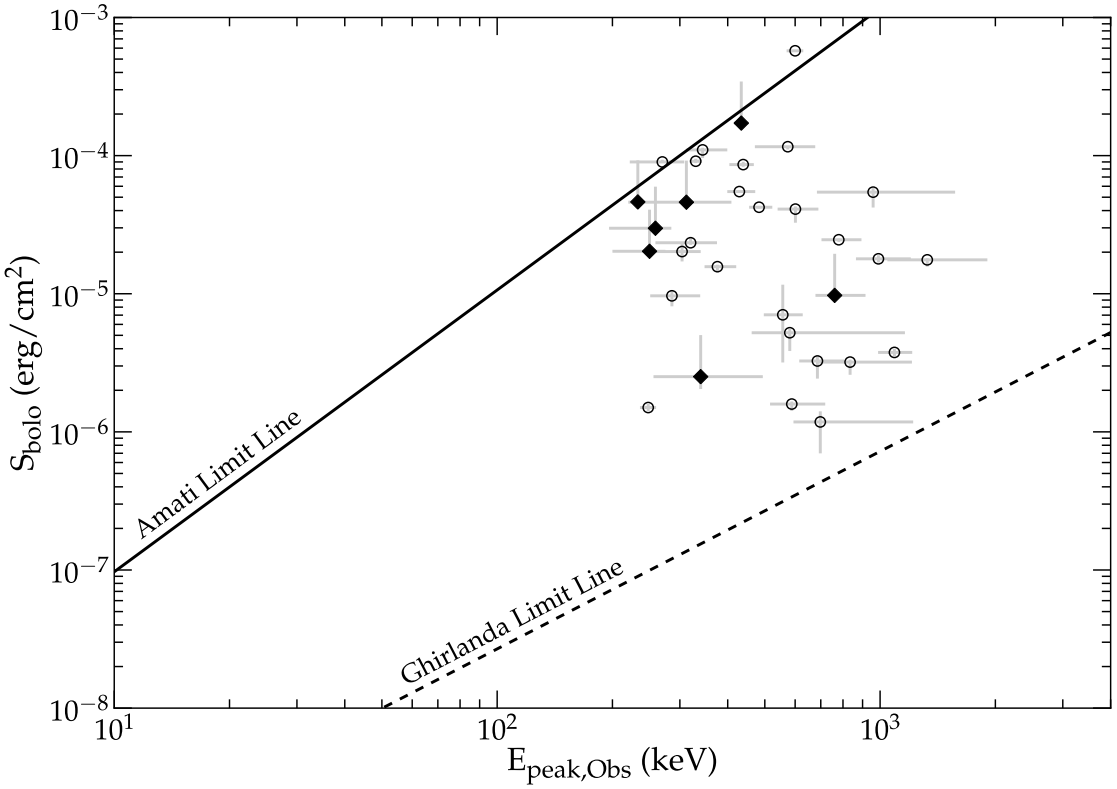

Figure 6.10 *Suzaku* data. Only bursts for which the time-integrated E_{peak} are reported. The fluences are also reported in these notices, typically over the 100 keV to 1 MeV range. These fluences had to be converted to bolometric fluences using the provided spectral parameters. Of the 32 bursts used, 94% are violators of the Amati limit. The 7 bursts that have associated spectroscopic redshift have a 100% violator rate. Again, the bursts with known redshift are not different from the overall sample. Filled diamonds represent bursts for which there is a measured redshift, unfilled circles are bursts for which there is no redshift.

The joint sample largely stretches between the Amati limit line and the Ghirlanda limit line (Figure 6.11). The fraction of violators is 86% for the 28 bursts with spectroscopic redshifts and 74% for the 38 bursts without redshifts. Again, the Amati relation fails, and there is no significant difference related to whether the burst has a spectroscopic redshift or not. No burst significantly violates the Ghirlanda limit.

6.3.8 *Konus* Data

The GRB detectors on the Wind satellite (Aptekar et al., 1995) are long-running instruments with a stable background that has measured many bursts, with the fluence and $E_{peak,obs}$ values promptly reported in the GCN circulars. These reported value are preliminary, with no final analysis having been published, but any plausible errors due to the preliminary nature of the report are greatly smaller than the observed scatter in the $S_{bolo}-E_{peak,obs}$ diagram (see Figure 6.12). A total of 97 bursts were found, 33 of which have associated spectroscopic redshifts, with reported fluences and $E_{peak,obs}$ for the entire burst interval. A bolometric correction factor was applied, based on the given spectral fits. This factor was typically very small, due to the large range the reported *Konus* fluences usually cover.

The distribution of the *Konus* bursts in the $S_{bolo}-E_{peak,obs}$ diagram has a flat lower cutoff, likely due the trigger threshold (although this cutoff is higher the reported trigger threshold in Aptekar et al. (1995) of $\sim 5 \times 10^{-7}\,\mathrm{erg\,cm^{-2}}$). The distribution also shows a fairly high upper limit on $E_{peak,obs}$ due to the sensitivity of the detectors to high photon energies. From 22% to 27% of the bursts are above the Amati limit line, while all the bursts are above the Ghirlanda limit line. The Amati relation fails for the *Konus* bursts. Again, the bursts with redshifts are distributed identically to those without, so there is no apparent selection effect based on spectroscopic redshifts.

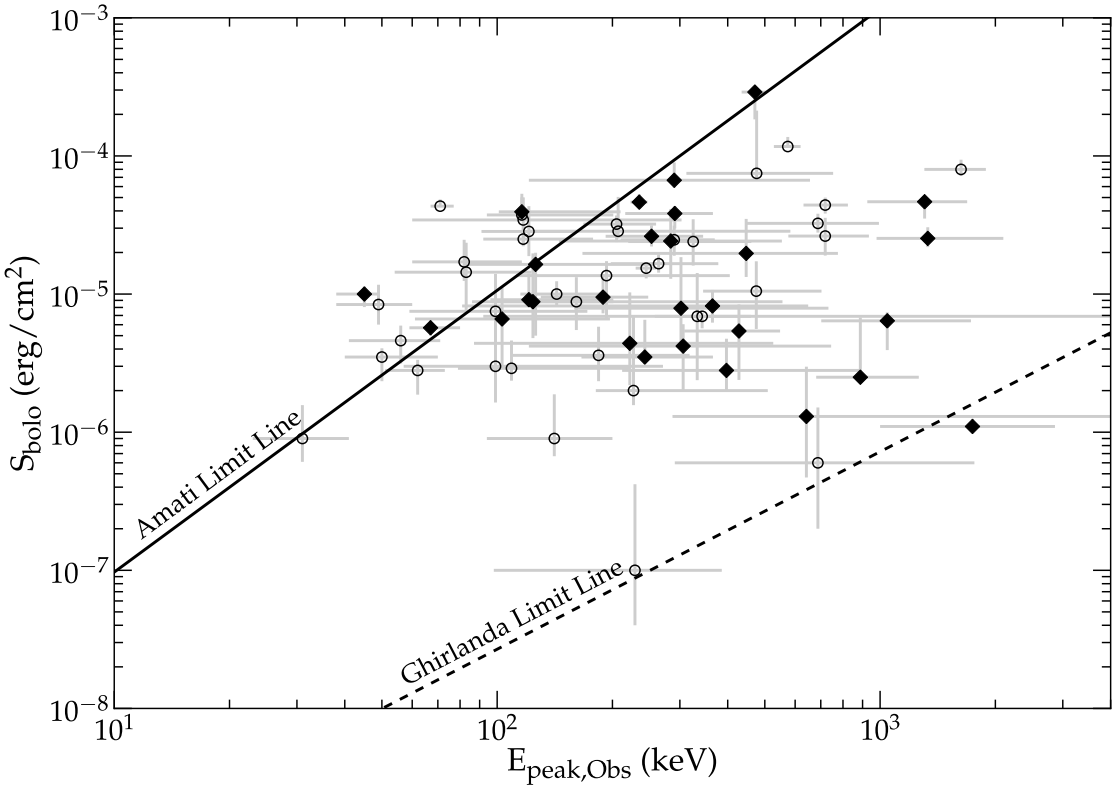

Figure 6.11 Combined data from *Swift* and *Suzaku* . Krimm et al. (2009) took the raw data from both detectors and fit the combined spectra to get a better measurement of E_{peak} for a large sample of bursts. Their E_{peak} values are used as found from the Band function. 38 of the 66 usable bursts do not have spectroscopic redshifts, of which 86% are violators. These bursts have an average log of the energy ratio of 9.63±0.85, whereas the Amati relation requires that this average must be less than 9.05. 28 of the bursts have spectroscopic redshifts, 86% of those busts are violators, with an average log of the energy ratio of 10.01±1.01. Even with the broad spectral range provided by combining the *Swift* and *Suzaku* data, the Amati relation fails. Filled diamonds represent bursts for which there is a measured redshift, unfilled circles are bursts for which there is no redshift.

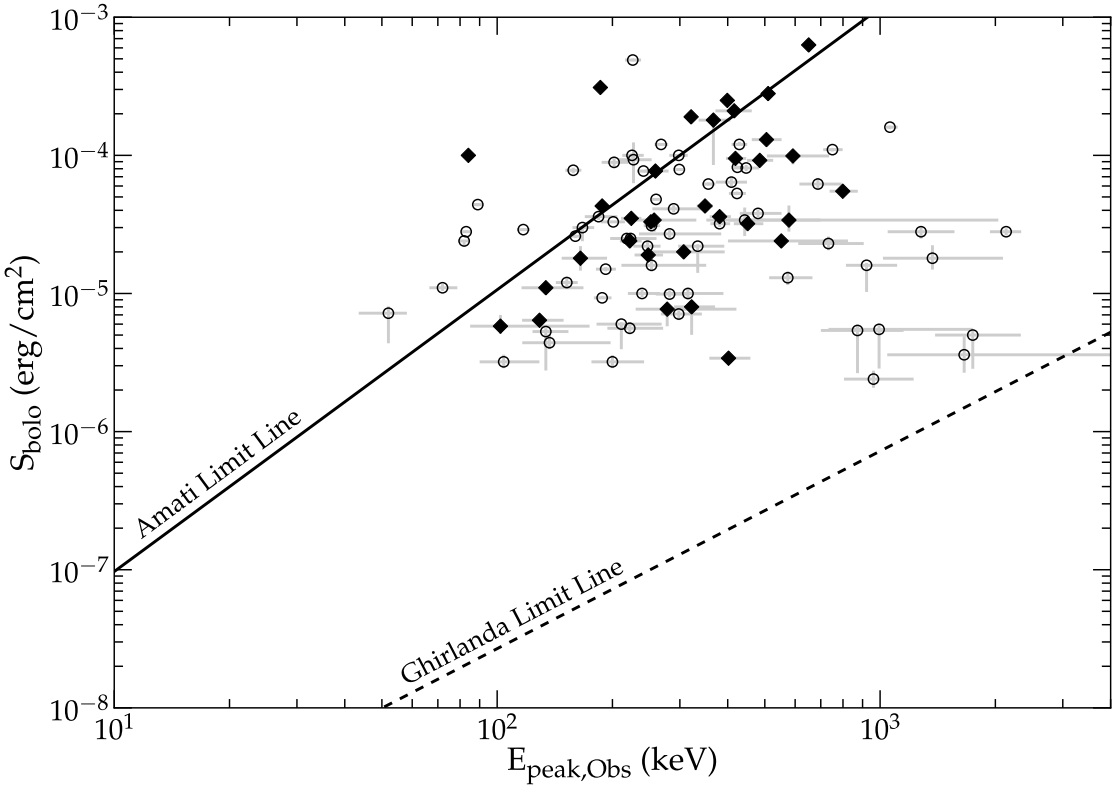

Figure 6.12 *Konus* bursts. This distribution of bursts has a fairly flat bottom corresponding to the trigger threshold for the detector. The very broad energy range of Konus allows for $E_{peak,obs}$ values to be measures from 30 keV to 2000 keV. The fraction of bursts violating the Amati limit is 73% for the 33 bursts with spectroscopic redshifts and 78% for the the 64 bursts without redshifts. With bursts extending down to near the Ghirlanda limit line, the observed distribution is clearly not that of the Amati relation plus some ordinary measurement errors. In other words, the Amati relation fails for this sample. Filled diamonds represent bursts for which there is a measured redshift, unfilled circles are bursts for which there is no redshift.

6.3.9 *Beppo-Sax* Data

Guidorzi et al. (2011) provides a large catalog of both E_{peak} and S from the *Beppo-Sax* GRBM. In the catalog, data for the brightest 185 bursts are given; for which 129 are used. Of the useable 129 bursts, only 10 bursts have spectroscopic redshifts. The provided S_{bolo} were over the 40-700 keV range. The same type of bolometric correction is applied as before, using the provided spectral indices for the CPL used. This correction is typically small, with a typical correction value of 1.5.

While it is impossible to make a strong statement about the shape of the distribution of *Beppo-Sax* bursts with only the bright bursts, there is still an important result from the data. The data is plotted in Figure 6.13. Even among the brightest bursts, 90% of bursts with redshifts and 90% of bursts without redshifts are violators. What is particularly provocative about this result is that these are the *brightest* bursts, and thus the *most* likely to not be violators. It is unlikely that there are a significant number of 'missing' bursts that would be non-violators. Any such burst would have to be both bright and have a low E_{peak} while still being dim enough to be missed in the bright burst catalog. Finally, information is provided as to the average energy ratio of these bursts, but once again, it should be stressed that these are only the brightest bursts in the catalog. Therefore, these values should be taken with caution. Nonetheless, it can be said with confidence that the Amati relation fails for *Beppo-Sax* bursts, although this statement is not as strong as it is for other detectors because of the sample used.

6.3.10 Overview of Results

Previously, Butler et al. (2007) had pointed out that the normalization constant for the Amati relation was slightly different depending on whether *Swift* or pre-*Swift* bursts were

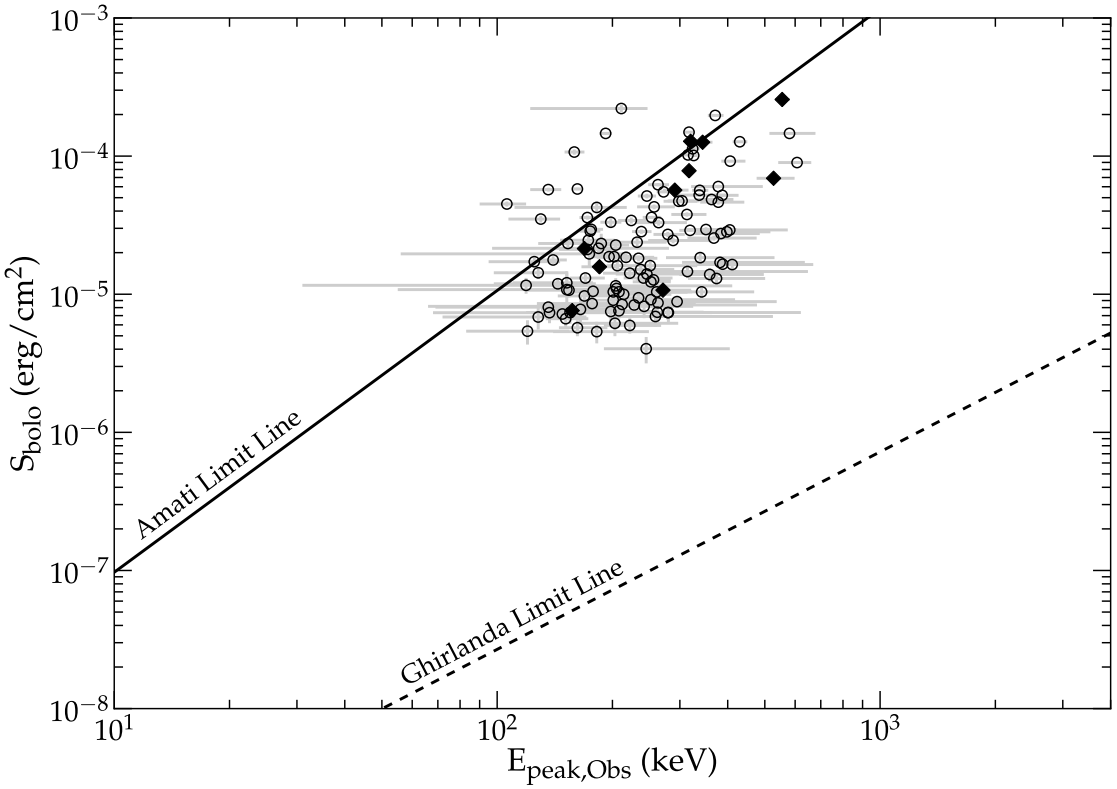

Figure 6.13 *Beppo-Sax* bursts. These bursts are taken from the Guidorzi (2011) bright *Beppo-Sax* burst catalog, of which 119 bursts are used. It is found that the fraction of bursts violating the Amati relation is 85% for bursts without spectroscopic redshifts, and 90% for bursts with redshifts. Because these are only the bright bursts, no commentary can be made as to the distribution of bursts like was done with other detectors. Despite these being the brightest bursts, this sample has a high violator rate. Since the brightest bursts are the most likely to pass the Nakar and Piran test, one can say with some confidence that the Amati relation fails for *Beppo-Sax* bursts. Filled diamonds represent bursts for which there is a measured redshift, unfilled circles are bursts for which there is no redshift.

used, and this is like noting that $\langle \log \frac{E_{peak}^{2.04}}{S_{bolo}} \rangle$ has changed. Previously, Band & Preece (2005) and Goldstein et al. (2010) pointed out that $> 80\%$ of BATSE bursts violate the Amati limit. In this section, these analyses have been generalized, both to looking at many GRB detector instruments and to looking at the two dimensional distribution in the $S_{bolo}-E_{peak,obs}$ diagram.

All of these data sets give consistent conclusions: (1) The distribution of bursts in the $S_{bolo}-E_{peak,obs}$ diagram varies significantly and greatly from satellite-to-satellite. (2) The only data sets to pass the generalized Nakar & Piran test for the Amati relation are the early heterogeneous sample of bursts with measured spectroscopic redshifts. (3) The bursts detected by BATSE, *Swift*, *Suzaku*, and *Konus* all have a high fraction ($\xi > 70\%$) of bursts which violate the Amati limit, with the violations being highly significant and by large factors. That is, the Amati relation fails for bursts from these four satellites. (4) The Amati limit is satisfied for the *HETE*-2 bursts, to the extent that the violator fraction is consistent the Amati relation plus normal observational scatter, however, the scatter in the $S_{bolo}-E_{peak,obs}$ diagram is so large that the conclusion is that the Amati relation does not satisfactorily apply to the *HETE*-2 data. (5) No bursts are found, from any satellite, that significantly violate the Ghirlanda limit. (6) These conclusions are true whether examining only bursts with spectroscopic redshifts or without redshifts.

The normalization factor for the Amati relation will scale closely with $\langle \log \frac{E_{peak}^{2.04}}{S_{bolo}} \rangle$. From Table 6.1, one sees that the Amati relation must vary from detector-to-detector by over an order of magnitude. With the bursts seen in the sky not depending on the satellite, the large variations in the Amati relation from detector-to-detector imply that there must be some selection effect which biases the visible bursts, with these biases being instrument-specific.

Every burst detector has a substantially different distribution of bursts in Figures 6.7-6.12. Since the population of bursts that appear in the skies above the Earth does not change with the satellite, so the large changes from detector-to-detector can only be due to some selection effect where bursts in various regions of the $S_{bolo}-E_{peak}$ diagram are not selected. The next section will investigate and identify these selection effects that create the Amati relation.

6.4 The Amati Relation Comes from a Combination of Selection Effects

The distributions of bursts in the $S_{bolo}-E_{peak,obs}$ diagram are caused by a variety of effects. Some of these effects are caused by detector limitations that prevent a burst from appearing in some parts of the $S_{bolo}-E_{peak,obs}$ diagram (Sections 6.4.1 and 6.4.2), while other effects make for rare bursts in other regions of the $S_{bolo}-E_{peak,obs}$ diagram (Sections 6.4.3 and 6.4.4). The combination of these effects will produce the observed distributions (Section 6.4.5). For some detectors, the selection effects will force the observed bursts to follow a roughly diagonal region (with wide scatter) that will appear as the Amati relation (Section 6.4.6).

6.4.1 Trigger Thresholds

The best known selection effect is the detector trigger threshold. For example, a burst would trigger BATSE only if it was produced a peak flux (in a 0.064, 0.256, or 1.024 second time bin) brighter than 5.5-σ above background in at least two detectors over the 50-300 keV energy range. Other satellites have more complex trigger algorithms (for example, GBM has overlapping triggers), but they all come down to the same essentials. The trigger threshold

depends on the $E_{peak,obs}$, the spectral energy range of the trigger, the background flux, and the effective area of the detector. The triggers operate off the peak flux (P_{max}), so the limiting fluence will depend on the effective duration (S_{bolo}/P_{max}), which can vary widely from burst to burst. Thus, the limit due to trigger thresholds will be 'fuzzy', with no sharp edge but rather a gradient as S_{bolo} is reduced. Approximately, the trigger threshold will produce a horizontal cutoff at the bottom of the $S_{bolo}-E_{peak,obs}$ diagram.

In principle, the exact trigger thresholds can be calculated for every detector and burst. In practice, the conditions ($E_{peak,obs}$, background flux, incidence angle, burst light curve) vary greatly from burst to burst, creating substantial scatter in the thresholds. For this chapter, an accurate distribution for the S_{bolo} threshold is not needed, so instead the typical S_{bolo} threshold is calculated as a function of $E_{peak,obs}$ for average conditions. In particular, an average spectral shape as the Band function (Band et al. 1993) is adopted with a low-energy power law index of -1.0 and a high-energy power law index of -2.0. The effective duration of the peak (S_{bolo}/P_{max}) is adopted such that it fits the observed distribution of the detectors. For each detector, values for the trigger energy range, face-on effective area, and the average background flux are taken. The formalism and many of the input parameters were taken from Band (2003). The result is a lower limit in the $S_{bolo}-E_{peak,obs}$ diagram, as displayed in Figure 6.7 for BATSE, Figure 6.8 for HETE, and Figure 6.9 for *Swift* . There is not enough information to calculate trigger thresholds for some satellites, but the threshold is usually fairly obvious (e.g., Figure 6.12 has a nearly flat and moderately sharp lower limit to S_{bolo}). These thresholds are not sharp, so bursts can easily appear somewhat below the threshold. Indeed, by varying the input conditions somewhat, the trigger threshold lines can be translated up and down substantially.

6.4.2 Threshold For Measuring $E_{peak,obs}$

A second detector selection effect is that the burst must have enough photons recorded for the analyst to be able to determine the $E_{peak,obs}$ value. This will depend on both S_{bolo} and $E_{peaks,obs}$ as well as the detector properties. For example, a burst just above the trigger threshold will have just enough photons to be detected but not enough photons to allow any constraints on the $E_{peak,obs}$ value, so this burst will not be included in a sample for plotting on the $S_{bolo}-E_{peak,obs}$ diagram. For another example, consider a burst with $E_{peak,obs}$ at the upper edge of the measured spectral range for a detector, such that a very bright burst will have a well-measured turnover that accurately defines the fitted $E_{peak,obs}$ value, whereas a fainter burst will have poor photon statistics near the turnover in the spectrum and the $E_{peak,obs}$ value will remain unmeasured and the burst will not be included in any of the samples.

In general, for a given $E_{peak,obs}$, there will be some lower limit on S_{bolo}, below which there will be too few photons to measure $E_{peak,obs}$. As $E_{peak,obs}$ moves to higher energies, the limit on S_{bolo} will sharply increase. The result will roughly be a diagonal line across the $S_{bolo}-E_{peak,obs}$ diagram, from lower left to upper right, with any burst below that line not having a measured $E_{peak,obs}$ and not appearing in any sample of bursts in Section 6.3.

Calculations were made of this threshold curve for BATSE, *HETE*-2, and *Swift*. To do this, in a Monte Carlo sense, many simulated bursts were constructed over each detector's spectral range for many values of $E_{peak,obs}$ where the normalization and error bars of the spectra were determined by the burst fluence. These spectra were then fitted by a power law times an exponential model (with the calculated $E_{peak,obs}$ value) and a simple power law model. If the chi-square values for the two fits differed by more than 15.0 (so that the model with the peak was a sufficiently good improvement on power law model given the

extra degree of freedom), then the S_{bolo} for the burst was taken to be above the threshold. By varying the $E_{peak,obs}$, the threshold for measurement as a curve in the $S_{bolo}-E_{peak,obs}$ diagram was determined. As these lines are merely for illustration, the DRM is *not used* for these simulations. For BATSE, *HETE*-2 , and *Swift* , the calculated thresholds are presented as curves in Figures 6.7, 6.8, and 6.9.

6.4.3 The $E_{peak,obs}$ Distribution

Amongst bursts appearing in the skies, the $E_{peak,obs}$ distribution is not flat, but rather bursts appear with a roughly log-normal distribution of $E_{peak,obs}$. For bright bursts, the mean value is 335 keV, with the FWHM stretching from roughly 150-700 keV (Mallozzi et al. 1995). This mean value shifts significantly as the bursts get dimmer, being 175 keV just above the BATSE trigger threshold (Mallozzi et al. 1995). The so-called 'X-ray Flashes' are simply bursts in the low-energy tail of the distribution (Kippen et al. 2004; Sakamoto et al. 2005; Pélangeon 2008). The existence of this single peak in the $E_{peak,obs}$ histogram is highly significant and not from any instrumental or selection effect (Brainerd et al. 1999). In all, most bursts are between 100-700 keV, and bursts <30 keV or >1000 keV are rare. This will directly translate to unpopulated regions of the $S_{bolo}-E_{peak,obs}$ diagram. A direct simulation of this distribution is given in Figure 6.4.

The $E_{peak,obs}$ distribution will cause definite but gradiated cutoffs in the $S_{bolo}-E_{peak,obs}$ diagram. These cutoffs will be nearly vertical. The drop in the average $E_{peak,obs}$ will make the cutoff on the right have a slope down to the lower left.

6.4.4 The S_{bolo} Distribution

Unsurprisingly, bright bursts are rare, while faint bursts are more frequent. The distribution of burst fluences is traditionally represented by the $\log N(>P) - \log P$ curve, for which

the best observations come from the BATSE catalog (Fishman et al. 1994; Paciesas et al. 1999). For bright bursts, the slope of the curve is nearly the ideal -$\frac{3}{2}$. The slope flattens out for faint bursts, approaching -0.7. In the $S_{bolo}-E_{peak,obs}$ diagram, the density of bursts falls off drastically from bottom to top (see Figure 6.4).

6.4.5 The Effects in Combination

The intrinsic distribution of bursts in the $S_{bolo}-E_{peak,obs}$ diagram is determined by the $E_{peak,obs}$ log-normal distribution that changes with S_{bolo} (Mallozzi et al. 1995) and by the log N($>$ P) $-$ log P distribution (Fishman et al. 1994). With these two effects, the burst density across the diagram is displayed in Figure 6.4. Together, the two effects produce burst density in the diagram Figure 6.14, and the parabolic threshold line in Figure 6.14. These combined effects dictate that bursts in the upper-left corner of the $S_{bolo}-E_{peak,obs}$ will be doubly rare, as bursts in this region will be very bright *and* have a low $E_{peak,obs}$. In other words, these distributions show a natural cutoff such that bursts that are below the Amati limit are rare.

The detector selection effects then operate on the natural distribution. The well known trigger threshold is actually below the threshold for measuring an $E_{peak,obs}$ value, so only the later selection effect is really operating. This selection effect cuts on a sort of diagonal from lower-left to upper-right, and its position depends greatly on the detector sensitivity and energy band for the trigger. For a relatively poor sensitivity and a trigger energy band that effectively does not get much above a few hundred keV, the threshold will be quite high. Indeed, for many detectors, the threshold will be just below the Amati limit line (Figure 6.14), so there will be few bursts significantly below the Amati limit line. That is, there is

a selection effect from the intrinsic distribution of bursts such that there is a natural cutoff below the Amati limit.

For some detectors, it is seen that the Amati relation is a natural and expected consequence of the intrinsic burst distribution combined with normal detector selection effects. This is illustrated in Figure 6.14, where the allowed region is confined to an area along the Amati limit line. From Figure 6.3, it is known that bursts along the Amati limit in the $S_{bolo}-E_{peak,obs}$ diagram will then imply a relation close to the Amati relation. Thus, the natural distribution of bursts makes for bursts above the Amati limit (i.e., the very-bright low-$E_{peak,obs}$ bursts) to be rare, while the detector selection effects makes for bursts below the Amati limit (i.e., the faint high-$E_{peak,obs}$ to be too faint to have a measured $E_{peak,obs}$. With the only bursts remaining being close to the Amati limit line, a relation like the Amati relation would be apparent. Thus, the conclusion is that the Amati relation is simply a result of selection effects and there is no physical basis.

For the original bursts used to define the Amati relation (Amati 2003), an additional selection effect is operating, in that the burst must also have a measured spectroscopic redshift for inclusion in the sample used for calibration. The selection effects for measuring a redshift are complex. There is certainly a selection based on redshift, with the cause being that more distant bursts are fainter, hence less likely to have a visible optical transient or host galaxy bright enough to get lines in a spectrum. An additional effect on redshift relates to the availability of spectral lines in the optical band. The efficiency of measuring redshift as a function of redshift has been quantified in Xiao & Schaefer (2011), with this effect being roughly an order of magnitude between z =5 and nearby bursts. The efficiency of measuring redshifts also presumably depends on S_{bolo} which will roughly scale as the burst brightness in the optical band. The redshift measurement efficiency also is time dependent, as optical

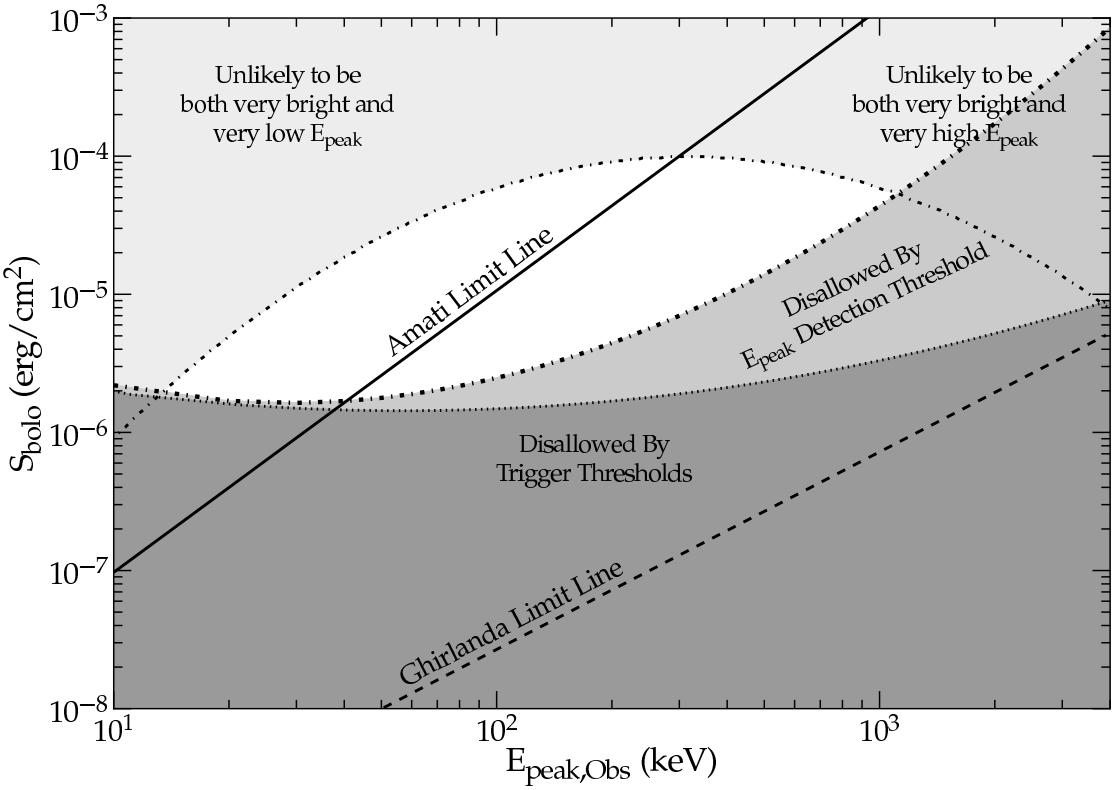

Figure 6.14 The selection effects. The two selection effects based on the intrinsic distribution of the burst population are combined and displayed as contours of burst density. These appear as two roughly concave-down parabolas, with each representing a different density level. The outside region is shaded darkly so as to indicate that bursts in those regions are rare, while the middle region is shaded a light gray to indicate that bursts in those areas of the diagram are less common than those in the central area. Of the two detector selection effects, the more restrictive is the requirement that the burst be bright enough to measure $E_{peak,obs}$. Versions of these detector effects are shown in a way to illustrate how the Amati relation bursts could be seen. The lower line illustrates a poor detector threshold (with shading below to indicate that no bursts in that area can be measured and placed onto the plot). The other line illustrates the result of a detector with both a poor detector threshold and low energy range (with shading below it). For a poor detector, the bursts that can be published and placed on this diagram are all in the unshaded and unhatched regions. The point of this diagram is that the selection effects will force the plotted bursts to roughly lie along the Amati limit line, and these bursts will then appear to obey the Amati relation. Thus, simple selection effects create the Amati relation, at least for some samples of bursts.

follow-up strategies and capabilities change within the community. Thus, *Swift* bursts started out with an average redshift of 2.8 in the first year after its launch (Jakobsson et al. 2006), while the average redshift has steadily declined to 2.1 over the last year (Jakobsson et al. 2009). The reason for this shift is unknown, but it must come from overall follow-up practices in the community. The bursts with redshift used in the *original* calibration of the Amati relation have an average redshift of 1.5, indicating that the effective threshold for this sample is quite high.

The distribution of bursts in the $S_{bolo}-E_{peak,obs}$ diagram will depend greatly on the detector. The threshold for measuring $E_{peak,obs}$ varies substantially detector to detector. For example BATSE has a low threshold while *Konus* has a high threshold. The shape of the threshold (as a function of $E_{peak,obs}$) also varies, from a flat bottom for *Konus* due to its sensitivity to high energy, to the up-sloping threshold for *Swift* due to its lack of high energy sensitivity and even more exaggerated in *HETE*-2 with its small area. The ability to measure $E_{peak,obs}$ depends critically on the energy range of the spectra. The *Konus* detectors have a very wide range of spectral energy resulting in a wide range of measured $E_{peak,obs}$ values, the *Swift* detectors cutoff around a few hundred keV, while the *Suzaku* detectors can only record $E_{peak,obs} \gtrsim 200$ keV. The combination of these selection effects makes the distribution of bursts different for each detector, and accounts for the wide range of distributions seen in Figures 6.5 - 6.12.

Still, the issue has been raised in recent tests (e.g. Ghirlanda 2011) that what is being seen in these failures is just the scatter about a relation which is ever changing with new bursts every day. The primary argument is that the Nakar and Piran test limit should be formulated from the 3-sigma line about the model, instead of the model line itself. As a result, the Amati limit would be considerably higher. There are a variety of problems with

this argument. The first of which being that there is already an allowance made for the Amati relation to have up to 40% violators and not be considered as failing for the data set. Therefore, the scatters are already being accounted for, and it is overkill to use such a generous limit to perform the test. If the test is done in this manner, no longer can allowances be made for any violators (or, more precisely, there needs to be less than 0.3% violators). Even by the groups own tests, there are violators on the order of a few percent, depending on the test. This is an unacceptable violator rate considering they are violating a limit from the three-sigma deviation from the model. Finally, another question that arises is that the bursts seen all seem to be biased in one direction. If these results were merely the of measurement scatter about the Amati relation, an equal fraction of bursts should been seen well above the limit line. Instead, for almost all data sets, the bursts are systematically in one direction from the limit.

The Amati relation will certainly see improvement in these tests in the future. With increasing number of *Swift* bursts with spectroscopic redshifts, it will undoubtedly eventually lie right in the middle of the *Swift* data set. Even then, the Amati relation will be failing for the best data sample, the BATSE data. So the argument is that there are undeniable systematic effects at play that are causing the Amati relation, and therefore even these 'improvements' would be fairly meaningless as there would still be systematic differences in where bursts are observed in the diagrams. Therefore, the Amati relation is simply not good for making any kind of predictions, cosmological or otherwise.

Perhaps the simplest disproof of the Amati relation is simply that the violator fraction is greatly too high in most data sets. And perhaps the simplest proof that the Amati relation is caused by selection effects is the large differences between the various $S_{bolo}-E_{peak,obs}$ diagrams for the many detectors.

6.5 Beaming Factor and the $S_{bolo}-E_{peak}$ Diagram

The Ghirlanda relation is greatly tighter than the Amati relation, and this provides confidence that a real physics relation is involved. Indeed, the physics behind the Ghirlanda relation has been easily explained as the simple consequence of relativistic effects and the viewing geometry within the usual jet model (Bloom et al. 2003; Yamazaki et al. 2004; Eichler & Levinson 2004; Levinson & Eichler 2005; Rees & Mészáros 2005). Thus, it appears that the Ghirlanda relation is true and physical for bursts. In the $S_{bolo}-E_{peak,obs}$ diagram, the Ghirlanda limit line (see Eq. 8 and many of the Figures) is reached only for bursts with no beaming (i.e., $F_{beam} = 1$) for a single high redshift. For $F_{beam} = 1$, a range of redshifts will produce bursts that are close to and just above the Ghirlanda limit line. This situation is illustrated in the upper-left panel of Figure 6.15. Most of the simulated bursts are well below the extreme case, so none of the bursts are actually on the Ghirlanda limit line.

The effect of beaming is easy to see, as it will only raise the bursts vertically in the $S_{bolo}-E_{peak,obs}$ diagram. (The real physics of the jets might result in correlations between F_{beam} and $E_{peak,obs}$, with this raising complications.) The Ghirlanda limit line (Equation 6.8) will have to be raised by the inverse of F_{beam}. Figure 6.15 displays the limit lines for beaming factors of 0.1, 0.01, and 0.001. The same figure also shows simulated bursts for the same sets of beaming factors. Bursts for a given beaming factor are fairly tightly confined to a narrow diagonal region just above the corresponding limit line. The center line for each of the panels is roughly parallel to and a factor of three above the limit line. Each of the limit lines has a constant value for $E_{peak,obs}^{1.43}/S_{bolo}$. With Equation 6.8 for $F_{beam} = 1$ and the approximate factor of three rise, the beaming factor can be approximated as

$$F_{beam} \approx \left(\frac{E_{peak}^{1.43}\, S_{bolo}^{-1}}{2.7 \times 10^{10}\, erg^{-1}\, cm^{2}} \right). \tag{6.9}$$

That is, one can estimate the beaming simply by looking at the position of the burst in the $S_{bolo}-E_{peak,obs}$ diagram. The bursts low down near the Ghirlanda limit line have nearly no beaming, while the bursts high in the diagram are highly beamed.

While only approximate, the $S_{bolo}-E_{peak,obs}$ diagram suddenly allows for measuring the beaming distribution for all GRBs, an idea first observed by Goldstein et al. (2011b). This is valuable because beaming can be otherwise measured only for the rare bursts with observed jet break times, with such a restriction being realized only for heavily selected bursts. Table 6.2 presents the logarithmic average of F_{beam} and θ_{jet} for the various burst samples. The majority of the BATSE bursts extends from beaming factors of near unity to 0.001, with a few bursts exceeding these values. By the average and RMS of the beaming factor, it is seen that most bursts are between 0.004-0.135. This sample has the lowest threshold across the bottom, and thus represents the most complete sample. Other satellites have higher thresholds that cutoff the derived beaming factor distribution from the bottom end. With this, it seems that the full population of GRBs has a typical beaming angle of $\sim 12^{\circ}$, and a typical range of around $5^{\circ} - 30^{\circ}$. This implies beaming angles substantially wider than realized only from those bursts with θ_{jet} derived from jet break times.

The position of the bursts used to calculate the original Amati relation (see Figure 6.5) is confined to a relatively narrow range of beaming factors from 0.001-0.01 (see Figure 6.15). This corresponds to $2.6^{\circ} < \theta_{jet} < 8^{\circ}$, which is close to the range derived from detailed analysis of multi-wavelength afterglow light curves (Panaitescu & Kumar 2002). It is as if the early bursts with redshifts were some selected for having a relatively narrow range of beaming angles. A better way to say this is to realize that the early thresholds for getting the redshifts were restricted to fairly bright bursts, and this allowed primarily bursts with high beaming factors to be selected (and bursts with very high beaming factors are rare),

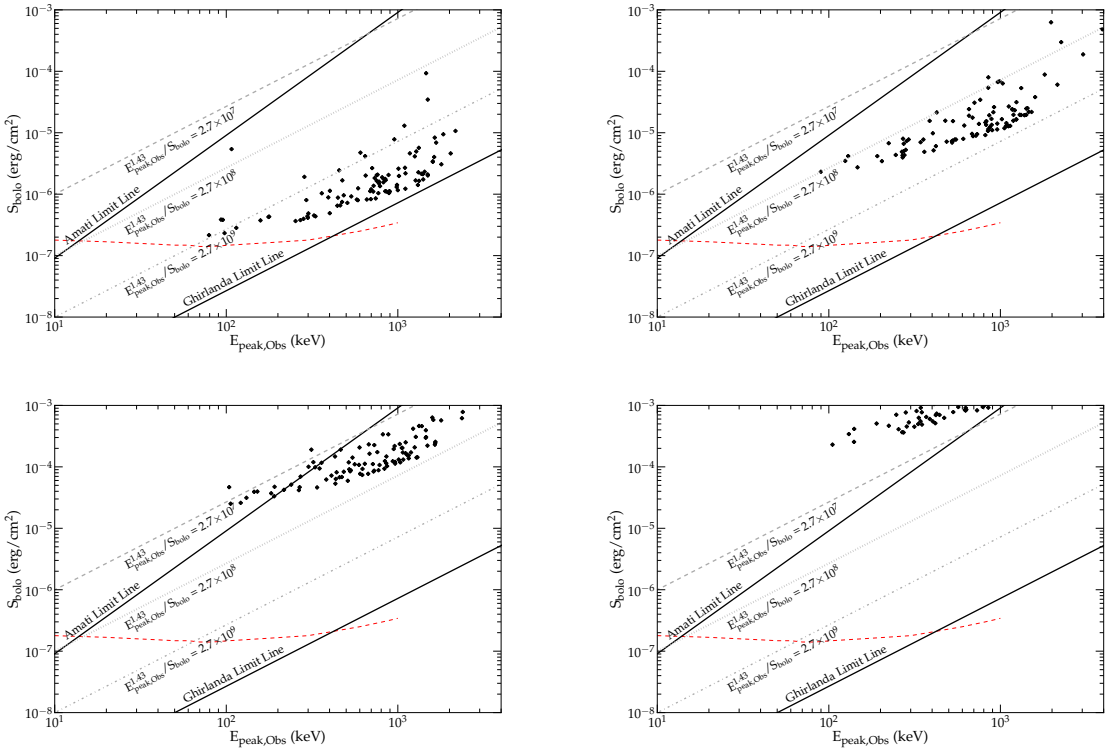

Figure 6.15 Beaming and the Ghirlanda limit. From Equation 8, the Ghirlanda relation demands that no burst be below some diagonal line in the $S_{bolo}-E_{peak,obs}$ diagram, with this line corresponding a burst with no beaming (isotropic emission with $F_{beam} = 1$). In principle, with beaming factors of 0.1, 0.01, and 0.001, corresponding limit lines can be drawn, as shown in each of the panels of this figure. As in Figure 6.2, the Ghirlanda relation as applied to a population of bursts with realistic distributions of redshift and $E_{peak,obs}$ will produce a diagram with points just above the limit line. The upper-left panel shows a set of 100 bursts from a Monte Carlo simulation with no beaming. No detector selection has been applied to these bursts. The bursts naturally lie typically a factor of three above the Ghirlanda limit line, although there is a scatter of around a factor of two. The other three panels show identical Monte Carlo simulations for 100 bursts each for which $F_{beam} = 0.1$ (upper-right panel), $F_{beam} = 0.01$ (lower-left panel), and $F_{beam} = 0.001$ (lower-right panel). With this, the position of a burst in the $S_{bolo}-E_{peak,obs}$ diagram can be used to read off its approximate beaming factor. Bursts along the Amati limit line will have beaming factors of 0.001-0.01. Indeed, the selection effects for some samples that allow only bursts to appear near the Amati limit line are equivalent to a selection on the beaming of the burst. With the realization that the position in the $S_{bolo}-E_{peak,obs}$ diagram gives the beaming, a beaming distribution for all bursts can now be constructed, not just those biased few for which a redshift and jet break have been measured.

Table 6.2. Beaming Factors for Each Data Sample

Data Set	$\#_{\mathrm{w}/z}$	$\langle \log \mathrm{F}_{\mathrm{beam}} \rangle_{\mathrm{w}/z}$[a]	$\#_{\mathrm{w/o}\ z}$	$\langle \log \mathrm{F}_{\mathrm{beam}} \rangle_{\mathrm{w/o}\ z}$[a]
Amati et al. 2006	50	-2.80±0.50	0	...
Schaefer 2007	27	-2.78±0.53	0	...
BATSE	0	...	1654	-1.64±0.77
HETE-2	12	-2.90±0.61	24	-2.45±0.67
Swift	25	-2.15±0.47	46	-2.17±0.48
Suzaku	7	-1.96±0.65	25	-1.60±0.76
Swift - *Suzaku*	25	-1.93±0.82	38	-2.19±0.70
Konus	33	-2.48±0.58	64	-2.20±0.68
Beppo-Sax	10	-2.57±0.33	119	-2.36±0.37

[a]For this, F_{beam} is *not* found with the use of a jet break time. Rather, $\mathrm{F}_{\mathrm{beam}}$ (and hence θ_{jet}) is found for individual bursts in a sample from Equation 6.9. The tabulated numbers are the average values over the given sample, while the RMS scatter over the whole sample is given after the average.

with the resulting sample strung out along a line which then was identified as the Amati relation.

6.6 Short Bursts

The short-hard GRBs, with the 90% duration (T_{90}) less than two seconds, are apparently a separate population from the long duration bursts talked about in al the previous sections. Goldstein et al. (2010) have presented the $S_{bolo}-E_{peak,obs}$ diagram for 168 short GRBs from the BATSE data. They point out that the use of an 'energy ratio' (i.e., $E^{1.43}_{peak,obs}/S_{bolo}$) provides an excellent discriminator between long and short GRBs. This would replace the distinction between the two classes as based on two properties (duration and hardness) with a distinction based on only one property (the energy ratio). This new criterion has a further advantages that it avoids a property (the hardness ratio) that is highly instrument dependent and arbitrary, and it avoids the sticky issue of measuring the T_{90} duration. A further advantage is that the energy ratio has only a relatively small dependence on the redshift of a burst, in that the exact same burst as viewed over a range of redshifts will have a relatively small change in the energy ratio, whereas the $1 + z$ factor applied to the T_{90} duration will substantially blur the 2-second paradigm.

For this chapter, the important point is that a short-long distinction based on the energy ratio implies that the short and long bursts occupy largely separate ranges in the $S_{bolo}-E_{peak,obs}$ diagram. Indeed, Figure 3 of Goldstein et al. (2010) demonstrates that the short bursts lie just above the Ghirlanda limit line and generally below the long bursts. Therefore, if the Ghirlanda relation applies to short GRBs, then they should all have $F_{beam} \approx 1$. If short GRBs are found to have significant beaming, then the Ghirlanda relation cannot apply to them.

While two-seconds is often used as a a cutoff between short and long GRBs, there is an overlap between the two populations. That is, some hard bursts that last longer than 2 seconds, and there are bursts that are shorter than 2 seconds that are soft. Unfortunately, Goldstein et al. (2010) finds overlap between the long and short bursts using the energy ratio that is comparable to the overlap seen using T_{90}. Therefore, while the energy ratio is a good way of delineating short and long bursts, it does not appear to do any better to distinguish bursts that are ambiguous as to their classification.

6.7 Conclusions

The $S_{bolo}-E_{peak,obs}$ diagram has two limit lines, where bursts cannot be below that line if the Amati or Ghirlanda relation holds. Actually, with the fairly large total uncertainties, substantially larger than the simple measurement errors quoted in the literature, nearly half of the bursts can be expected to be scattered below the Amati limit line. So a simple test of the Amati relation is whether the *average* burst falls below the Amati limit. (This is similar to the original test proposed by Nakar & Piran, except that agreement with the Amati relation corresponds to about 40% violators.) This test was applied to many burst samples. The samples of early bursts with spectroscopic redshifts (as originally used to calibrate the Amati relation) pass the test, as does the sample of *HETE*-2 bursts (even though the scatter about the Amati relation is unusably large). All other satellites have a large fraction of violators far below the Amati limit line. This is true whether looking at bursts with or without measured spectroscopic redshifts. This constitutes a proof that the Amati relation could possibly apply, at best, to only a small and unrecognizable fraction of GRBs. Indeed, the wide variations in distribution from detector to detector constitute a proof that selection effects must dominate the Amati relation.

Four selection effects are found that restrict the distribution on all sides. The best known detector selection effect is the trigger threshold, which produces a roughly horizontal and fuzzy cutoff. A more subtle and more restrictive selection effect is that for an $E_{peak,obs}$ value to be reported, the burst must be brighter than some threshold, with this threshold rising fast with increasing $E_{peak,obs}$. These two detector selection effects will cut out bursts that are some combination of faint and hard, with these effects changing greatly from detector to detector. The third and fourth selection effects operate to restrict the burst population as it appears in the sky. The third selection effect is that bursts have a log-normal distribution of $E_{peak,obs}$ with the mean value shifting to lower values for faint bursts. This effect will also reduce the number of detectable bursts that are faint and hard. The fourth selection effect is that bright bursts are much rarer than faint bursts, as quantified by the usual power-law $\log[N(>P)] - \log[P]$ curve. The combination of the third and fourth effects means that the bright and soft bursts are doubly-rare, so that the upper-left side of the $S_{bolo}-E_{peak,obs}$ diagram will be empty.

For a detector with a range of spectral sensitivity and a low detection threshold, the distribution in the $S_{bolo}-E_{peak,obs}$ diagram will extend relatively low, with a large fraction of violators below the Amati limit (like for BATSE). For a detector with a low energy range of sensitivity and a low detection threshold, the cutoff will be a diagonal line just below the Amati limit. When combined with the paucity of bright-soft bursts in the GRB population (i.e., those above the Amati limit line), there is a combined selection effect that picks out bursts near the Amati limit. Such a burst sample would then appear to follow the Amati relation. Thus, the very strong selection effects for the early bursts with spectroscopic redshifts will create the Amati relation without any need for a physical connection between the $E_{peak,obs}$ and S_{bolo}. That is, the Amati relation is not real, but its appearance in some

data sets is simply a result of various selection effects by the detectors and within the GRB population.

There are still strong reasons to believe that the Ghirlanda relation is a valid physical law for GRBs. With this, the position of a burst in the $S_{bolo}-E_{peak,obs}$ diagram will be a function of its beaming factor. Along lines parallel to the Ghirlanda limit, the beaming factor is given by Equation 6.9. This allows one to construct an approximate distribution of F_{beam} for the BATSE bursts without any selection effects. The typical beaming factor is found to be 0.02 ($\theta_{jet} = 12°$), most bursts have beaming factors in the range 0.004-0.1 ($5° < \theta_{jet} < 30°$), while the extreme values of the beaming factor *tending to* range from 0.001-1 (from $\theta_{jet} = 2.6°$ to isotropic). The bursts in the original sample for the Amati relation are stretched out along the Amati limit line, and these correspond to beaming factors of 0.001-0.01 ($2.6° < \theta_{jet} < 8°$).

With these strong results, the Amati relation should clearly not be used for purposes of cosmology, as has been previously done by many groups. It should be noted that for the GRB HD, the Amati relation has not been used for any cosmological purpose *by the LSU GRB group* (e.g., Schaefer 2007; Xiao & Schaefer 2011).

It needs to be emphasized that the failure of the Amati relation in no way carries any implications for any other GRB luminosity relation. The fault of the Amati relation can be viewed as if it is merely a version of the Ghirlanda relation except that the beaming correction is unknown, so isotropic emission was assumed. The result, however, is that the Amati relation is biasing itself towards some average of whatever the beaming factors of the calibrating bursts are. All the other GRB luminosity relations do *not* involve beaming corrections, and the known physics of the beaming is already accounted for in the physics derivations of these laws. The Ghirlanda relation is in essence just a conservation of energy statement, while the other luminosity relations (all involving the peak flux, not the fluence)

just involve relativistic effects in the visible region of colliding jets. Indeed, most of the other GRB luminosity relations were *predicted* from the physics and then later confirmed. In all, the failure of the Amati relation is zero evidence for the validity of the other relations (many of which were confirmed predictions) and there are good physical reasons to know that they are valid physical laws for GRBs.

7. The Burst Pulse Paradigm

This chapter covers work that is a preliminary investigation into whether the burst pulse paradigm can be used to improve the GRB luminosity relations.

7.1 Introduction

Recently, a number of good arguments have been made that some burst properties are really based on individual pulses of the burst (e.g. Hakkila et al. 2008; Ghirlanda et al. 2009; Hakkila & Preece 2011). In particular, the rise time, $\tau_{\rm rise}$, the lag time, $\tau_{\rm lag}$, the peak flux, $P_{\rm bolo}$, and the time-resolved $E_{\rm peak}$. It makes good physical sense to consider these values on a pulse-by-pulse basis as opposed to some value over the whole burst. As different pulses will vary in luminosity, the values for these time-resolved quantities will change greatly over the course of the burst over the course of various pulses.

Work has already been done in extracting burst pulse properties of bursts over several detectors, including BATSE, *HETE*-2 and *Fermi* (e.g. Hakkila 2008; Hakkila & Nemiroff 2009; Hakkila & Preece 2011; Arimoto et al. 2010; Ghirlanda et al. 2010). These groups have found a consistent (and unsurprising) trend that within an individual burst, a pulse's peak flux is significantly correlated with shorter $\tau_{\rm lag}$, $\tau_{\rm rise}$, and durations. Despite all this work, the groups have yet to apply it to *Swift* bursts, and no work has been done towards using this information with the GRB luminosity relations. The majority of the work in the literature has been to advertise and test the robustness of the pulse paradigm.

The formalism in idenifying and fitting pulses has been laid out in the literature. In Hakkila et al. (2008), this is described as using the following fitting model to pulses

$$\mathrm{I(\,t)} = \mathrm{A}\exp\left[2\left(\frac{\tau_1}{\tau_2}\right)^{1/2}\right]\exp\left[-\frac{\tau_1}{\mathrm{t}-\mathrm{t_s}}-\frac{\mathrm{t}-\mathrm{t_s}}{\tau_2}\right]. \tag{7.1}$$

In this equation, A is the amplitude of the pulse, $\mathrm{t_s}$ is the start time of the pulse, and τ_1 and τ_2 and a rise and decay time of the pulse. This routine has found to be quite successful in the literature, particularly with BATSE data. Hakkila et al. (2008) described a procedure in which a Bayesian Blocks (Scargle 1998) method was used to identify possible pulses in the burst. In addition, $\mathrm{E_{peak}}$ varies with time over the course of a GRB, and tends to spike when a new pulse starts (Hakkila 2011). Nonetheless, this method cannot be completely automated, and requires human intuition to determine pulses on a case by case basis.

This formalism provides several advantages for pulling out GRB luminosity indicators. The most obvious is that pulling the peak flux is much more accurate when taking a fitted light curve as opposed to some average over the brightest second of the burst. The other advantage is that using the values from a fitted pulse would provide a purer estimate of pulse parameters than those that have been derived from the whole burst. This is due to the pulse parameters from the whole burst being the result of some sort of convolution of a number of pulses. Finally, as the majority of bursts have multiple pulses, a redundancy can be developed to improve the accuracy of a distance measure to the burst.

Swift has the largest number of GRBs with measured redshifts, and represents an untapped source to apply the burst pulse paradigm to the GRB luminosity relations. A simple way to test this is to take *Swift* bursts for which pulses are well separated. This idealized case would provide a measurement of how well the luminosity relations can be improved.

This chapter highlights an investigation into such an 'idealized' sample. *Swift* bursts are analyzed for the means of applying the burst pulse paradigm to the GRB luminosity relations.

Overall, the Hakkila model for pulses is found to be unstable for the bursts used. The model is not robust, an suffers from large cross terms in the covariance matricies. In addition, a two sided Gaussian model is used on the data. While this model has less trouble converging, it still has unacceptably large uncertainties. As such, the conclusion is that the sample is not good for using the $\tau_{\rm rise} - {\rm L}$ or $\tau_{\rm lag} - {\rm L}$ relations. In addition, there are a number of issues that confuse the accuracy of $E_{\rm peak}$ over these pulses. Therefore, the $E_{\rm peak} - L_{\rm iso}$ relation will also be not useful for the sample. As the 'best case' data does not work with the *Swift* data, this will likely lead to no good uses for the luminosity relations.

7.2 Data

As the luminosity relations can only be calibrated on bursts for which the distance is known, the candidate list starts with just the *Swift* bursts for which there is a measured spectroscopic redshift. The first cut made was to remove bursts for which there were obviously more than one pulse overlapping (which was a sizable majority). Still more bursts were rejected for being too noisy. These initial cuts were made via direct observation of the light curves on the online *Swift* quick look data table[1].

For the remaining bursts, the *Swift* BAT (Burst Alert Telescope) data was downloaded through the *Swift* portion of the HEASARC (High Energy Astrophysics Science Archive Center) database[2]. This database provides a simple means download the relevant data to a local device.

The data was then processed through a series of routines as described in the BAT user's manual available on the *Swift* webpage[3]. These commands were used to update the data files

[1] http://swift.gsfc.nasa.gov/docs/swift/archive/grb_table/
[2] http://heasarc.gsfc.nasa.gov/cgi-bin/W3Browse/swift.pl
[3] http://swift.gsfc.nasa.gov/docs/swift/analysis/

using the latest calibration files, and create light curves and spectra. These processes were checked multiple times against existing examples to ensure that the commands were being executed properly. *Batbinevt* and *batgrbproduct* are largely the two most commonly used routines. *Batbinevt* being the command for making lightcurves and spectra, and *batgrbproduct* runs this routine for a variety of different time intervals and energy ranges (in addition to other tasks irrelevant to this investigation).

Having confidence that these routines were being run in the proper way, light curves were generated for the remaining set of $\sim$ 15 GRBs. These light curves were binned by the normal *Swift* operating mode of 64ms per bin, and used the latest *Swift* calibration files to automatically remove the background. This is another important strength of *Swift* , as it removes any kind of arbitrary background subtraction that has to be done manually (like with BATSE). The *Swift* data analysis programs take into account the various different contributions to background that need to be considered (e.g. spacecraft motion, variations in pointing).

The output of the light curves is generally output as a binary table (FITS). This was converted into an ASCII (American Standard Code for Information Transfer) table for easier use in codes by means of a personally written script in the *Python* coding language. The *Python* package PyFITS[4], as distributed by STScI (Space Telescope Science Institute), was very useful in this task.

The light curves were once again critiqued for various quality issues. Even at this stage, some bursts were rejected for having overlapping pulses. These pulses were averaged out when first observed on the 1-second light curves, but appeared with the finer time resolution. In addition, some pulses that appeared separated were merged when looked at with the finer

[4]http : //www.stsci.edu/resources/software_hardware/pyfits

resolution data. Still other pulses had to be removed for having pulses that were barely above the noise and thus were too faint. The full *Swift* data set was reassessed to attempt to find any additional bursts to add to the sample. For example, some bursts were included that had two pulses, but the second pulse was far too faint to readily measure (e.g. 060904B). In the end, the sample included 13 bursts with one good pulse (050908, 051111, 060206, 060904B 060912, 070306, 070318, 070612, 070810, 071010B, 080413B, 091018, 091020). In addition, and only one burst with multiple pulses was suitable for use, 091208B.

7.3 The Hakkila Pulse Model

With the data set now settled upon, the next step was to fit the data to the Hakkila pulse model (equation 7.1). The first attempt made is the simplest approach in optimization, a brute force method. By 'brute force', the meaning is that every combination of reasonable fit parameters is attempted, and the combination that provides the best fit is taken. One 'smart' way to perform this method is to start with a low-resolution parameter space, and once the general area of the minima is found, then move to successfully higher resolutions. This was done with simple coding in *Python*. Unfortunately, the model created a 'wrinkly' chi square surface, creating many local minima. There was no simple and quick way to converge on a solution, even with a 'smart' approach. Given the computational time required to run a brute force method, another solution was sought out.

The next attempt was to try the *fmin* function within Scipy, a *Python* package. *Fmin* is a package that uses the Nelder-Mead simplex algorithm (e.g. Nelder & Mead, 1965). The general idea of a simplex is to start with a number of attempts of finding the minima, and to gradually replace the worst of the points with a value that goes through the center of the

worst of the others. Eventually, the simplex works its way down the slope of the chi-square surface until it reaches the minimum.

This function converged to a solution in a much quicker manner than the brute force method. These solutions did not prove to be very robust, and very often gave different solutions for small changes in the initial parameters. Several attempts were made to resolve this issue, including giving the algorithm many different starting points, setting absolute bounds on fitting parameters, and varying the tolerance in the convergence parameters. While these steps did seem to improve the fits somewhat, they did not resolve the underlying issue. Computing time was going to be entirely too high to confidently identify the global minimum. In this sense, the simplex approach was only marginally better than the brute force method.

The Levenberg-Marquardt optimization method (Levenberg 1943; Marquardt 1963) is a gradient-based optimization method that uses the slope of the chi-square surface to find minima. It is generally used in non-linear optimization problems although like the simplex, can converge on local minima easily. MPFIT is routine originally written on IDL based on this method is also available on *Python* through STScI. Likewise, leastsq is another routine in *Python* that uses this method. Both these algorithms failed for many of the same reasons that the simplex method failed. There was no confidence in the results being given by the optimization software.

At this point, there was concern that the routines failing due to poor implementation. All previous codes (for all routines) were run for a much simpler set of data - a Gaussian function with some arbitrary noise. These routines worked quickly and efficiently in finding the correct answer for the data. These checks provided confidence that these routines were being run in the correct manner.

Curve_fit, another Scipy optmizer in *Python* also uses the Levenberg-Marquardt method. This routine provided a more reliable fit than the other routines, even fitting 'known data' quicker and more accurately than other routines. Unfortunately, *curve_fit* also had many of the same problems with robustness as previous routines. Small changes in the initial conditions yielded considerably different optimization parameters. This was true regardless of the brightness of the pulse. Even when given realistic starting parameters, the routine would return unrealistic fits.

Another problem was that even when the routine returned reasonable values, the uncertainties were entirely too large, often anywhere between one and ten times that of the actual value. The cross terms were of similar size, only further demonstrating the poor quality of the fits. With such uncertainties, there was no confident way to declare any set of fit parameters as optimal.

At this point, the usage of the Hakkila formulation was questioned. The same burst data however, seemingly had no problems being fit to Gaussian pulse models. This once again suggested that the problem was not in how the fits were being executed, but in the model itself. The fits were much more stable with Gaussian functions, with very little of the local minima issues seen with the Hakkila model. As such, a new model was adopted.

7.4 The Two Sided Gaussian Pulse Model

A new model was therefore adopted, a two-sided Gaussian.. As the model implies, it is a Gaussian function, but with different widths on either side of the peak. The function is made continuous by ensuring the amplitude is the same. Specifically, the fitting model used

was

$$I(t) = \begin{cases} A\, e^{-\frac{(t-t_p)^2}{2\sigma_1^2}} & : t < t_p \\ \\ A\, e^{-\frac{(t-t_p)^2}{2\sigma_2^2}} & : t \geq t_p \end{cases} . \tag{7.2}$$

Where the amplitude A retains the same meaning as the Hakkila pulse model in equation 7.1. The standard deviations for each side of the Gaussian, σ_1 and σ_2, will be analogs to the values of τ_1 and τ_2 in the Hakkila model respectively. The new value t_p, represents the time of the peak.

The two sided Gaussian resolved some of the issues seen within the Hakkila model. It was far more robust, and did not suffer from the same problems with local minima as seen previously. In most cases, with even vaguely reasonable starting parameters, the same values were returned. Unfortunately, the error bars were still large, and still had fairly high cross terms. These uncertainties, however, were nowhere near as large as what was being consistently seen using the Hakkila model. Since this new model was robust, the entire data set was fit to it. The results in these tables were further tested for robustness by varying the fit intervals. The model provided stable results regardless of fit interval, giving confidence in the fit values. The fit results are in Table 7.1 and Table 7.2. *Swift* data is typically broken down into four channels. Channel 1 covers 15-25 keV, channel 2 cover 25-50 keV, channel 3 covers 50-100 keV, and channel 4 covers 100-350 keV. The data was fit to all individual channels in Table 7.1 and the sum of all four channels in Table 7.2.

Physically, one should expect that the higher the energy bands will have earlier peaks. That is, the higher the energy range of the 'channel', the earlier the value for t_p should be. This is a direct result of the Liang-Kargatis relation (Liang & Kargatis 1996; Crider et al. 1999; Ryde & Svensson 2000; 2002), which dictates that $dE_{peak}/dt \propto L$. This is established by the expected case of shocked material cooling at a rate dominated by radiative cooling.

That is, the shocked material will cool as a function of how quickly it radiates energy away (its luminosity). Explicitly, as the emitting region of a luminous GRB cools, the 'peak' of a pulse will be seen to occur close in time between the high and low energy channels as the burst is quickly radiating its energy away. Conversely, a dimmer burst will radiate its energy away much more slowly and thus have a longer delay in the peaks in the high and low energy channel. Surprisingly, the idea of using this as a form of luminosity indicator was missed originally, and it was not until Schaefer (2004) the $\tau_{\rm lag} - {\rm L}$ relation was explained.

One of the first things to look for in Table 7.1 is t_p in the individual channels. In many cases, the peak of the pulse did not uniformly get earlier for higher energies, and in other cases, the time of the higher energy channels had error bars too large to confidently calculate a lag time. In still other cases, no good fit was obtained in the highest energy band due to lack of photons. It was only for the bright bursts of the sample that a lag time could even reasonably be obtained.

Still, most lags were unreliable. They were often too large, and very often negative, meaning that the lag times were doing the exact opposite of what has been seen in the literature, and what is expected physically. Table 7.3 shows a list of bursts for which lags were obtained. These lags were between the 25-50 keV and 100-350 keV *Swift* channels (channels 2 and 4), which is the traditional way of measuring lag in *Swift* bursts. For bursts where no fourth channel data exists, no lag is recorded. One can see that almost all the lags are bad in one or more of these ways described.

Table 7.1. Two-Sided Gaussian Fits to *Swift* Data - Individual Channel Data

BURST	CH[a]	A (cts s^{-1} $detector^{-1}$)	t_p (s)	σ_1 (s)	σ_2 (s)	χ^2	dof
050908	1	$1.50\times10^{-2}\pm2.38\times10^{-6}$	301.801±7.732	10.535±6.515	8.521±6.077	1165.5	1251
	2	$2.80\times10^{-2}\pm5.44\times10^{-6}$	300.450±1.223	3.650±0.903	5.876±1.092	1227.1	1251
	3	$1.80\times10^{-2}\pm5.22\times10^{-6}$	302.165±1.622	3.576±1.307	3.338±1.265	1121.9	1251
	4	$3.00\times10^{-3}\pm4.81\times10^{-6}$	299.491±20.305	1.367±14.544	3.823±21.749	1183.9	1251
051111	1	$5.80\times10^{-2}\pm5.47\times10^{-6}$	298.810±0.552	3.066±0.366	13.721±0.698	1584.6	1564
	2	$9.30\times10^{-2}\pm6.60\times10^{-6}$	296.434±0.152	1.648±0.096	15.124±0.277	1646.2	1564
	3	$8.70\times10^{-2}\pm6.65\times10^{-6}$	296.444±0.172	2.045±0.104	12.661±0.242	1673.8	1564
	4	$3.00\times10^{-2}\pm5.85\times10^{-6}$	297.456±1.036	2.723±0.674	7.312±1.034	1553.0	1564
060206	1	$1.01\times10^{-1}\pm1.33\times10^{-5}$	301.454±0.033	1.353±0.022	2.433±0.028	551.7	626
	2	$1.34\times10^{-1}\pm2.09\times10^{-5}$	301.436±0.024	1.401±0.016	1.949±0.018	663.1	626
	3	$9.70\times10^{-2}\pm1.70\times10^{-5}$	301.514±0.028	1.475±0.021	1.360±0.020	632.3	626
	4	$2.10\times10^{-2}\pm1.10\times10^{-5}$	302.563±0.142	1.870±0.198	0.350±0.095	639.8	626
060904B	1	$5.30\times10^{-2}\pm1.57\times10^{-5}$	240.282±0.156	0.640±0.106	5.528±0.306	1563.9	1563
	2	$8.80\times10^{-2}\pm2.13\times10^{-5}$	240.215±0.095	0.993±0.060	4.451±0.120	1582.3	1563
	3	$9.80\times10^{-2}\pm2.30\times10^{-5}$	240.402±0.061	1.113±0.039	2.969±0.058	1450.7	1563
	4	$2.30\times10^{-2}\pm1.51\times10^{-5}$	239.936±0.593	0.781±0.394	3.207±0.686	1539.3	1563
060912	1	$2.61\times10^{-1}\pm1.39\times10^{-4}$	239.805±0.007	0.301±0.004	1.698±0.009	917.9	939
	2	$3.73\times10^{-1}\pm2.49\times10^{-4}$	239.670±0.003	0.208±0.002	1.293±0.004	968.8	939
	3	$2.50\times10^{-1}\pm1.89\times10^{-4}$	239.508±0.005	0.198±0.003	1.299±0.007	969.2	939
	4	—	—	—	—	—	—
070306	1	$1.02\times10^{-1}\pm8.11\times10^{-6}$	337.013±0.188	3.484±0.139	8.406±0.150	1219.8	938
	2	$1.27\times10^{-1}\pm1.01\times10^{-5}$	336.994±0.130	3.209±0.094	7.989±0.101	1286.1	938
	3	$1.00\times10^{-1}\pm9.35\times10^{-6}$	337.558±0.136	3.232±0.098	5.888±0.101	1185.7	938
	4	$2.00\times10^{-2}\pm3.48\times10^{-6}$	339.444±1.595	6.978±1.825	3.290±1.047	924.7	938
070318	1	$3.00\times10^{-2}\pm2.33\times10^{-6}$	176.753±0.801	1.779±0.526	20.732±1.631	1622.4	1564
	2	$5.30\times10^{-2}\pm3.50\times10^{-6}$	175.947±0.086	0.513±0.055	16.483±0.392	1578.8	1564
	3	$4.40\times10^{-2}\pm3.80\times10^{-6}$	176.047±0.157	0.743±0.099	13.820±0.480	1690.0	1564
	4	$9.00\times10^{-3}\pm1.74\times10^{-6}$	175.233±0.601	0.184±0.383	20.317±9.313	1608.3	1564
070612	1	$2.40\times10^{-2}\pm7.50\times10^{-6}$	240.473±14.164	3.563±9.574	36.173±33.512	2180.7	2189
	2	$3.90\times10^{-2}\pm9.85\times10^{-6}$	235.884±3.925	2.028±2.488	34.467±11.794	2205.9	2189
	3	$6.60\times10^{-2}\pm1.72\times10^{-5}$	232.962±0.193	0.052±0.112	21.014±1.886	2270.3	2189
	4	$1.90\times10^{-2}\pm1.01\times10^{-5}$	235.587±18.710	5.176±12.760	16.193±19.620	2207.5	2189
070810	1	$5.80\times10^{-2}\pm1.39\times10^{-5}$	240.379±0.277	1.848±0.190	4.307±0.265	880.8	939
	2	$8.00\times10^{-2}\pm2.27\times10^{-5}$	239.929±0.121	1.237±0.083	3.323±0.117	949.0	939
	3	$3.90\times10^{-2}\pm1.89\times10^{-5}$	239.543±0.285	0.963±0.196	2.879±0.313	939.7	939
	4	—	—	—	—	—	—
071010B	1	$2.57\times10^{-1}\pm1.56\times10^{-5}$	240.268±0.013	1.221±0.008	6.625±0.017	1322.5	1095
	2	$3.17\times10^{-1}\pm2.25\times10^{-5}$	240.422±0.010	1.149±0.006	5.697±0.012	1435.7	1095
	3	$2.01\times10^{-1}\pm1.72\times10^{-5}$	240.330±0.013	0.976±0.008	4.650±0.015	1244.7	1095
	4	$3.00\times10^{-2}\pm6.83\times10^{-6}$	240.001±0.248	1.135±0.162	3.892±0.289	1095.5	1095

Table 7.1—Continued

BURST	CH[a]	A (cts s^{-1} $detector^{-1}$)	t_p (s)	σ_1 (s)	σ_2 (s)	χ^2	dof
080413B	1	$5.04\times10^{-1}\pm3.55\times10^{-4}$	239.294±0.009	0.615±0.005	1.676±0.008	529.1	469
	2	$7.50\times10^{-1}\pm6.89\times10^{-4}$	239.270±0.005	0.500±0.003	1.430±0.004	624.6	469
	3	$6.26\times10^{-1}\pm6.06\times10^{-4}$	239.291±0.005	0.477±0.003	1.019±0.003	491.0	469
	4	$1.48\times10^{-1}\pm2.61\times10^{-4}$	239.153±0.028	0.436±0.017	0.844±0.023	467.7	469
091018	1	$4.53\times10^{-1}\pm8.60\times10^{-5}$	243.642±0.003	0.601±0.002	1.669±0.002	511.7	469
	2	$4.53\times10^{-1}\pm1.08\times10^{-4}$	243.638±0.003	0.654±0.002	1.315±0.002	545.0	469
	3	$1.80\times10^{-1}\pm6.65\times10^{-5}$	243.540±0.012	0.699±0.008	1.100±0.009	515.7	469
	4	—	—	—	—	—	—
091020	1	$9.60\times10^{-2}\pm1.73\times10^{-5}$	241.605±0.392	3.928±0.277	6.720±0.330	844.3	783
	2	$1.49\times10^{-1}\pm2.48\times10^{-5}$	240.486±0.102	1.818±0.064	6.408±0.109	795.1	783
	3	$1.49\times10^{-1}\pm3.17\times10^{-5}$	240.220±0.074	1.203±0.044	5.622±0.087	898.4	783
	4	$4.60\times10^{-2}\pm1.97\times10^{-5}$	240.027±0.400	0.904±0.267	5.845±0.603	822.3	783
091208B[b]	1	$3.04\times10^{-1}\pm6.91\times10^{-4}$	367.986±0.045	0.633±0.029	1.450±0.039	165.4	157
	2	$6.38\times10^{-1}\pm2.45\times10^{-3}$	367.817±0.007	0.192±0.004	0.843±0.007	177.9	157
	3	$5.16\times10^{-1}\pm2.17\times10^{-3}$	367.802±0.009	0.228±0.005	0.780±0.009	189.1	157
	4	$1.77\times10^{-1}\pm1.14\times10^{-3}$	368.035±0.041	0.409±0.026	0.400±0.025	138.2	157
091208B[c]	1	$9.90\times10^{-2}\pm2.09\times10^{-4}$	359.929±0.270	0.569±0.167	2.711±0.316	121.7	150
	2	$2.24\times10^{-1}\pm4.58\times10^{-4}$	359.365±0.009	0.080±0.006	1.803±0.033	124.7	150
	3	$2.36\times10^{-1}\pm5.36\times10^{-3}$	359.424±0.542	0.000±0.564	0.919±0.158	142.9	150
	4	—	—	—	—	—	—

[a]Channels here refer to *Swift* data channels. Channel 1 covers 15-25, channel 2 covers 25-50, channel 3 covers 50-100, channel 4 covers 100-350 keV.

[b]Pulse 1.

[c]Pulse 2.

These worries were compounded when comparing them to existing lags in the literature. In Table 7.3 a list of lags from Xiao & Schaefer (2009) for the same bursts is provided. This paper obtained lags from a cross-correlation technique using the same data, but measures the lag over the whole body of the burst. For the few bursts for which there was a positive lag time obtained (regardless of how t_p behaves), the difference is taken, along with the statistical significance of that difference. These lags are grossly different from those found in Xiao & Schaefer (2009). In addition, for many bursts for which lags were found in Xiao & Schaefer (2009), there was difficulty in obtaining lags using the fitting technique. For all

Table 7.2. Two-Sided Gaussian Fits to *Swift* Data - Summed 4 Channel Data[a]

BURST	A (cts s^{-1} $detector^{-1}$)	t_p (s)	σ_1 (s)	σ_2 (s)	χ^2	dof
050908	$6.169\times10^{-2}\pm1.45\times10^{-5}$	301.341±1.010	5.127±0.787	6.015±0.838	1187.455	1251
051111	$2.653\times10^{-1}\pm2.43\times10^{-5}$	296.692±0.073	1.940±0.046	13.766±0.115	1720.409	1564
060206	$3.485\times10^{-1}\pm6.49\times10^{-5}$	301.504±0.011	1.392±0.008	1.903±0.009	683.713	626
060904B	$2.615\times10^{-1}\pm7.51\times10^{-5}$	240.356±0.034	-0.988±0.022	3.879±0.040	1519.993	1563
060912	$8.990\times10^{-1}\pm6.90\times10^{-4}$	239.727±0.002	0.253±0.001	1.489±0.003	1075.425	939
070306	$3.518\times10^{-1}\pm4.42\times10^{-5}$	337.308±0.071	3.432±0.052	7.197±0.054	1686.447	938
070318	$1.368\times10^{-1}\pm1.28\times10^{-5}$	176.112±0.064	0.674±0.041	16.950±0.243	1792.030	1564
070612	$1.425\times10^{-1}\pm3.86\times10^{-5}$	236.098±1.351	2.826±0.854	29.504±2.803	2144.177	2189
070810	$1.788\times10^{-1}\pm6.24\times10^{-5}$	239.950±0.081	1.389±0.057	3.612±0.082	925.751	939
071010B	$7.998\times10^{-1}\pm7.85\times10^{-5}$	240.399±0.006	1.139±0.003	5.695±0.007	1735.342	1095
080413B	$2.034\pm2.44\times10^{-3}$	239.354±0.002	0.533±0.001	1.289±0.002	710.577	469
091018	$1.092\pm3.17\times10^{-4}$	243.660±0.002	0.629±0.001	1.467±0.001	585.627	469
091020	$4.457\times10^{-1}\pm1.06\times10^{-4}$	240.251±0.038	1.393±0.024	6.485±0.046	940.245	783
091208B[b]	$1.693\pm9.72\times10^{-3}$	367.915±0.005	0.269±0.003	0.857±0.005	256.941	157
091208B[c]	$5.520\times10^{-1}\pm1.89\times10^{-3}$	359.577±0.013	-0.199±0.008	1.547±0.023	139.612	150

[a]Channels here refer to *Swift* data channels. The summed 4-channel data covers the 15-350 keV energy range. Refer to Table 7.1 for breakdown of what energy range each channel covers.

[b]Pulse 1.

[c]Pulse 2.

these reasons, the hope of using the $\tau_{\rm lag}-$ L relation on well-separated *Swift* pulses seems to be defeated. There is no reliable way to obtain good, reliable values for the $\tau_{\rm lag}$, even with this idealized set of data.

Next, consider the $\tau_{\rm rise}-$ L relation. The rise time of a GRB is a direct result of the geometry of a GRB, and was predicted to correlate with luminosity in Schaefer 2002. The idea is that the rise time is the delay between the arrival time of photons from the center of the emitting region and the edge of the emitting region. The photons on the edge of the emitting region will take longer to be observed simply due to the longer path length they take to Earth. The size of the visible region is dependent on the beaming factor of the jet of the burst, $\Gamma_{\rm jet}$. So in turn the rise time of a burst will be proportional to $\Gamma_{\rm jet}^{-2}$. As the burst luminosity also scales with a power of $\Gamma_{\rm jet}$ (usually accepted to be a power of about 3), the

Table 7.3. Double Sided Gaussian Fits to *Swift* Data

BURST	$\tau_{\rm lag}$ [a] (s)	$\tau_{\rm lag}$ [b] (s)	Δ (s)	Significance
050908	0.959±20.341[c]	—	—	—
051111	-1.022±1.047[c]	1.7±0.07	—	—
060206	-1.127±0.144[c]	0.01±0.03	—	—
060904B	0.279±0.601[c]	0.36±0.09	-0.08	0.13
060912	—	0.07±0.01	—	—
070306	-2.451±1.600[c]	1.27±0.07	—	—
070318	0.715±0.817[c]	—	—	—
070612	0.297±19.117	0.77±0.43	-0.47	0.02
070810	—	1.09 ±0.23	—	—
071010B	0.420±0.248[c]	0.84±0.04	-0.42	1.67
080413B	0.117±0.028[c]	0.23±0.01	-0.11	3.76
091018	—	—	—	—
091020	0.458±0.413	—	—	—
091208B[b]	-0.218±0.042	—	—	—
091208B[c]	—[c]	—	—	—

[a]Lags as measured from the two-sided Gaussian.

[b]Lags as measured from a cross-correlation function (Xiao & Schaefer 2009).

[c]The time of the peak of this burst behaves in an unexpected way. This can be either the time of peak is not getting earlier as a function of higher energy channels, or the time of peak goes oscillates across the energy bands. This is a general warning that the lag time is likely no good, in addition to any concerns that may be raised by error bar size.

$\tau_{\rm rise} - {\rm L}$ relation comes out of simple geometry. Explicitly, the higher the $\Gamma_{\rm jet}$, the higher the luminosity, and the higher the $\Gamma_{\rm jet}$ the shorter the rise time.

Recall that for the model used, σ_1 is representative of the rise time of the burst. Looking at Table 7.1, many of the same problems are seen as were seen with t_p. The uncertainties are often too high to be confident in the returned values. For many bursts, the rise time is just as ill-behaved as t_p. Here, 'ill-behaved' carrying the same connotation as it did before. There is not enough confidence in these fits to use the $\tau_{\rm rise} - {\rm L}$ relation on this sample of *Swift* pulses.

7.5 Calculating $\mathbf{E}_{\rm peak}$

The one burst parameter that stayed reasonably constant throughout this whole process was the amplitude (see Table 7.1 and Table 7.2). The amplitude consistently returned nearly exactly the same results every time, and generally had considerably small error bars. The cross terms related to the amplitude were also negligible. This is fairly reasonable, as small shifts in the other burst parameters will generally not change how high the fitted curve must be fit to the data. This gave promise that regardless of how good the other parameters were, the peak flux could be taken out to extract luminosities for the $E_{\rm peak} - L_{\rm iso}$ relation. This meant that at least one of the luminosity relations might be useful with individual pulses. The simplest case to start with involves the most photons, the full four-channel data.

XSPEC is a HEASARC tool designed to fit spectra that is used widely by many different astronomers. The BAT user's manual explicitly states that spectra created in the bat analysis tool *batbinebt* are made to be used in XSPEC. There are various step-by-step guides on how to create and fit BAT spectrum including the BAT user's manual, and online guides[5].

[5] e.g., http : //swift.gsfc.nasa.gov/docs/swift/analysis/threads/batspectrumthread.html
http : //grbworkshop.wikidot.com/s9 − 10 − swift − bat

Generally, E_{peak} refers to the time integrated E_{peak}, that is, the E_{peak} over the entire burst. For the $E_{peak} - L_{iso}$ relation, the 'peak E_{peak}' is needed, often called the 'time-resolved' E_{peak} (see Chapter 6 for differences in defining E_{peak}). This is because the $E_{peak} - L_{iso}$ relation uses E_{peak} as a sort of peak flux. As such, the time of interest (i.e. the time for which to take E_{peak} over) is going to be some interval around the peak brightness of the pulse.

As has been covered in previous chapters, there are generally three types of models used in fitting GRB spectra. The first is a simple power law,

$$\frac{dN}{dE} = A\left(\frac{E}{50.0\,\mathrm{keV}}\right)^{-\alpha}. \tag{7.3}$$

Where A is a normalization constant, α is the photon index, and there is no break in the spectrum. If this model is the best fit for a GRB spectrum it is considered to have no measurable E_{peak}. The second model is a 'cut-off' power law (CPL),

$$\frac{dN}{dE} = A\left(\frac{E}{50.0\,\mathrm{keV}}\right)^{-\alpha} \exp\left[-\frac{E\,(2.0 - a)}{E_{peak}}\right] \tag{7.4}$$

So the CPL model gets its name from the exponential cut off that is introduced into the equation. Here, the extra fit parameter is E_{peak}, which is related to the break in the spectrum. As there is now an extra fit parameter, the chi-square of the fit will usually improve (due to the extra degree of freedom). As a sort of F-test, the BAT team generally suggests an absolute minimum of an improvement of 6.0 in the value of chi-square before the model can be considered a better fit after considering the extra degree of freedom. Finally, the Band function is also commonly used, and has yet another degree of freedom. It is generally described as a broken power law smoothed by an exponential, (see equation 5.1).

All the pulses were fit to all three models in XSPEC. For all pulses, the Band function showed no significant improvement over the simpler models. In Table 7.4, the results of the fits are presented. These fits are done over two time intervals, the full-width and half-width

Table 7.4. XSPEC E_{peak} Fits to *Swift* Data

BURST	Interval	Model	α	E_{peak} (keV)	A ph cm^{-2} s^{-1} keV^{-1}	χ^2	χ^2_r
050908	FWHM	PL	1.76±0.10	—	$3.03\times10^{-3}\pm2.96\times10^{-4}$	90.0	1.58
	HWHM	PL	1.58±1.03	—	$4.38\times10^{-3}\pm3.71\times10^{-4}$	71.4	1.25
051111	FWHM	CPL	0.99±0.13	192.22±56.07	$2.04\times10^{-2}\pm2.58\times10^{-3}$	46.6	0.83
	HWHM	PL	1.23±0.04	—	$1.90\times10^{-2}\pm3.62\times10^{-4}$	58.8	1.03
060206	FWHM	CPL	1.07±0.17	76.53±8.62	$3.42\times10^{-2}\pm6.65\times10^{-3}$	49.5	0.88
	HWHM	CPL	0.87±0.20	77.37±8.53	$4.89\times10^{-2}\pm1.11\times10^{-2}$	50.7	0.91
060904B	FWHM	CPL	1.07±0.17	76.53±8.62	$3.42\times10^{-2}\pm6.65\times10^{-3}$	49.5	0.88
	HWHM	CPL	0.87±0.20	77.37±8.53	$4.89\times10^{-2}\pm1.11\times10^{-2}$	50.7	0.91
060912	FWHM	PL	1.75±0.05	—	$4.80\times10^{-2}\pm1.29\times10^{-3}$	39.9	0.70
	HWHM	CPL	1.13±0.21	79.29±12.52	$1.18\times10^{-1}\pm2.74\times10^{-2}$	80.7	1.05
070306	FWHM	PL	1.60±0.03	—	$1.86\times10^{-2}\pm2.71\times10^{-4}$	45.6	0.80
	HWHM	PL	1.60±0.03	—	$2.42\times10^{-2}\pm4.01\times10^{-4}$	43.7	0.77
070318	FWHM	CPL	1.10±0.16	141.47±41.62	$1.17\times10^{-2}\pm1.98\times10^{-3}$	35.9	0.64
	HWHM	CPL	1.00±0.17	123.50±28.56	$1.79\times10^{-2}\pm3.25\times10^{-3}$	32.6	0.58
070612A	FWHM	PL	1.01±0.07	—	$8.28\times10^{-3}\pm3.47\times10^{-4}$	57.1	1.00
	HWHM	PL	0.92±0.08	—	$1.03\times10^{-2}\pm4.65\times10^{-4}$	67.5	1.18
070810A	FWHM	CPL	0.38±0.39	44.39±0.11	$7.03\times10^{-2}\pm3.40\times10^{-2}$	67.6	1.21
	HWHM	CPL	1.19±0.37	50.07±7.30	$2.66\times10^{-2}\pm1.25\times10^{-2}$	55.1	0.98
071010B	FWHM	CPL	1.41±0.10	55.48±2.38	$7.29\times10^{-2}\pm7.48\times10^{-3}$	35.0	0.62
	HWHM	CPL	1.16±0.11	61.61±2.40	$1.10\times10^{-1}\pm1.22\times10^{-2}$	68.9	0.89
080413B	FWHM	CPL	0.98±0.14	87.11±7.86	$2.17\times10^{-1}\pm3.18\times10^{-2}$	103.3	1.34
	HWHM	CPL	0.99±0.17	93.73±12.51	$2.74\times10^{-1}\pm4.90\times10^{-2}$	32.2	0.58
091018	FWHM	PL	2.34±0.04	—	$1.81\times10^{-2}\pm3.96\times10^{-4}$	54.3	0.95
	HWHM	CPL	1.30±0.25	43.58±0.17	$3.53\times10^{-2}\pm1.11\times10^{-2}$	53.0	0.95
091020	FWHM	PL	1.40±0.04	—	$2.73\times10^{-2}\pm5.42\times10^{-4}$	39.18	0.69
	HWHM	PL	1.30±0.04	—	$3.29\times10^{-2}\pm7.82\times10^{-4}$	58.70	1.03

half-maxima (FWHM and HWHM). These were estimated by using the best-fits of the total four channel data in Table 7.2. Using the definition that a FWHM is $\sim 2.35\sigma$, the rise and decay times were each multiplied by a factor of $\sim$1.18 to obtain the start and stop times for the FWHM interval. Likewise, a factor of $\sim$0.59 was used to find the start and stop times of the HWHM interval. In the table, if the CPL model is not better by at least 6.0 greater in chi-square, the PL model is listed instead. Burst 091208B had too few photons to adequately fit any models, and thus is not present in the tables.

Four of the thirteen pulses have no E_{peak} found, and bursts, 051111 and 070318 have very high error bars. So the sample is not large enough to convince anyone as to the usefulness of the $E_{peak} - L_{iso}$ relation for pulses.

Once again, a check was needed to ensure the fits were performed correctly. Sakamoto et al. (2011) that explicitly gives CPL fits for various bursts over explicit intervals. These intervals are for time-integrated bursts, and cover the entirety of the burst. In Table 7.5 the results these fits are presented for five such bursts. In Table 7.6, the differences along with the significance of that difference are given. The significance is determined by dividing the difference by an uncertainty value where the uncertainty is determined by adding the separate measurements in quadrature.

While the fits agree within error bars, they do not yield exactly the same results. As both fits are using the *Swift* BAT data over the exact same time interval, and both are using XSPEC to make the fits, both fits should return the same values. The problems with measuring E_{peak} have been well documented (e.g. Preece 2011; Collazzi et al. 2011; Chapter 5). What is being observed here is very likely some combination of E_{peak} evolving over the course of the burst, and fairly high (and unavoidable) values of σ_{Choice} (see Chapter 5). Given

Table 7.5. Sakamoto Check

BURST	Sakamoto et al. (2011) α	Sakamoto et al. (2011) E_{peak} [a]	Sakamoto et al. (2011) A [b]	This Work α	This Work E_{peak} [a]	This Work A [b]
041224	$-0.984^{+0.281}_{-0.264}$	$68.9^{+11.7}_{-7}$	$10.1^{+3.7}_{-2.6}$	-0.929±0.163	67.6±4.5	10.69±1.90
050117	$-1.171^{+0.182}_{-0.172}$	$130.3^{+70.6}_{-26.7}$	$6.4^{+1.3}_{-1}$	-1.162±0.110	119.0±18.7	6.00±18.67
050219B	$-0.919^{+0.236}_{-0.224}$	$107.9^{+30.2}_{-15.2}$	$41.4^{+10.6}_{-8.1}$	-0.925±0.137	105.6±11.4	41.97±0.56
050306	$-1.086^{+0.281}_{-0.265}$	$140.3^{+171.5}_{-35.8}$	$9.3^{+2.9}_{-2.1}$	-1.054±0.170	129.0±28.9	9.80±1.66
050416B	$-0.391^{+0.679}_{-0.585}$	$95.7^{+65.5}_{-19.4}$	$76.2^{+75.1}_{-34.4}$	-0.239±0.382	85.8±12.1	93.90±37.11

[a] keV

[b] 10^{-3} ph cm^{-2} s^{-1} keV^{-1}

Table 7.6. Sakamoto Check 2

BURST	$\Delta\alpha$	Significance	Δ E_{peak} [a]	Significance	Δ A [b]	Significance
041224	-0.06	0.17	1.3	0.16	-0.59	0.14
050117	-0.01	0.04	11.3	0.35	0.40	0.02
050219B	0.01	0.02	2.3	0.12	-0.57	0.05
050306	-0.03	0.10	11.3	0.25	-0.50	0.15
050416B	-0.15	0.20	9.9	0.43	-17.70	0.21

[a] keV

[b] 10^{-3} ph cm^{-2} s^{-1} keV^{-1}

Table 7.7. Robustness Test

BURST	Start[a] (s)	End[a] (s)	α	E_{peak} (keV)	A (10^{-3} ph cm^{-2} s^{-1} keV^{-1})
050117	-5.72	215.86	-1.164±0.111	120.6±18.9	6.5±0.9
	4.28	225.86	-1.177±0.111	121.9±19.6	6.4±0.9
	-5.72	225.86	-1.191±0.111	126.0±22.8	6.0±0.9
	-15.72	225.86	-1.178±0.113	124.2±23.2	5.9±0.8
	-5.72	235.86	-1.189±0.113	126.2±22.8	5.8±0.8
	-15.72	235.86	-1.188±0.114	126.7±23.5	5.6±0.8
	-25.72	235.86	-1.200±0.115	126.6±24.5	5.3±0.8
	-15.72	245.86	-1.160±0.115	122.6±21.3	5.5±0.8
	-25.72	245.86	-1.175±0.116	122.5±21.8	5.3±0.8
050219B	-15.59	18.57	-0.915±0.121	110.0±10.9	82.7±9.6
	-25.59	18.57	-0.972±0.124	116.1±13.8	61.8±7.3
	-15.59	28.57	-0.860±0.128	103.7±9.3	68.9±8.5
	-25.59	28.57	-0.918±0.130	108.5±11.5	54.2±6.9
	-25.59	38.57	-0.602±1.359	114.6±9.6	48.5±6.0
	-35.59	28.57	-0.601±0.135	109.9±8.7	51.0±6.3
	-35.59	38.57	-0.925±0.137	105.6±11.4	42.0±5.6
	-45.59	38.57	-0.449±0.150	107.0±7.9	42.9±5.8
	-35.59	48.57	-1.008±0.140	109.9±14.3	34.8±4.8
	-45.59	48.57	-0.567±0.150	111.2±9.7	35.3±4.9
	-55.59	48.57	-0.627±0.153	115.0±11.3	30.3±4.2
	-45.59	58.57	-0.562±0.157	108.8±9.5	32.4±4.7
	-55.59	58.57	-0.975±0.154	104.7±13.5	26.8±4.1
050306	-13.42	187.84	-1.055±0.170	130.2±29.7	9.4±1.6
	-3.42	197.84	-1.035±0.171	127.7±27.8	9.6±1.7
	-13.42	197.84	-1.037±0.171	128.9±27.8	9.2±1.6
	-23.42	197.84	-0.929±0.167	118.9±19.3	9.5±1.6
	-13.42	207.84	-0.972±0.176	120.4±22.5	9.4±1.7
	-23.42	207.84	-0.978±0.179	121.1±23.9	8.9±1.7
	-33.42	207.84	-0.952±0.183	118.6±22.5	8.7±1.7
	-23.42	217.84	-0.985±0.182	119.5±23.4	8.6±1.7
	-33.42	217.84	-0.960±0.185	117.1±22.2	8.4±1.7
050416B	-9.94	4.2	-0.151±0.671	97.1±21.7	29.3±18.7
	0.06	14.2	-1.102±0.470	106.7±61.6	15.1±78.5
	-9.94	14.2	-0.935±0.610	146.3±126.9	8.2±5.7
	-9.94	24.2	-0.615±0.789	95.6±45.6	8.7±7.7
	-19.94	14.2	-1.055±0.746	119.1±112.7	5.7±6.0
	-19.94	24.2	-0.846±0.879	86.9±65.5	6.1±6.8
	-29.94	24.2	-0.077±1.172	62.8±15.6	13.1±17.4
	-19.94	34.2	-0.621±1.048	105.2±72.7	4.7±7.1
	-29.94	34.2	-0.217±1.221	78.5±30.4	7.0±10.9

[a]Time in seconds from the trigger time.

all these uncertainties in E_{peak} , there is little point in attempting the $E_{peak} - L_{iso}$ relation on a pulse by pulse basis.

A robustness test was performed where fits were performed over different time intervals. These time intervals all contained the full burst, the results of which are in Table 7.7. While the values are all within error bars, the error bars are too large, making such a statement fairly meaningless. So there is very little confidence in what values of E_{peak} to use.

7.6 Conclusions

The reality of this investigation is that *Swift* data cannot be used to calibrate any pulse-based luminosity relations. In the best cases (i.e. cases where bursts are well-separated), the bursts are either too faint to measure, or, the fits are unreliable and not robust. Large cross terms dominate any fits looking for rise or lag times, which leads to no confidence in any of the values obtained. In addition, when measuring E_{peak} , even with the same data as other groups, many of the same scatter issues seen earlier dominate. As a result, none of the three relations, $\tau_{rise} - L$, $\tau_{lag} - L$, or $E_{peak} - L_{iso}$, can be used. Since they can not be done even in the Earth's rest frame, they most certainly will not be able to be done in the burst's frame (see Chapter 2), with less photons.

In the future, it is possible that using the less-ideal bursts for which there are overlapping pulses can be used. In these cases, the $E_{peak} - L_{iso}$ relation could not be used. This is because there is no way to determine what photons come from what pulses under such circumstances. Still, the lag and rise times might be salvaged from these bursts. Unfortunately, given the error bars on an 'ideal' set of data, there is little optimism that it yield a significant improvement. It is unlikely that the pulse paradigm can be used for *Swift* bursts, which as the largest sample of GRBs with known redshift, is disappointing. As *Fermi* gets more and

more bursts with redshifts, perhaps a better data set will emerge to try this study again. As *Fermi* is much more like BATSE in operation, the fitting methods might transfer more easily to that data. The outlook, however, is not optimistic.

8. Conclusions

8.1 This Work

When this work first began, there were eight luminosity relations generally accepted by the GRB community. As has been discussed at length, these luminosity relations were known to have various problems, and were in need of improvement. Improving the GRB luminosity relations would greatly improve the GRB HD, and eventually could answer questions regarding the high-z Universe.

The first steps in the investigation were promising. The luminosity relations were successfully defended against a number of good arguments against them (chapter 3). Unfortunately, a more in-depth investigation of the Amati relation, $E_{peak} - E_{\gamma,iso}$, revealed that it owed its existence to a combination of selection effects. Therefore, the Amati relation is not good for cosmological purposes (chapter 6).

A different investigation went to show that the Firmani relation, $L_{iso} - E_{peak}\, T_{0.45}$, was no improvement over the $E_{peak} - L_{iso}$ relation (chapter 4). The first reason for this was that the Firmani relation gained significant scatter when using independent data sets, especially when expanded to a larger data set. Another reason for rejecting the Firmani relation is that it is not independent of already existing GRB luminosity relations. Therefore, the Firmani relation is not useful for cosmological purposes.

So one result of this work is that two GRB luminosity relations have been shown to be not useful. Worse yet, there is still the case of the two relations that are of limited usefulness ($N_{peak} - L$ and $V - L$). So in reality, only four relations can be confidently use for cosmological purposes. One side effect of this is that the other four relations will suffer

from a sort of guilt by association. That is, a GRB worker could incorrectly judge that the remaining luminosity relations are also not useful simply as a result of the failures of others.

In addition, chapter 5 highlighted some very serious issues with the measurements of E_{peak}. That is, the scatter in the luminosity relations can only be reduced so much because of unavoidable sources of scatter beyond the normal Poisson scatter. Even if the community were to adopt a strict standard, the improvement that can be gained through such standardization is questionable. That is, there will always be some irreducible amount of $\sigma_{\rm Choice}$. It is also reasonable to assume that these uncertainties are present in the measurement of other burst parameters, implying that *other* luminosity relations have some amount of irreducible scatter.

In chapter 7, attempts to reduce some of this scatter by dividing apart GRBs into individual pulses were not successful. Even with the 'best case' of well separated *Swift* bursts, no conclusive data could be obtained to perform calibrations. While the burst pulse paradigm makes good physical sense, it appears as if any uncertainties lost by breaking convolutions of multiple pulses will simply be replaced by uncertainties in the measurement of pulse parameters. Therefore, it is not clear as to how much can be gained by using the pulse paradigm for future cosmology.

There have been *some* positive results as a result of this work. The analysis in chapter 5 led to the discovery that GRBs *might* be thermostated. This is simply a result of observing that the distribution of observed E_{peak} values is of the similar width to the normal observational errors as calculated in chapter 5. As such, the intrinsic distribution of E_{peak} must be small, indicating that some emission mechanism must exist to thermostat GRBs. As the average value of the intrinsic E_{peak} is close to 511 keV, this implies that the emission mechanism that is acting as a thermostat could be electron-positron annihilation.

8.2 New Luminosity Relations?

In recent years, there have been a number of claims made for new GRB luminosity relations. These relations are often only found empirically, with little to no physical explanation for their existence. Unfortunately, these luminosity relations have had considerable doubts raised against them. There does not appear to be any 'new' luminosity relation in the literature that has any promise.

For example, Danotti et al. (2008; 2010; 2011) proposed a correlation between the break-time in the X-ray afterglow light curve (T_a) to the luminosity in X-rays at that time (L_x). The break time here is defined as the time where the afterglow light-curve transitions from an exponential to a power law decay. However, recent work by Cannizzo et al. (2010) suggest that the relation may be due to a kind of Malmquist bias where the breaks in faint bursts are not observed. Indeed, the Dainotti group itself has recently softened its statements as to the strength of the relation in recent work.

Panaitescu and Vestrand (2008) proposed a similar idea using optical afterglows. Here, the peak flux in the optical is correlated in a simple power law with the time of that peak. This relation then only applies to the small subset of bursts that not only have an optical transient, but also have this peak observed early in the optical transient. Recently, enough new bursts have been observed to warrant a recheck of the original analysis. In two separate studies, several new bursts were tested against this relation, and no convincing correlation was found (Klotz et al. 2009; Kann et al. 2010). Recently, this same finding was made independently by Bradley Schaefer and Rebecca Fitzgerald at LSU. Consequently, the last two attempts at finding new GRB luminosity relations have failed.

Tsutsui et al. (2009) makes a similar suggestion as made by Firmani et al. (2006) that the addition of a duration will improve the $E_{peak} - L_{iso}$ relation. The proposed duration is

$T=E_{peak}L$, which is a sort of equivalent width. This idea, however, was already disproven in Collazzi & Schaefer (2008) (also see Chapter 4). In that work, one of the alternative durations used was S_{bolo}/ P_{bolo}. By simple application of the inverse square law, one finds that these are exactly the same duration. Collazzi & Schaefer (2008) found that S_{bolo}/ P_{bolo} yielded no significant improvement to the $E_{peak}- L_{iso}$ relation.

8.3 The Path Forward

There are a few studies that can be done in the near future to further assess the GRB luminosity relations. One such path is to perform the same type of analysis of chapter 5 on other GRB luminosity indicators. Indeed, in Chapter 7, it was seen how greatly lag and rise time can vary as a result of analyst choices. This gives cause to believe that all the other luminosity indicators might have similar size widths in σ_{Total} as was seen in E_{peak} . This again suggests a need for standardization in the measurement of these burst parameters. However, this is very difficult given the chaotic nature of GRBs, vast differences in detector thresholds, and general disagreements in how the parameters should be measured.

This also introduces the common question of what is the best detector to use. The answer, unsurprisingly, is that it depends on what question is being asked. For example, *Swift* and *Konus* have the largest numbers of bursts with known redshift, and would therefore be the obvious choice for calibrating GRB luminosity relations. However, the *Konus* team has never released an official catalog of bursts. Most of the results must be taken from preliminary analysis in the GCNs. In addition, *Swift* data and analysis tools are far more accessible, making it the better choice of the two. If the worker is trying to answer a question for which the redshift is unneeded (e.g. chapter 6), BATSE would be the obvious choice. BATSE

covers the widest range of energies and has the most bursts seen of any detector. Therefore, BATSE would be the obvious best choice for demographic studies.

A revisit of all GRB luminosity relations for all bursts with cosmological redshifts is needed. The last such test, Schaefer (2007) is now nearly five years old, and the data set can easily be tripled. This investigation would go far beyond a simple 'redo' with an expanded data set. Some of the lessons learned over the last few years can be applied to a new investigation. As an example, it would be appropriate to construct and calibrate the GRB luminosity relations just for *Swift* bursts, and compare those fits to the calibrations for the total data set. This would be building based on the lessons of chapter 6, which showed that different groups with different detectors can add significant scatter. Chapter 6 also demonstrated how greatly different the time-resolved and time-integrated E_{peak} can be. Therefore the $E_{peak} - L_{iso}$ relation should really be calibrated with *just* the time-resolved E_{peak}, not a mix of time-resolved and time-integrated E_{peak}. Another attempt would be to compare the scatter in the luminosity relations from data in the literature as compared to data derived independently.

The future of the GRB luminosity relations lies chiefly with what predictions can be made from them. The ideal scenario would be a type of rapid-response system where the GRB luminosity relations are used to predict the redshift of a new burst accurately and reliably. This is not a new idea, but the current accuracy of the luminosity relations has made this difficult to do. Ultimately, however, the best way to convince the community is to demonstrate consistency between the GRB HD and the SN HD (i.e. for $z<1.4$). In addition, the GRB HD would need to have a narrow distribution of hundreds of bursts around some plausible cosmology.

Bibliography

Amati, L. 2003, Chinese Journal of Astronomy and Astrophysics, 3, 455.

Amati, L. 2006, Monthly Notices of the Royal Astronomical Society, 372, 233.

Amati, L. et al. 2009, Astronomy & Astrophysics, 508, 173.

Amati, L. et al. 2002, Astronomy & Astrophysics, 390, 81.

Aptekar, R.L. et al. 1995, Space Science Reviews, 71 265.

Arimoto, M. et al. 2010, PASJ, 62, 487.

Astier, P. et al. 2006, Astronomy & Astrophysics, 447, 31.

Band, D.L. 2003, The Astrophysical Journal, 588, 945.

Band, D.L. & Preece, R.D. 2005, The Astrophysical Journal, 627 319.

Band, D.L. et al. 1993, The Astrophysical Journal, 413, 281.

Barraud, C. et al. 2003, in AIP Conf. Ser. 662, Gamma-Ray Burst and Afterglow Astronomy 2001: A Workshop Celebrating the First Year of the HETE Mission, ed. G. R. Ricker & R. K. Vanderspek (Melville, NY: AIP), 59.

Barthelmy, S. D. et al. 2007, GCN Circ. 6390.

Bellm, E. et al. 2007, GCN Circ. 6399.

Briggs, M.S. et al. 1996, The Astrophysical Journal, 459, 40.

Bloom, J. S. et al. 2003, The Astronomical Journal, 125, 999

Blustin, A.J. et al. 2006, The Astrophysical Journal, 637, 901.

Bromm, V. & Loeb, A. 2002, The Astrophysical Journal 575, 111.

Bromm, V. & Loeb, A. 2006, The Astrophysical Journal, 642, 382.

Bromm, V. & Loeb, A. 2007, in AIP Conf. Proc. 937, Supernovae 1987A: 20 Years After: Supernovae and Gamma-Ray Bursters, ed. S. Immler & K. Weller (Melville, NY: AIP), 532.

Bouwens, R.J. et al. 2006, The Astrophysical Journal, 653, 53.

Brainerd, J. J. et al. 1999, in AIP Conf. Proc. 526, Gamma-Ray Bursts: 5th Huntsville Symposium, ed. R. Marc Kippen, R. S. Mallozzi, & G. J. Fishman (Melville, NY: AIP), 150.

Butler, N.R., et al. 2007, The Astrophysical Journal, 671, 656.

Butler, N. R. et al. 2010, The Astrophysical Journal, 711, 495.

Cabrera, J.I. et al. 2007, Monthly Notices of the Royal Astronomical Society, 382, 342.

Campana, S. et al. 2006, Nature, 442, 1008.

Cannizzo, J.K. et al 2011, The Astrophysical Journal, 734, 35.

Collazzi, A.C. & Schaefer, B.E. 2008, The Astrophysical Journal, 688, 456.

Collazzi, A.C. et al. 2011, The Astrophysical Journal, 729, 89.

Collazzi, A.C. et al. 2011b, The Astrophysical Journal, submitted.

Costa, E. et al. 1997, Nature, 387, 783.

Crider, A. et al. 1999, ApJ, 519, 206.

Dainotti, M.G. et al. 2008, Monthly Notices of the Royal Astronomical Society: Letters, 391, L79.

Dainotti et al. 2010, The Astrophysical Journal, 722, L215.

Dainotti et al. 2011, The Astrophysical Journal, 730, 135.

Eichler, D. & Levingston, A. 2004, The Astrophysical Journal Letters, 614, L13.

Fenimore, E.E. et al. 1993, Nature, 366, 40.

Fenimore, E.E. & Ramirez-Ruiz, E. 2000, astro-ph/0004176.

Firmani, C. et al. 2006, Monthly Notices of the Royal Astronomical Society: Letters, 372, L28

Fishman, G.J. 1991, Bulletin of the American Astronomical Society, 23, 1404.

Fishman, G. J., & Meegan, C. A. 1995, Annual Reviews of Astronomy & Astrophysics., 33, 415.

Fishman, G.J. et al. 1994, The Astrophysical Journal Supplement, 92, 229.

Foley, S. et al. 2008, Astronomy & Astrophysics, 484, 143

Ford, L.A. et al. 1995, The Astrophysical Journal, 439, 307.

Frail, D. et al. 1998, The Astrophysical Journal Letters, 502, L119.

Galama, T.J. et al. 1998, Nature, 395, 670.

Gehrels, N. et al. 2006, Nature, 444, 1044.

Ghirlanda, G. et al. 2004, The Astrophysical Journal, 616, 331.

Ghirlanda, G. et al. 2005, Monthly Notices of the Royal Astronomical Society: Letters, 361, L10

Ghirlanda, G. et al. 2010, Astronomy & Astrophysics, 511, 43.

Ghirlanda, G., et al. 2011, in "The Prompt Activity of Gamma-Ray Bursts: their Progenitors, Engines, and Radiation Mechanisms" Conference: North Carolina State University at Raleigh, NC.

Giannios D., & Spruit, H.C. 2007, Astronomy & Astrophysics, 469, 1.

Goldstein, A. et al. 2010, The Astrophysical Journal, 721, 1329.

Goldstein, A. et al. 2011, The Astrophysical Journal, in prep.

Goldstein, A. et al. 2011b, The Astrophysical Journal, submitted, astro-ph/1101.2458.

Golenetskii, S. V. 1988, Advances in Space Research, 8, 653.

Golenetskii, S. et al. 2005a, GCN Circ. 3474.

Golenetskii, S. et al. 2005b, GCN Circ. 4078.

Golenetskii, S. et al. 2007, GCN Circ. 6403.

Greiner, J. 2010, in "Gamma-Ray Bursts", http : //www.mpe.mpg.de/ jcg/grbgen.html

Guidorzi, C. et al. 2005, MNRAS, 363, 315

Guidorzi, C. et al. 2011, Astronomy & Astrophysics, 526, 49.

Hakkila, J. 2011, Private Communication.

Hakkila, J. & Nemiroff, R.J. 2009, The Astrophysical Journal, 705, 372.

Hakkila, J. & Preece, R.D. 2011, The Astrophysical Journal Submitted, arXiv:1103.5434

Hakkila, J. et al. 2008, The Astrophysical Journal Letters, 677, L81.

Hamuy, M. et al. 1996, The Astronomical Journal, 112, 2391.

Higdon, J.C. & Ligenfelter, R.E. 1990, Annual Reviews of Astronomy & Astrophysics, 1990, 28, 401.

Higdon, J.C. & Schmidt, M. 1990, The Astrophysical Journal, 335, 13.

Hjorth, J. et al. 2003, Nature, 423, 847.

Hopkins, A.M. & Beacom, J.F. 2006, The Astrophysical Journal, 651, 142.

Hubble, E. 1929, Proceedings of the National Academy of Science, 15, 168.

Jakobsson, P. et al. 2006, Astronomy & Astrophysics, 447, 897.

Jakobsson, P. et al. 2009, in AIP Conf. Proc. 1133, Gamma-Ray Bursts, 6th GRB Symposium, ed. C Meegan, N. Gehrels, & C. Kouveliotou (Huntsville, AL: AIP), 455.

Jarosik, N. et al. 2011, The Astrophysical Journal Supplement, 192, 15.

Jimenez, R., Band, D., & Piran, T. 2001, The Astrophysical Journal, 561, 171.

Kann, et al. 2010, The Astrophysical Journal, 720, 1513.

Kaneko, Y. et al. 2006, The Astrophysical Journal Supplement, 166, 298

Kazanas, D. & Mannheim, P.D. 1991, The Astrophysical Journal Supplement, 76, 431.

Kim, A., Goobar, A., & Perlmutter, S. 1996, Publications of the Astronomical Society of the Pacific, 108. 190.

Kippen, R.M. et al. 2003, in AIP Conf. Proc. 662, Gamma-Ray Bursts and Afterglow Astronomy, ed. G. R. Ricker & R. Vanderspek (Melville, NY: AIP), 244.

Kippen, R.M., et al. 2004, in AIP Conf. Proc. 727, Gamma-Ray Bursts: 30 Years of Discovery: Gamma-Ray Symposium, e. E.E. Fenimore, M. Galassi, (Melville, NY: AIP), 119.

Klebesadel, R. W., Strong, I.B., & Olson, R.A. 1973, The Astrophysical Journal, 182, L85.

Klotz, A. et al. 2009, The Astronomical Journal, 137, 4100.

Kobayashi, S. et al. 2002, The Astrophysical Journal, 577, 302.

Kocevski, D. & Butler, N. 2008, The Astrophysical Journal, 680, 531.

Koshut, T. M. et al. 1996, The Astrophysical Journal, 463, 570.

Kowalski, M. et al. 2008, The Astrophysical Journal, 686, 749.

Krimm et al. 2009, The Astrophysical Journal, 704 1405.

Kulkarni, S.R. et al. 1998, Nature, 393, 35.

Lamb, D.Q. & Reichart, D.E. 2000, The Astrophysical Journal Letters, 536, 1.

Leith et al. 2008, The Astrophysical Journal Letters, 672, L91.

Levenberg, K. 1944, The Quarterly of Applied Mathematics, 2, 164.

Levinston, A. & Eichler, D. 2005, The Astrophysical Journal Letters, 629, L13.

Li, L.-X., 2007, Monthly Notices of the Royal Astronomical Society, 374, L20.

Li, L.-X. & Paczynski, B. 2006, Monthly Notices of the Royal Astronomical Society, 366, 219.

Liang, E. & Kargatis, V. 1996, Nature, 381, 49.

Liang, E. W. et al. 2004, The Astrophysical Journal Letters, 606, L29.

Lloyd-Ronning, N.M. et al. 2002, The Astrophysical Journal, 574, 554.

Lloyd-Ronning, N. M., & Ramirez-Ruiz, E. 2002, The Astrophysical Journal, 576, 101.

MacFadyen, A.I. et al. 2001, The Astrophysical Journal 550, 410.

Malesani, D. et al. 2004, The Astrophysical Journal Letters, 609, L5.

Mallozzi, R.S. et al. 1995, The Astrophysical Journal, 454, 597.

Mannheim, P.D. 2006, Progress in Particle and Nuclear Physics, 56, 340.

Marquardt, D. 1963, SIAM Journal on Applied Mathematics, 11, 431.

Meegan, C. et al. 1992, Nature, 355, 143.

Melandri, A. et al. 2008, The Astrophysical Journal, 686, 1209.

Metzger, M.R. et al. 1997, Nature, 387, 878.

Mézáros, P. & Rees, M.J., 1997, The Astrophysical Journal, 476, 232.

Mészáros, P. et al. 2002, The Astrophysical Journal, 578, 812.

Murakami, T., et al. 1988, Nature, 335, 234.

Nakar, E. & Piran T. 2005, Monthly Notices of the Royal Astronomical Society, 360, L73.

Nava, L. et al. 2006, Astronomy & Astrophysics, 450, 471.

Nava, L. et al. 2008, Monthly Notices of the Royal Astronomical Society, 391, 639.

Nava, L. et al. 2009, AIPC, 1133, 350.

Nelder, J.A. & Mead, R. 1965, The Computer Journal, 7, 308.

Norris, J.P. et al. 2000, The Astrophysical Journal, 534, 248.

Norris, J.P. et al. 1995, The Astrophysical Journal, 439, 542.

Norris, J.P. et al. 1996, The Astrophysical Journal, 459, 393.

Ohno, M. et al. 2005, GCN Circ. 4297.

Paciesas, W.S. et al. 1999, The Astrophysical Journal Supplement, 122, 465.

Panaitescu, A. & Kumar, P. 2002, ApJ, 571, 779.

Panaitescu, A. & Vestrand, W. T. 2008, Monthly Notices of the Royal Astronomical Society, 387, 497.

Pélangeon, A. et al. 2008, Astronomy & Astrophysics, 491, 157.

Perlmutter, S. et al. 1999, The Astrophysical Journal, 517, 565.

Phillips, M. 1993, The Astrophysical Journal Letters, 413, L105.

Podsiadlowski, Ph. et al. 2004, ApJ, 607, L17.

Preece, R.D. 2011, in "The Prompt Activity of Gamma-Ray Bursts: their Progenitors, Engines, and Radiation Mechanisms" Conference: North Carolina State University at Raleigh, NC.

Price, P.A. et al. 2003, The Astrophysical Journal, 589, 838.

Reichart, D.E. et al. 2001, The Astrophysical Journal, 552, 57.

Riess, A.G. et al. 2004, The Astrophysical Journal, 607, 665.

Rees, M. J. & Mészáros, P. 1992, Monthly Notices of the Royal Astronomical Society, 258, 41.

Rees, M. J. & Mészáros, P. 1994, The Astrophysical Journal, 430, L93.

Rees, M. J. & Mészáros, P. 2005, The Astrophysical Journal, 628, 847.

Rhoads, J.E. 1997, The Astrophysical Journal Letters, 487, L1.

Rizzuto, D., et al. 2007, Monthly Notices of the Royal Astronomical Society, 379, 619

Rossi, F., et al. 2008, Monthly Notices of the Royal Astronomical Society, 388, 1284.

Ryde, F. & Svensson, R. 2000, The Astrophysical Journal, 529, 13.

Ryde, F. & Svensson, R. 2002, The Astrophysical Journal, 566, 210.

Sakamoto, T., et al. 2005, The Astrophysical Journal, 629, 311.

Sakamoto, T., et al. 2008a, The Astrophysical Journal Supplement, 175, 179.

Sakamoto, T., et al. 2008b, The Astrophysical Journal, 679, 570.

Sakamoto et al. 2011, ApJS, Accepted, astro-ph/1104.4689

Sari, R. et al. 1998, The Astrophysical Journal Letters, 497, L17.

Sari, R. et al. 1999, The Astrophysical Journal, 519, L17.

Salvatera, R. et al. 2009, Nature, 461, 1258.

Sandage, A. 1958, The Astrophysical Journal, 127, 513.

Scargle, J. D. 1998, The Astrophysical Journal, 504, 405.

Schaefer, B. E. 2002, Gamma-ray Bursts: The Brightest Explosions in the Universe (Cambridge, MA: Harvard Univ. Press).

Schaefer, B.E. 2003a, The Astrophysical Journal Letters, 583, L67.

Schaefer, B.E. 2003b, The Astrophysical Journal Letters, 583 L71.

Schaefer B.E., 2004, The Astrophysical Journal, 602, 306.

Schaefer, B.E. 2007, The Astrophysical Journal, 660, 16.

Schaefer, B.E. & Collazzi, A.C. 2007, The Astrophysical Journal Letters, 656, L53.

Schaefer, B.E. et al. 1994, The Astrophysical Journal Supplement, 92, 285.

Schaefer, B.E. et al. 2001, The Astrophysical Journal Letters, 563, L123.

Schmidt, M. 1968, The Astrophysical Journal, 151, 393.

Schmidt, M. et al. 1988, The Astrophysical Journal Letters, 329, L85.

Stanek, K.Z. et al. 2003, The Astrophysical Journal, 591, L17.

Tanvir, N.R. et al. 2009, Nature, 461, 1254.

Thompson, C. et al. 2007, The Astrophysical Journal, 666, 1012.

Tsutsui, R. et al. 2009, Journal of Cosmology and Astroparticle Physics, 8, 15.

Uehara, T. et al. 2007, GCN Circ. 6396.

van Paradijs, J. et al. 1997, Nature, 386, 686.

Vianello, G. et al. 2009, Astronomy & Astrophysics, 495, 1005.

Wiltshire, D.L. 2007, Physical Reviews Letters, 99, 251101.

Woosley, S.E. 1993, The Astrophysical Journal, 405, 273.

Woosley, S.E. & Bloom, J.S. 2006, Annual Reviews of Astronomy & Astrophysics, 44, 507.

Wright, E.L. 2007, The Astrophysical Journal, 664, 633.

Xiao, L. & Schaefer, B.E. 2009, The Astrophysical Journal, 707, 387.

Xiao, L., & Schaefer, B. E. 2011, The Astrophysical Journal, accepted.

Yamazaki, R. et al. 2004, The Astrophysical Journal, 606, L33.

Yonetoku, D. et al. 2004, The Astrophysical Journal, 609, 935.

Appendix

Letters of Permission

A.1 Permission to Reproduce Previously Published Work

Permissions to reproduce material appearing throughout this thesis (most notably in Chapters 2, 3, 4, and 5) were obtained through direct contact with the Institute of Physics Publishing department of Copyright and Permissions. The material is reproduced by permission of the American Astronomical Society. Each chapter specifically references the papers involved, but the full references are also here for completeness:

Schaefer, B.E. & Collazzi, A.C. 2007, The Astrophysical Journal Letters, 656, L53.

Collazzi, A.C. & Schaefer, B.E. 2008, The Astrophysical Journal, 688, 456.

Collazzi, A.C. et al. 2011, The Astrophysical Journal, 729, 89.

A.2 Permission to Reproduce Figure 1.2

This figure was reproduced by the permission of the American Astronomical Society.

Vita

Andrew Charles Collazzi was born in Ridgewood, New Jersey, on March 16, 1984. He earned his bachelor's degree in physics and mathematics with honors in astronomy in 2006 from Vanderbilt University, and his master's degree in physics in 2010 from Louisiana State University. The degree of Doctor of Philosophy in physics will be conferred on him by Louisiana State University at the August 2011 commencement ceremony.